SAPIENZA
UNIVERSITÀ DI ROMA

PhD COURSE IN PHARMACEUTICAL SCIENCES
XXVI CYCLE

# DISSERTATION

**Title of dissertation**

## *Chromatography and mass spectrometry in the study of structure and dynamics of chiral molecules.*


Author
Rocchina Sabia

Advisor
Prof. Claudio Villani


aa 2013-2014

## Table of contents

## Abstract

### Part A

Dynamic high performance liquid chromatography on chiral stationary phases is a consolidated technique that allows the investigation of chiral molecules with labile stereogenic elements that interconvert very quickly at room temperature and result in stereoinversion processes occurring on the time scale of the separation process. Kinetic parameters for on-column interconversions can be extracted from exchange-deformed experimental peak profiles by computer simulation. The technique has been used in a wide range of temperatures and is complementary in scope to dynamic nuclear magnetic resonance spectroscopy.

Here we report, in the first part, the separation of the enantiomers of benzodiazepines, a class of molecules whose conformational enantiomers interconvert not only through a single bond rotation but also via “ring-flip” inversion. The second part concerns the first HPLC resolution of the conformational enantiomers of tri-O-thymotide (TOT) a

macrocyclic trilactone existing in fast-exchanging multiple chiral conformations. Variable chromatography on brush type stationary phases showed dynamic features due to on-column interconversions of TOT.

**Part B**

Chiral recognition is a branch of chemistry aimed at understanding the reactivity as well as the size- and shape-specificity of non-covalent interactions between molecular aggregates formed by chiral species. Mass spectrometry (MS) is a powerful tool for investigating chiral recognition in the gas phase in the absence of perturbing environmental phenomena and discriminating and even quantifying chiral species by interaction with chiral reference molecules.

A small library of synthetic receptors was prepared by macrocyclization of complementary A and B fragments to yield $A_2B_2$ macrocycles, where A are activated forms of isophthalic acid derivatives and B are chiral, $C_2$ symmetric 1,2-diamines derived from 1,2-diphenylethylendiamine. Their enantioselectivity was investigated by ESI-MS and

revealed large enantioselectivities towards the enantiomers of aminoacids and peptide guests. The stability of the complexes increases with the size of guests and with large aromatic portions on the guest.

**Part C**

This part of my academic program was developed at the University of California, Davis, under the supervision of prof. Carlito Lebrilla, during the last period of my Ph.D. activity.

An important goal in proteomic is to quantify the profile changes of protein abundances in biological systems. Quantifying these changes is a key to understand changes in cell state at a molecular level.

In the last years label-free quantitation using MRM (multiple reaction monitoring), which correlates the mass spectrometric signal of intact proteolytic peptides with the relative or absolute protein quantity, is become a powerful tool for accurate quantitation. Here we report a label-free method to quantify proteins and their glycoforms in biologic

fluids (milk, feces and urine) by MRM, including the selection of proteotryptic peptides and the optimization and validation of transitions.

# PART A

# *Stereodynamics of chiral stereolabile compounds*

## General Introduction

Louis Pasteur, in 1848, was the first to recognize the omnipresence and significance of chirality [1]. Today chirality can indeed be found at all levels in nature, in the form of the elementary particle known as the helical neutrino, inherently chiral
DNA, or helical bacteria, plants and sea shells.

Chiral objects exist as a pair of enantiomorphous mirror images that can exhibit different chemical and physical properties in a chiral environment. Stereolabile conformational enantiomers and diastereoisomers cannot be separated at room temperature and spectroscopic or chromatographic techniques are often unable to differentiate the rapidly interconverting species. Many biologically active compounds, such as pharmaceuticals, agrochemicals, flavors, fragrances, and nutrients, are chiral and this increases the demand in progress in asymmetric synthesis and catalysis, and in the development of analytical techniques for the determination of the stereochemical

purity of chiral compounds. Stereoselective analysis usually entails chiroptical measurements, NMR and mass spectroscopic methods, electrophoresis, chiral chromatography or UV and fluorescence sensing assays, and it can provide invaluable information about the stability of chiral compounds to racemization and diastereomerization. One of the best way to obtain information in terms of enantiomeric composition and to separate enantiomers on large scale is represented by HPLC separation of enantiomers on chiral stationary phases. High-resolution enantioselective chromatography techniques based on the utilization of chiral stationary phases, are extremely useful for the study of conformational chirality. The simultaneous use of DNMR is of fundamental importance because it allows the complete elucidation and assignment of very complicated patterns. Separation of enantiomers on chiral stationary phases is realized through reversible formation of diastereomers, resulting from non-covalent interaction of the two enantiomers of the analyte with the chiral selector of the

stationary phase. This reversible interaction is usually referred to as primary equilibrium (Fig. 1) [2-6].

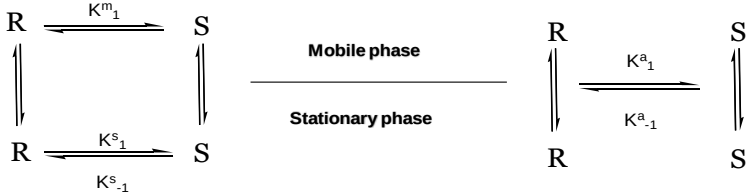


$K^m_1$ , $K^m_{-1}$ : rate costants for the interconversion in the mobile phase

$K^s_1$: rate costant for the R to S conversion in the stationary phase

$K^s_{-1}$: rate costant for the S to R conversion in the stationary phase

$K^a_1$: apparent rate costant for the R to S conversion

$K^a_{-1}$: apparent rate costant for the S to R conversion

**Figure 1:** Primary and secondary equilibria taking place during chromatography of two interconvertible enantiomers R and S on a CSP.

The secondary equilibria are related to the reversible exchange processes between R and S occurring in the mobile and stationary phases. If the mobile phase is achiral the two constants $k^m_1$ and $k^m_{-1}$ are equal, the two rate constants, $k^s_1$ and $k^s_{-1}$, are different if R and S have different retention times.

The apparent rate constants $k^a_1$ and $k^a_{-1}$ thus obtained are averaged values for the interconversion occurring in the mobile ($k^m_1=k^m_{-1}$) and in the stationary ($k^s_1 \neq k^s_{-1}$) phases. Although the values of the apparent rate constants obtained by simulation may differ in principle from $k^m$, in practice they are usually very close to those determined by independent measurements in free solution and can be used to determine the energy barrier for the dynamic process [7]. The equation (1) relates the chromatographic enantioselectivity ($\alpha$) with the energy difference of the transient diastereomers.

$$\Delta\Delta G^\circ_{2,1}=\Delta G^\circ_2 - \Delta G^\circ_1 = -RT \ln(k'_2/k'_1) = -RT \ln\alpha_{2,1} \qquad (1)$$

where $\Delta\Delta G^\circ_{2,1}$ is the difference in the interaction Gibbs energies between the two enantiomers and the selector, R is the gas constant, T is the absolute temperature and $\alpha_{2,1}$ is the ratio of the retention factors $k'_2$ and $k'_1$ of the two enantiomers.

Dynamic stereochemistry, in the form of variable temperature (for DNM and DHPLC) or variable flow chromatography, plays a crucial role in the study of stereodynamic processes that can be employed to determine the enantiomerization (the reversible isomerization of one enantiomer into the other) barrier of chiral stereolabile species when the interconversion takes place at the time scale of the separation process. A successful chromatographic separation of stereoisomers affords two distinct peaks. However, stereoisomers may undergo interconversion during the chromatographic process at elevated temperatures. The competition between resolution and isomerization results in an elution profile showing a plateau between the peaks. Since plateau formation is due to on-column isomerization, both the reaction rate and the height of the plateau increase with temperature (Fig. 2). When the interconversion process becomes much faster than the chromatographic separation, at high temperatures, only one peak is observed.

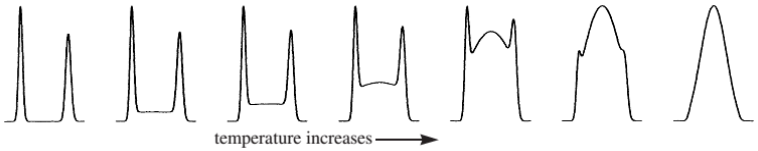


**Figure 2:** Temperature-dependent plateaus and peak coalescence due to simultaneous chromatographic resolution and on-column isomerization.

Three different chromatographic scenarios can be observed: (a) two baseline-separated peaks are obtained if enantiomerization is slow compared to the chromatographic time scale; (b) competition between chromatographic resolution and enantiomerization generates a temperature-dependent plateau between the two peaks; and (c) only one peak is observed when enantiomerization is fast relative to the time required for the separation.

Computer simulation of exchange-deformed elution profiles gives the apparent rate constants for the on column R/S interconversion and the associated barriers $\Delta G^{\ddagger}$.

The interconversion of stereoisomers exhibiting diastereotopic nuclei can be monitored by variable-temperature NMR spectroscopy (dynamic NMR) when

the reaction is slow on the NMR time scale. This is the case when:

$$k = \frac{1}{t} \ll \pi \frac{\Delta\nu}{\sqrt{2}}$$

where $k$ is the interconversion rate constant, $t$ is the interconversion time (in s) and $\Delta\nu$ is the NMR shift separation of the signals (in Hz) at low temperatures at which exchange does not occur. This equation indicates that same nuclei can show distinct signals when the chemical shift difference ($\Delta\nu$) corresponds to a time spent by the nuclei in different positions longer than the interconversion time $t$. Increasing the temperature, increases the exchange rate relative to the NMR time scale and only one averaged species is observed due to signal coalescence (Fig. 3) [8-9].

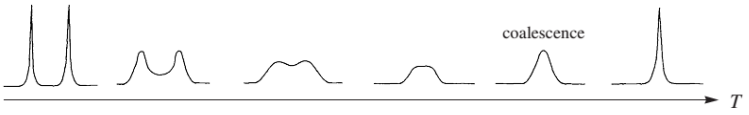


**Figure 3:** Variable-temperature NMR spectra.

Free Gibbs activation energy $\Delta G^{\ddagger}$ can be calculated in kcal/mol from eq. 1

$$\Delta G^{\ddagger} = 4.58*T_c*[10.32 + \log (T_c/k_c)] \qquad \text{(Eq. 1)}$$

The NMR time scale is different from HPLC time scale and dynamic spectra are observed across a higher temperature range compared to DHPLC.

DHPLC and DNMR are complementary methods that allow kinetic investigations of stereolabile compounds over a wide temperature range. DHPLC is well suited for operation in the cryo-temperature range (from -80 °C to 0 °C) and in the high temperature range (from ambient temperature up to 100 °C.)

## References

[1] Cahn, R. S.; Ingold, C. K.; Prelog, V. *Angew. Chem.*, Int. Ed. Engl.1966, 5, 385-415.

[2] Subramanian, G. (Ed.), A Practical Approach To Chiral Separations By Liquid Chromatography, Wiley-VCH, Weinheim 1994.

[3] Ahuja, S. (Ed.), Chiral Separations – Applications and Technology, American Chemical Society, Washington, DC 1997.

[4] Allenmark, S., Schurig, V., *J. Mater. Chem.* 1997, 7, 1955 –1963.

[5] Armstrong, D. W., *LC-GC Int*. 1998,4, 22 – 31.

[6] Gasparrini, F., Misiti, D., Villani, C., *J. Chromatogr A* 2001, 906, 35 – 50.

[7] D'Acquarica, I., Gasparrini, F., Pierini, M., Villani, C., Zappia, G. *J. Sep. Sci.* 2006, 29, 1508 – 1516.

[8] Gasparrini, F., Lunazzi, L., Misiti, D., and Villani, C. *Acc. Chem. Res.* 1995, Vol. 28, No. 4.

[9] C. Wolf, *Dynamic Stereochemistry of Chiral Compounds*, RSC Publishing, Cambridge, 2008.

# PART A-1

# *Dynamic HPLC on chiral stationary phases. Low temperature separation of the interconverting enantiomers of benzodiazepines*

# Benzodiazepines

## 1.1 Introduction

Most of commercially chiral drugs are either racemates or single enantiomers; the biological activity of chiral molecule differs from the racemate and the individual enantiomers, and it is well documented [1, 2].

Stereoisomers are isomeric molecules that have the same molecular formula and sequence of bonded atoms, but that differ only in the three-dimensional orientations of their atoms in the space. There is another, often overlooked, source of chirality: atropisomerism [3, 4]. Atropisomers are enantiomers or diastereoisomers resulting from slow axial rotation and that can interconvert thermally, slowly enough to allow analytical separation (~1000 s or longer). As bond rotation is time-depending, racemization for atropisomers can vary between minutes to years, depending on steric hindrance, electronic factors, temperature and solvents and has the potential to lead to sizeable pharmacological

consequence. Using quantum mechanics (QM), the calculation of energy barrier can predict atropisomerism. The increasing importance on atropisomers is due to their impact on pharmaceutical field to develop safe and stable substances that specifically target essential elements that cause disease. It is well-known the case of thalidomide, whose enantiomers differ dramatically and one is teratogen; the separation of each isomer in mixture is critical to assure the safety, quality and efficacy of drug [5, 6].

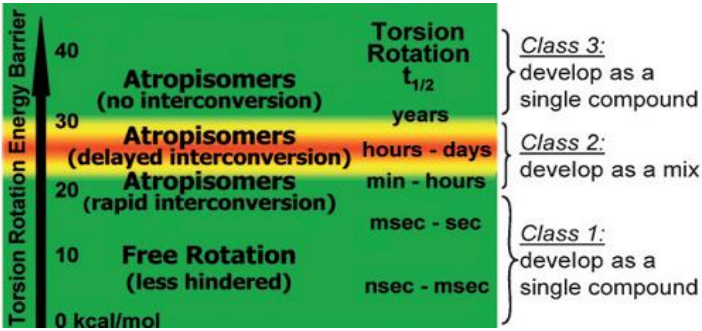


**Figure 1:** Correlation between calculated torsion rotation energy barriers, $t_{1/2}$, and compound classes.

Atropisomers can be classified into three groups according to their time-dependent properties, based on rotational energy barriers, and this can suggest accompanying development strategies (Fig. 1) [7].

Class 1 are compounds that possess fast axial rotation rates on the order of seconds or faster, exhibit no axial chirality at room temperature, and have energy barriers to rotations ($\Delta E_{rot}$) of < ~20 kcal/mol. These compounds do not have atropisomer properties.

Compounds with $\Delta E_{rot}$ > ~20 kcal/mol can form atropisomers and can be divided into two classes, class 2 and 3. Class 2 are compounds that present delayed axial interconversion with $t_{1/2}$ values in the range of minutes, days or months. Class 3 compounds ($\Delta E_{rot}$ > ~30 kcal/mol) are those that experience very slow torsion-rotation rates ($t_{1/2}$) on the order of years. These chiral compounds are stable over time and can thus be isolated as optically pure. Benzodiazepines, a well-known class of sedatives, hypnotics, anxiolytics and anticonvulsants, are a class of conformational enantiomers that present not only a single

bond rotation but also a "ring-flip" to switch from one enantiomer to the other. 1,4-benzodiazepines are characterized by a non-planar diazepine ring which inverts between two enantiomeric boat conformations [8]. The conformation of the diazepine ring presents four endocyclic torsion angles (τ2, τ3, τ4, and τ5), but the two conformers are described by the sign of τ3 (the angle defined by C(2), C(3), N(4), and C(5)), namely an (M)-conformer where τ3 is negative, and a (P)-conformer where it is positive (Fig. 2) [9]. These two conformers differ in the orientation of the $CH_2$ (3) group which lies above (M) or below (P) the plane defined by the fused benzene ring of the benzodiazepine.

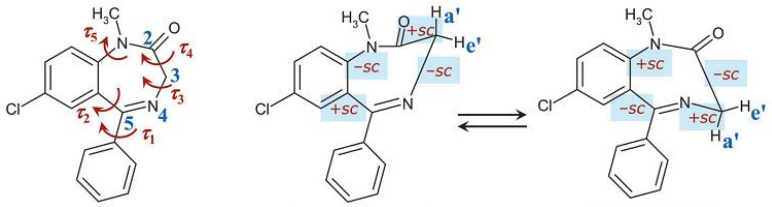


**Figure 2:** Diazepam enantiomeric conformers.

The two enantiomeric conformers of diazepam have the same conformational energy, the near-planar transition state is of ca. 17 kcal/mol above the low energy conformations, and its τ3 and τ4 assume synperiplanar geometries. The two conformers are in very rapid equilibrium and cannot be separated physically (Fig. 3).

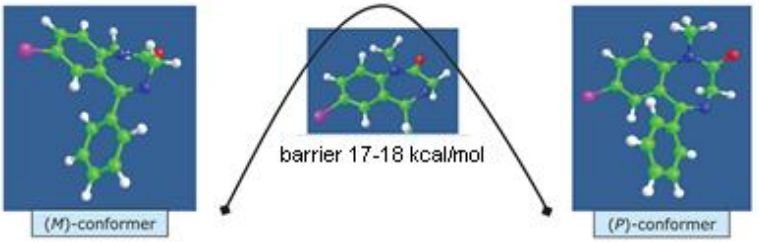


**Figure 3:** Enengy barrier of diazepam interconversion.

The stability to racemization of these seven-membered ring systems depends on the bulkiness of the substituent attached to the amide nitrogen. Substitution around the (medium) rings must impose severe steric restrictions to bond rotation before these molecules become class 3 atropisomer.

## 1.2 Results and discussion

### 1.2.1 Diazepam, prazepam, flunitrazepam and tetrazepam

*1.2.1 a Chromatographic resolution*

Diazepam and other glycine-derived 1,4-benzodiazepin-2-ones are examples of drugs that existed as mixtures of chiral conformations, that are not separable at room temperature cause their barriers to interconversion are sufficiently low.

These class of substances, lacking a chiral center, exist in the form of axially chiral enantiomers that usually show rapid interconversion due to facile ring flipping at room temperature.

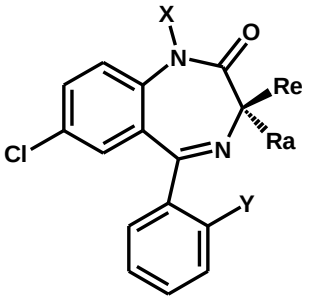


**Figure 4:** structure of 1,4-benzodiazepin-2-ones.

For BDZs unsubstituted at C3 (Ra=Re=H), such as diazepam (Fig. 5), the equilibrium in solution is extremely rapid, the calculated activation energy is ~ 17.6 kcal/mol (Fig. 3) [10].

We focused our attention on four benzodiazepines (Fig. 2), very close, in term of structure, to diazepam to explore the influence on chromatographic separation and on enantiomerization barriers of substituent in N1.

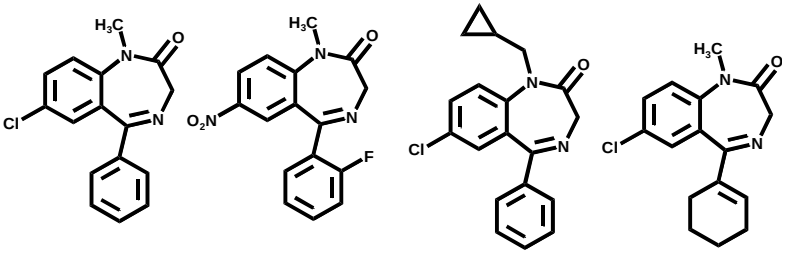


**Figure 5:** diazepam, flunitrazepam, prazepam and tetrazepam

Flunitrazepam differs from diazepam for the presence of a fluorine group on the aryl ring and for a nitro group in 7 position instead of chloride. Prazepam presents a ciclopropyl at the N1 and tetrazepam has a partially saturated, non planar ring in position 5.

The chromatographic separations were performed on a CSP, we selected Whelk-O1 for its extraordinary degree of generality. The Whelk-O1 CSP is based on 1-(3,5-dinitrobenzamido)-1,2,3,4,-tetrahydrophenanthrene, this π-electron acceptor/π-electron donor phase allows the resolution of a wide variety of underivatized racemates (see part A2 for the chemical structure). At room temperature the separation were unsuccessful for all of these drugs due to their rapid interconversion (explained before), they showed only one single peak. At sub-ambient temperatures, high values of enantioselectivity and resolution factors were obtained using hexane-$CH_2Cl_2$-MeOH 60/60/1 mixture as eluent, delivered at a flow rate of 1.0 ml/min. At -20 °C the chromatographic profile of diazepam shows two distinct peaks separated by a plateau, the on-column enantiomerization process is slower than the chromatographic resolution (Fig. 5). The on-column M/P interconversion process results completely locked at -66 °C.

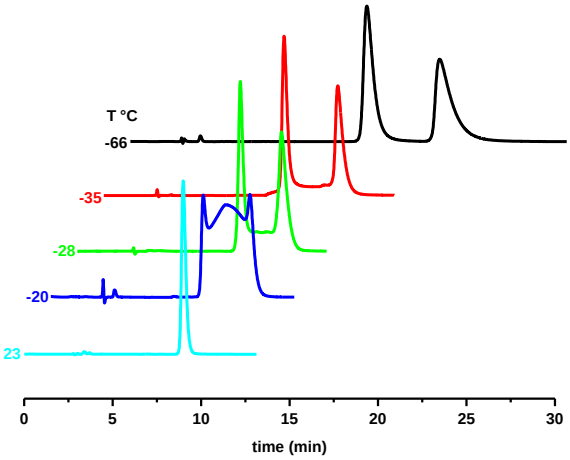


**Figure 5:** diazepam, column (R,R)-Whelk-O1, eluent hexane/$CH_2Cl_2$/MeOH 60/60/1, flow rate 1 ml/min, UV detection at 280 nm.

Flunitrazepam presents a nitro group instead of the chlorine atom and also presents a fluorine on the non-fused phenyl ring, these differences in the structure influence both the separation and the interconversion. At -32 °C the two enantiomers were still not resolved, we observed two distinct peaks at -55 °C with a plateau and the process was completed locked at T lower than -62 °C.

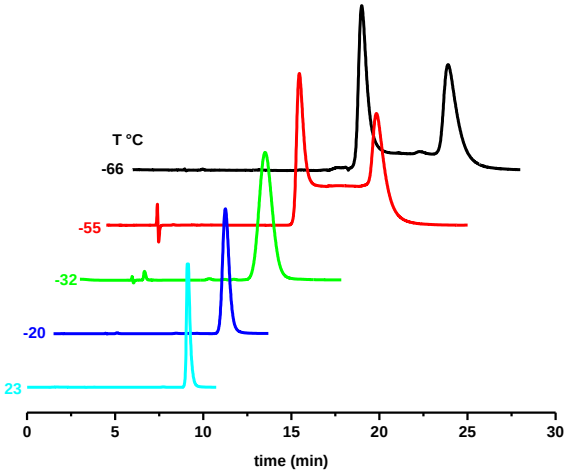


**Figure 6:** flunitrazepam, column (R,R)-Whelk-O1, eluent hexane/$CH_2Cl_2$/MeOH 60/60/1, flow rate 1 ml/min, UV detection at 280 nm.

Prazepam presents exactly the same structure of diazepam except for the substituent in N1, it presents a cyclopropyl methyl, a larger group than the methyl group.

In this case and also in the case of tetrazepam, the plateau is visible already at -11 °C and the interconversion is locked at -35 °C in the case of prazepam (Fig. 7), and at -66 °C in the case of tetrazepam (Fig. 7).

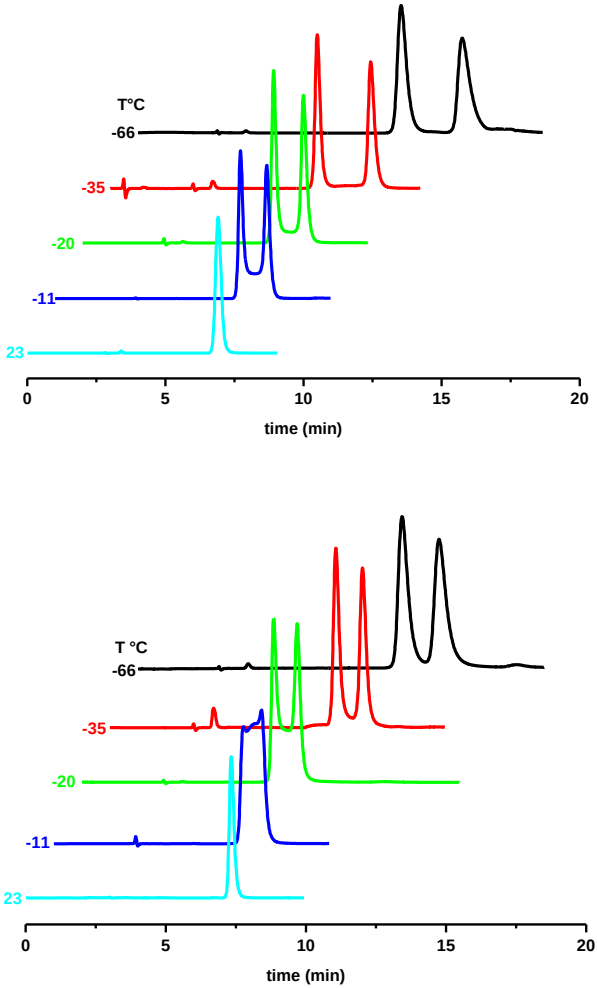


**Figure 7:** prazepam (top), tetrazepam (bottom) column (R,R)-Whelk-O1, eluent hexane/$CH_2Cl_2$/MeOH 60/60/1, flow rate 1 ml/min, UV detection at 280 nm.

*1.2.1 b Simulation of dynamic chromatograms*

The enantiomerization barriers of diazepam, tetrazepam, funitrazepam and prazepam have been determined by dynamic HPLC on the Whelk-O1 CSP. Interconversion profiles featuring plateau formation and peak broadening were observed and simulated by the lab-made computer program Auto DHPLC y2k based on the theoretical plate as well as on the stochastic model using the experimental data plateau height. Dynamic deformations of the experimental chromatograms were exploited to extract kinetic data pertinent to the enantiomerization process occurring during the chromatographic runs.

Program Auto DHPLC y2k [11] implements both stochastic and theoretical plate models according to mathematical equations and procedures described within ref. [11a,b], respectively. Figure 8 shows all the chromatographic profile, both experimental (black) and simulated (red).

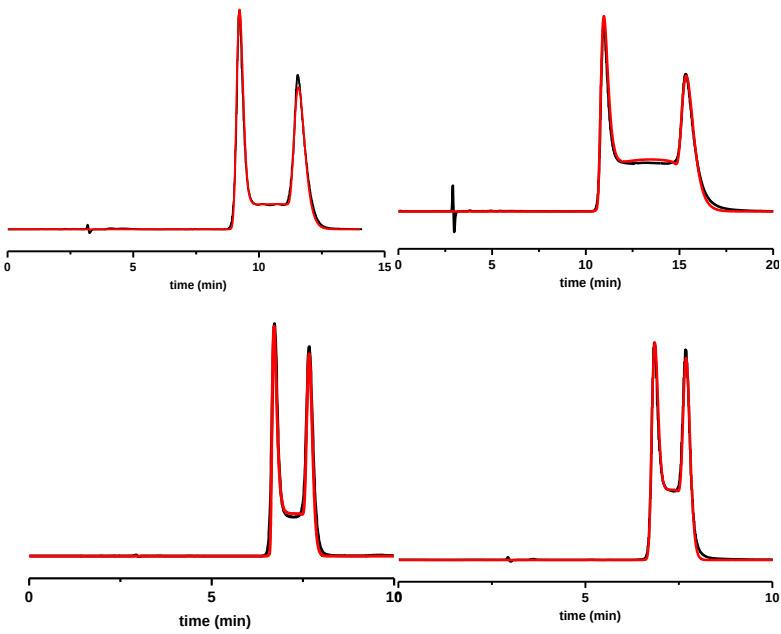


**Figure 8:** experimental (black) and simulated (red) profile of diazepam at -28 °C (top, left panel); flunitrazepam at -66 °C (top, right panel); prazepam at -20 °C (bottom, left panel) and tetrazepam -20 °C (bottom, right panel).

As shown in Tab 1 the stability towards racemization of these seven-membered ring systems depends on the bulkiness of the substituent attached to the N1 amide nitrogen. When observing the energy barriers listed in table

1, the lower values $\Delta G^{\ddagger}_{12}$ are the ones related to the conversion of the first eluted enantiomer into the second one, and are those closer to values recorded by other techniques in free solution (e.g. by D-NMR) in the absence of the usually retarding effect of the stationary phase. The calculated activation energy of diazepam is $\Delta G_{12}$ =17.60 kcal/mol ± 0.02 (in agreement with D-NMR literature data). A similar value is observed for tetrazepam, a result that is consistent with the energy barrier depending on the size of the N1 substituent. For prazepam, that has the largest group on N1, the energy barrier is significantly larger, around 18.65 kcal/mol. Flunitrazepam, on the other hand, has a lower barrier for the M/P interconversion: the presence of the two electron-withdrawing nitro and fluorine substituents on the two phenyl rings presumably decreases the electron density on the diazepine ring and facilitates the ring inversion process.

| *compound* | *T* | | $k^a_1$ *(min$^{-1}$)* | $k^a_{-1}$ *(min$^{-1}$)* | $\Delta G^{\ddagger}_{12}$ *(kcal/mol)* | $\Delta G^{\ddagger}_{21}$ *(kcal/mol)* |
|---|---|---|---|---|---|---|
| | *°C* | *K* | | | | |
| diazepam | -20 | 253 | 0.201 | 0.152 | 17.60 | 17.74 |
| | -28 | 245 | 0.039 | 0.031 | 17.83 | 17.95 |
| | -35 | 238 | 0.021 | 0.016 | 17.59 | 17.72 |
| prazepam | -11 | 262 | 0.069 | 0.061 | 18.79 | 18.87 |
| | -20 | 253 | 0.029 | 0.025 | 18.65 | 18.73 |
| tetrazepam | -11 | 262 | 0.152 | 0.138 | 18.39 | 18.44 |
| | -20 | 253 | 0,083 | 0,074 | 18,04 | 18,1 |
| flunitrazepam | -55 | 218 | 0.074 | 0.053 | 15.54 | 15.68 |

**Table 1:** Enantiomerization barriers (in kcal/mol) obtained by D-HPLC. T = column temperature within 0.1 °C. Errors in $\Delta G^{\ddagger}$ ± 0.02 kcal/mol.

### *1.2.1 c $^{1}$H-NMR and D-NMR of flunitrazepam*

The $^{1}$H-NMR spectrum (400 MHz, $CDCl_3$, 25 °C, TMS as external standard) of flunitrazepam showed a singlet at 3.5 ppm due to the methyl group, two distinct signal at 3.8 and 5.0 ppm corresponding to the two methylenic protons Ha and He, (J= 11.5 Hz) (Fig. 9). Downfield between 7.0 and 8.5 ppm a complex absorption pattern is observed, corresponding to the aromatic proton resonances.

The enantiomerization barrier of flunitrazepam was monitored also by variable-temperature NMR spectroscopy (dynamic NMR), because its enantiomerization barrier, previously calculated by D-HPLC, is so low in the NMR time scale to permit to see the exchange at value of T close to ambient temperature.

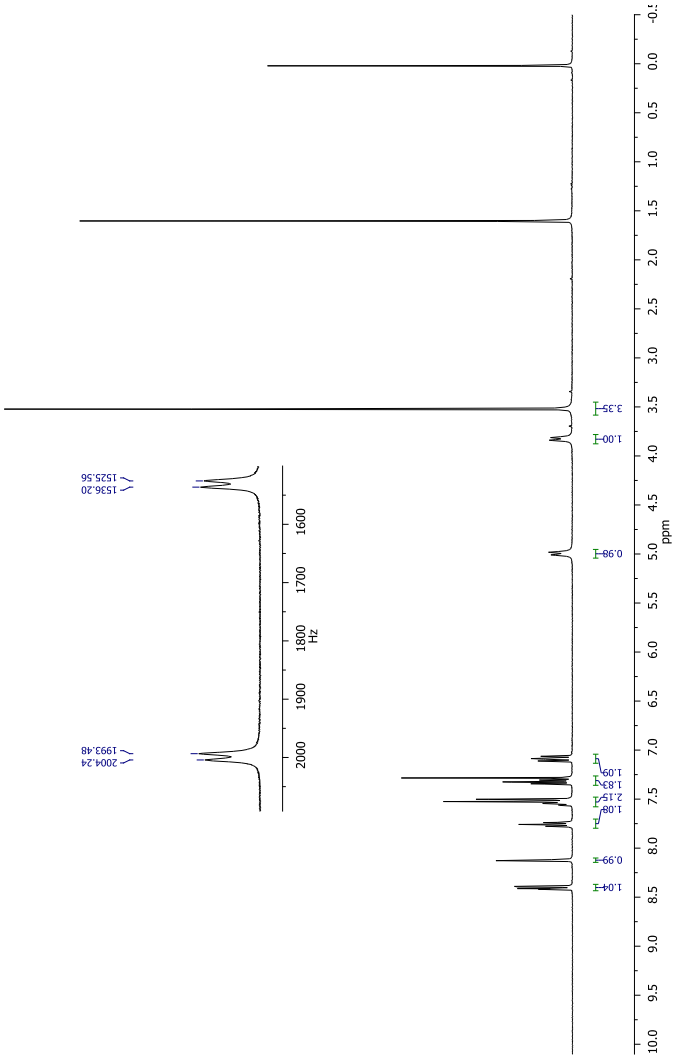


**Figure 9:** $^{1}$H-NMR spectrum of flunitrazepam in $CDCl_3$.

The experiments of dynamic NMR where carried out in two different solvent, $CD_3OD$ and $d_6$-DSMO, to evaluate also the influence of the solvent on the enantiomerization barrier. The experiments were performed in a temperature range between 27.5 and 92 °C in $d_6$-DMSO and 27.5 and 72.6 °C in the case of $CD_3OD$ (Fig. 10). At room temperature, for both the experiments, the methylenic protons of C3 gave two distinct peaks. When the temperature is raised above 27.5 °C, the rotation becomes faster and the M enantiomer into the P interconversion becomes increasingly faster on the NMR time scale. At the highest temperature the interconversion is so fast that the two protons are no longer diastereotopic and coalesce into a single averaged signal. Increasing the temperature didn't change all the spectrum but only the signals of methylenic protons. As the temperature is raised, the signals become first two broad signals and then they turn into a single signal (Fig. 10). The coalescence temperature observed for the experiments in DMSO was 64.9 °C and 72.6 °C for $CD_3OD$. The free activation energy was calculated according to the following

equation (derived from the Eyring equation $k=(k_BT/h)e^{-\Delta G^{\ddagger}/RT}$):

$$\Delta G^{\ddagger} = 4.58*T_c*[10.32 + \log (T_c/k_c)]$$

where $T_c$ is the coalescence temperature and $k_c$ is the kinetic constant of the interconversion process at coalescence temperature :

$k_c = 2.22*[(\Delta\nu^2 + 6(J_{AB})^2]^{1/2}$

where $\Delta\nu$ (Hz) is the frequency difference between the two signals in the absence of exchange, $J_{AB}$ is the J-coupling between A and B also in absence of exchange.

The $\Delta G^{\ddagger}$ was 15.72 ± 0.01 kcal/mol at $T_c$= 64.9 °C in $d_6$-DMSO and 16.01 ± 0.01 kcal/mol at $T_c$= 72.60 °C in $CD_3OD$, in agreement with the values previous determined by D-HPLC (15.61 ± 0.02 kcal/mol). As expected, the barriers of interconversion are unaffected by the nature of the solvent, as is usually the case for thermal enantiomerization processes occurring by conformational changes.

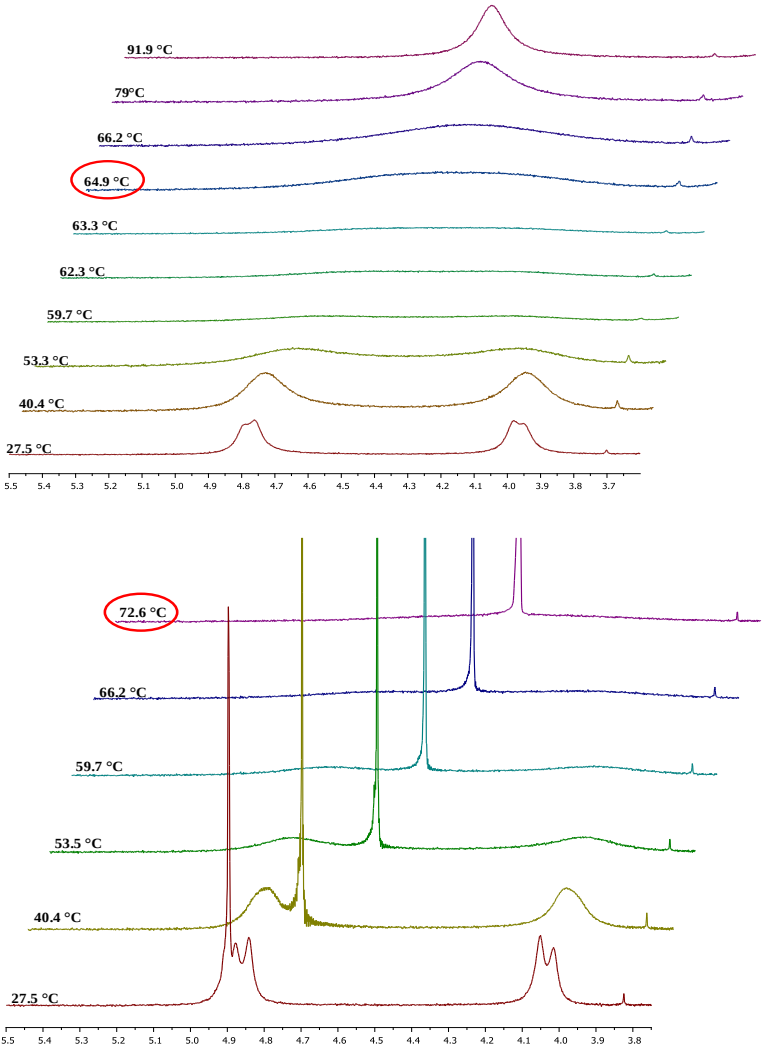


**Figure 10 :** flunitrazepam, DNMR, top DMSO, bottom $CD_3OD$.

*1.2.1 d diazepam ring-opening*

The diazepine seven-membered ring in BDZ is known to be highly sensitivity to hydrolysis in both acidic and basic media. The ring opening can occur by initial breakage of the amide functionality or the C—N bond, in both cases the final product being the substituted 2-aminobenzophenone. Gallardo Cabrera at all in their studies showed that, in addition to the expected 2-methylamino-5-chlorobenzophenone, other products were formed [12] when the experiments were carried out with HCl in aqueous MeOH media.

Our study on the seven-membered ring opening showed the breakage of the C-N bond, without employing acid or basic media. Dynamic chromatographic runs performed on a column of cyclodextrin and $H_2O$/MeOH/$AcONH_4$ (80/20; 20 mM) mixture as eluent at pH 3.5, showed two distinct peaks in a ratio of 95:5 whose signals are connected by an asymmetric plateau (Fig. 11) visible at T greater than 50 °C.

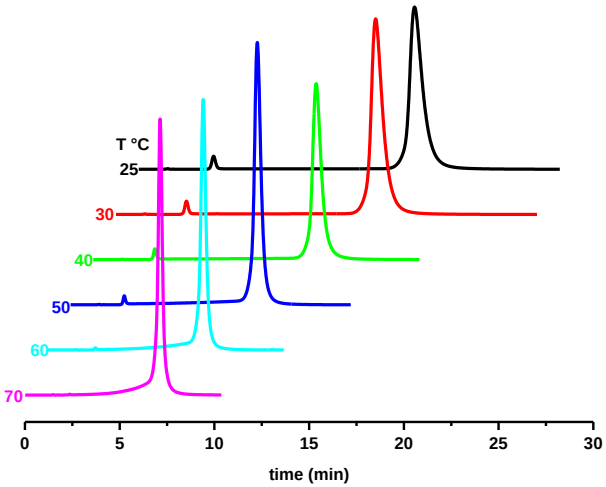


**Figure 11:** diazepam, column ACC-1-23, eluent $H_2O$/MeOH/$AcONH_4$ 80/20 20 mM pH=3.56, flow rate 1 ml/min, UV detection at 254 nm.

By using high resolution MS we assigned the exact structures of the species corresponding to these two peaks. Direct electrospray of a solution of diazepam in MeOH/$H_2O$ (1:1) showed two signal: one at *m/z* 285.07 corresponding to the protonated diazepam and the other at *m/z* 303.08 corresponding to the open ring (Fig. 12-13) form derived from the attack of one water molecule on the imine carbon C5. High resolution ESI_MS obtained on an orbitrap

instrument gave for the same two peaks the values of m/z = 285.0773 (calculated for $C_{16}H_{14}ClN_2O^+$, m/z = 285.0789 ) and m/z = 303.0895 (calculated for $C_{16}H_{16}ClN_2O_2^+$, m/z = 303.0895), thus confirming the assignment.

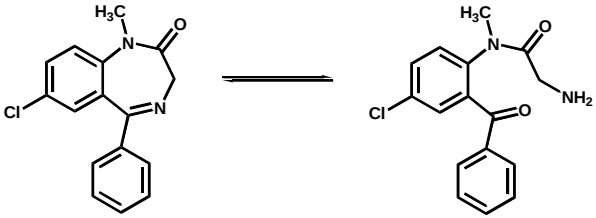


**Figure 12:** diazepam ring-opening.

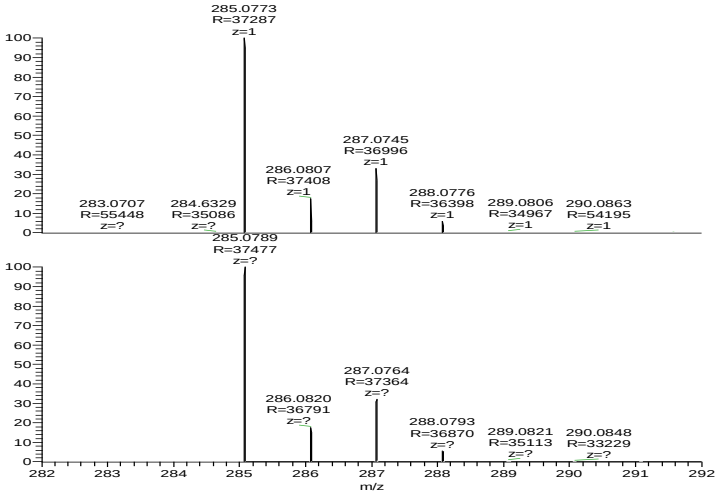

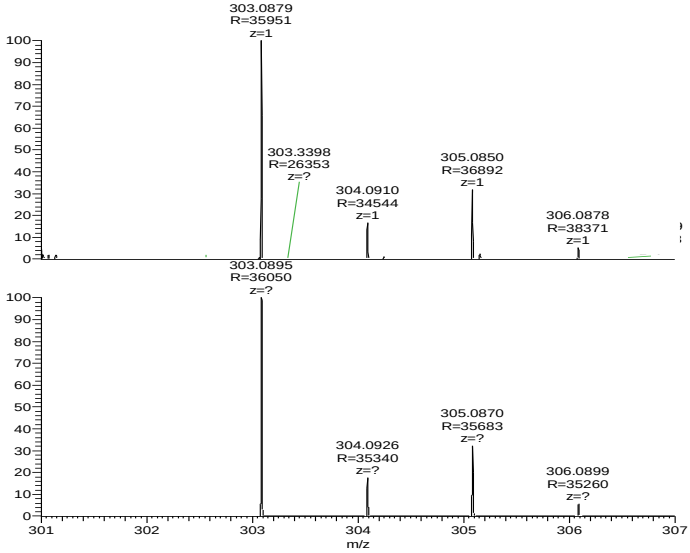


**Figure 13:** HR-ESI-MS of diazepam.

## 1.2.2 Midazolam, triazolam, alprazolam and estazolam

*1.2.2 a Chromatographic resolution*

These BDZ present a pentatomic ring fused on the N1-C2 bond of the diazepine ring: an imidazole, in the case of midazolam, and a triazole, in the other structures. These additional fused rings introduce another element of influence on the energy barrier $\Delta G^{\ddagger}$ for the M/P interconversion.

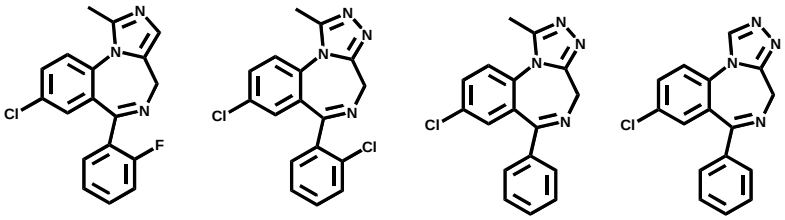

**Figure 14:** midazolam, triazolam, alprazolam and estazolam

As for the other BDZs investigated before, these class are chiral even if they lack a chiral center and their enantiomers cannot be isolated at room temperature. Their chromatographic behavior was studied by dynamic HPLC in

the form of variable temperature. The enantiomers of midazolam were resolved by HPLC on two columns: Chiralpak AD using hexane/isopropanol (70 : 30) as eluent and Chiralpak IA using hexane/$CH_2Cl_2$/MeOH 55/44/1. At 6 °C, in both the experiments, the enantiomerization is completed locked and the two peaks corresponding to the M/P enantiomers are completely resolved at the baseline. Due to the long runs (40 min for Chiralpak AD and ~30 min with Chiralpak IA) the second peak is broad but its area is the same as that of the first eluted enantiomer.

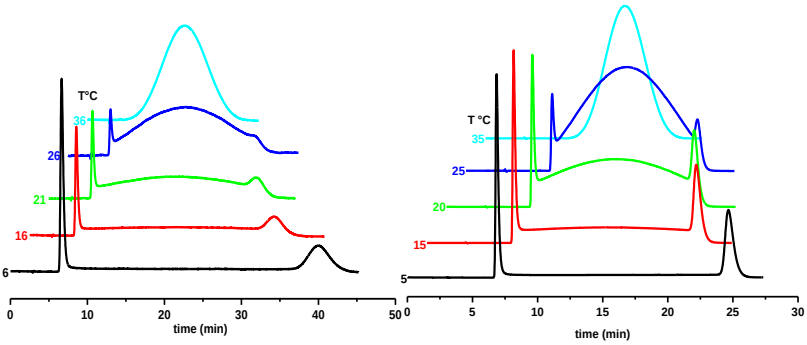


**Figure 15:** midazolam; left panel: Chiralpak AD, eluent hexane/IPA 70/30, flow rate 1 ml/min, UV detection at 280 nm; right panel: Chiralpak IA, eluent hexane/$CH_2Cl_2$/MeOH 55/44/1, flow rate 1 ml/min, UV detection at 265 nm.

Chiralpak AD afforded a good separation and resolution of the two enantiomers but long run time, so alprazolam and triazolam were only studied on Chiralpak IA.

Alprazolam differs from triazolam for the absence of chlorine group on the aryl ring. The electron-withdrawing behavior of this group influences the interconversion barrier of the BDZ that requires lower T to be separated, in analogy to the conformational behavior of flunitrazepam (Fig. 16).

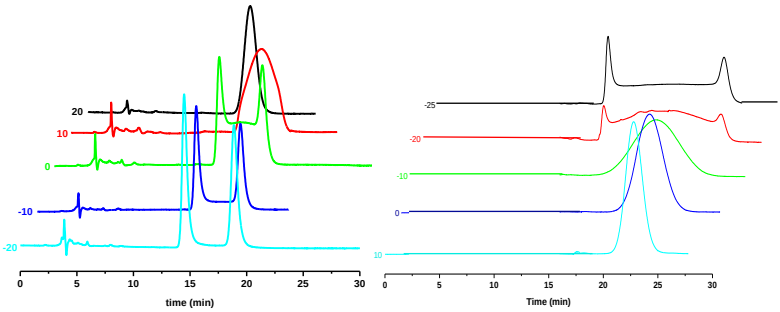


**Figure 16:** alprazolam (left panel), triazolam (right panel) column Chiralpak IA, eluent hexane/$CH_2Cl_2$/MeOH 55/44/1, flow rate 1 ml/min, UV detection at 265 nm.

*1.2.2 b Simulation of dynamic chromatograms*

Computer simulations (Fig. 17) of the chromatographic profiles yielded the isomerization barriers $\Delta G^{\ddagger}$= 20.54 ± 0.02 kcal/mol for midazolam, 19.72 ± 0.02 kcal/mol for alprazolam and 17.33 ± 0.02 kcal/mol for triazolam.

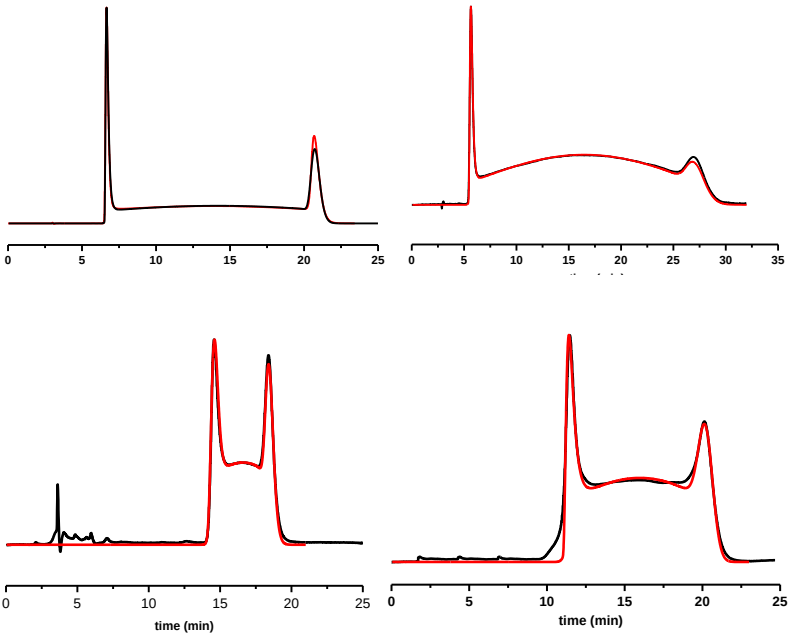


**Figure 17: experimental (black traces) and simulated (red traces) HPLC plots.** Top: midazolam Chiralpak IA, T 15 °C (right panel); Chiralpak AD, T 21 °C (left panel); Bottom: alprazolam T 0 °C; triazolam, T -25 °C.

Midazolam presents the largest $\Delta G^{\ddagger}$ value, and the measured barrier is independent on the structure of the CSP (cfr IA vs AD columns). Midazolam has an imidazole ring fused on the diazepine ring and, in spite of the presence of the electron withdrawing fluorine on the C5 phenyl ring, it shows the highest energy barrier, indicating the imidazole ring renders the 1,4-diazepine more rigid compared to the triazole ring. When alprazolam and triazolam are compared, the lower barrier of the latter can be ascribed to the additional chlorine atom in the C5 phenyl ring of triazolam.

| compound | T | | $k^{a}_{1}$ ($min^{-1}$) | $k^{a}_{-1}$ ($min^{-1}$) | $\Delta G^{\ddagger}_{12}$ (kcal/mol) | $\Delta G^{\ddagger}_{21}$ (kcal/mol) |
|---|---|---|---|---|---|---|
| | °C | K | | | | |
| midazolam AD | 16 | 289 | 0.246 | 0.046 | 20.07 | 21.02 |
| | 21 | 294 | 0.363 | 0.075 | 20.19 | 21.11 |
| midazolam IA | 15 | 288 | 0.180 | 0.057 | 20.17 | 20.83 |
| alprazolam | 0 | 266 | 0.063 | 0.050 | 19.66 | 19.79 |
| | -7 | 253 | 0.040 | 0.030 | 19.39 | 19.53 |
| | -10 | 263 | 0.023 | 0.018 | 19.46 | 19.59 |
| triazolam | -26 | 247 | 0.106 | 0.059 | 17.49 | 17.77 |

**Table 2:** Enantiomerization barriers (in kcal/mol) obtained by D-HPLC. T = column temperature within 0.1 °C. Errors in $\Delta G^{\ddagger}$ ± 0.02 kcal/mol.

*1.2.2 c Reverse-phase chromatography of midazolam*

Human serum albumin (HSA) is an abundant plasma protein that binds a remarkably wide range of drugs, thereby restricting their free, active concentrations. The fundamental role of human serum albumin is as carrier for a variety of endogenous and exogenous compounds in serum [13].

It is well known that the activity of benzodiazepines depends on their binding with HSA, which has a specific, high-affinity BDZ binding site and shows a stereospecificity of binding [14, 18], it has been demonstrated that serum albumin shows a preferential affinity for the (M)-conformer of diazepam [9].

The binding properties of HSA can change in pathological conditions either because of its concentration or because of the concentration of endogenous compounds that selectively bind to the carrier. The investigation of the physiological role of albumin in the human body, the pharmacological consequences of drug-albumin binding and the structure and the properties of the protein binding sites provides new insights into the architecture and specificity of each drug

pocket on HSA and it is important to understand the molecular basis of the adaptability of this transporter protein.

We investigated the conformation selectivity in the binding of midazolam to human serum albumin through dynamic HPLC and induced circular dichroism (ICD). Dynamic chromatographic experiments were carried out on a Chiralpak HSA, where human serum albumin is a selector immobilized on the silica, with an aqueous mobile phase containing a phosphate buffer at different pH. This type of stationary phase is sensitive to the composition of the mobile phase, temperature, flow rate, and pH [19]. Different pH were used to modify the retention time and also the peak shape. Increasing of pH, increase the retention times and the selectivity. Dynamic HPLC were performed in a range of T between 10 and 25 °C (Fig. 18).

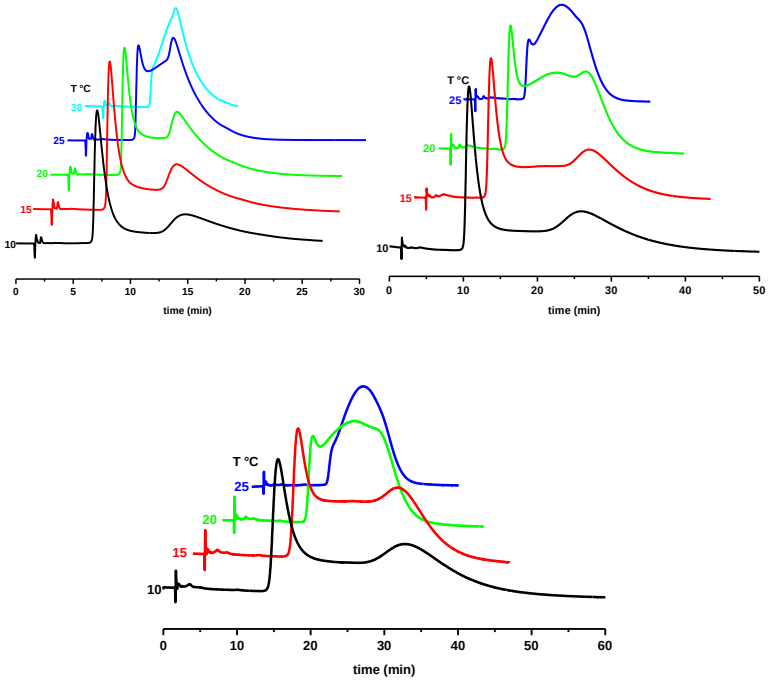


**Figure 18:** midazolam, column Chiralpak HSA, eluent phosphate buffer (0.1 M) 1-propanol 10% (pH 5.77 top left panel; pH 6.22 top right panel; pH 7 bottom); UV detection at 265 nm; flow rate 0.9 ml/min.

The best separation was obtained at pH 6.22 or higher. pH played an important role on the conformation of the HSA, changes in pH can produce structural transitions of the

protein, changes in the properties of a small molecule-protein complex and can produce alterations of the degree of ionization of the ligand molecule.

Computer simulation of elution profiles, that originate from simultaneous separation and interconversion of enantiomers during liquid chromatography, were used to determine rate constants and activation parameters of the isomerization in reverse phase.

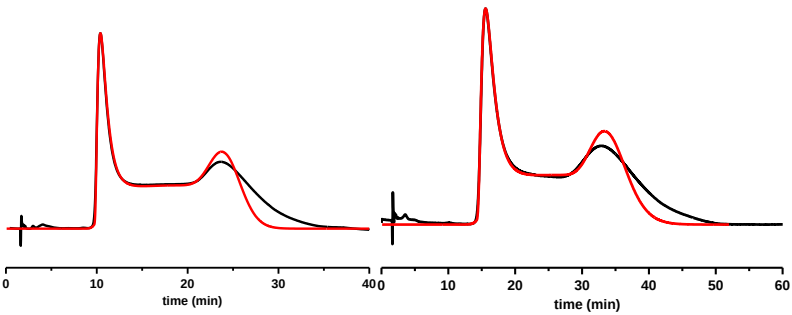


**Figure 19:** experimental (black traces) and simulated (red traces) HPLC plots of midazolam at pH 6.2 (left panel) and pH 7 (right panel).

Simulation of the experimental chromatographic profile (Fig. 19) showed and confirmed that the enantiomerization

barriers are not affected by the solvent, temperature and pH. $\Delta G^{\ddagger}$ was 20.77 ± 0.2 kcal/mol at pH 7 and T 9 °C, 20.54 ± 0.2 kcal/mol at pH 6.22, T 15 °C. The energy barrier for enantiomer interconversion, $\Delta G^{\ddagger}$, was between 20.19 and 20.87 ± 0.2 kcal/mol in organic solvents (measured by DHPLC on chiral stationary phases under normal phase elution mode, see table 2) and similar values were obtained in aqueous media (20.55-20.99 ± 0.2 kcal/mol, table 3).

| Column | T °C | $\Delta G_{1-2}$ | $\Delta G_{2-1}$ |
|---|---|---|---|
| Chiralpak AD Normal phase | 21 | 20.19 | 21.11 |
| Chiralpak IA Normal phase | 15 | 20.22 | 20.87 |
| Chiralpak HSA Reverse phase | 9 | 20.55 | 20.99 |

**Table 3:** Enantiomerization barriers (in kcal/mol) obtained by D-HPLC under normal phase and reversed phase elution conditions. T = column temperature within 0.1 °C. Errors in $\Delta G^{\ddagger}$ ± 0.02 kcal/mol.

When the HPLC separation of midazolam on the HSA column was monitored by CD detection at 265 nm, the plot showed (Fig. 20) a positive signal for the first eluted enantiomer and a negative signal for the second one at 265 nm.

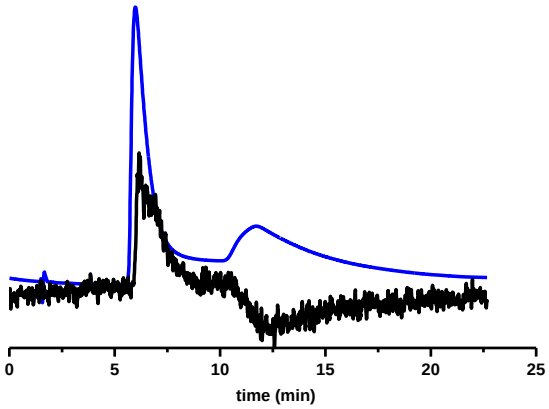


**Figure 20:** UV (blue line) and CD (black line) recorded at 265 nm.

Induced Circular Dichroism (ICD) spectrum detected for the interaction of midazolam with HSA is shown in Figure 21. The presence of HSA induces a CD positive signal in the region around 265 nm, and a negative band around 300 nm,

corresponding to the M chiral conformation for all the 1,4-benzodiazepines studied so far.

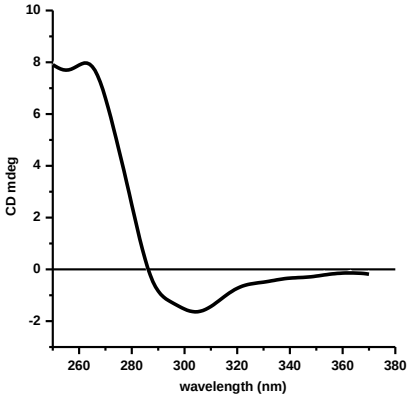


**Figure 21**: CD spectrum of a mixture of HSA ($3 \cdot 10^{-5}$ M) and midazolam ($3 \cdot 10^{-3}$ M) in phosphate buffer at room temperature.

This ICD has been interpreted as originating from an imbalance of the original 1:1 M:P ratio, induced by the HSA binding of the interconverting enantiomers of the benzodiazepine, and favoring the M conformation. The HPLC results collected on the surface immobilized HSA, however, shows an opposite preference for the enantiomers of midazolam, whose second eluted enantiomer (the one

showing greater affinity for the immobilized HSA) has a negative CD sign when monitored at 265 nm (P chiral conformation). The same behavior was earlier reported for a tbutyl N1 substituted benzodiazepine, that showed ICD in the presence of HSA favoring the M conformation and HPLC resolution on immobilized HSA favoring the P conformation [20, 21].

*1.2.2 d D-NMR of estazolam*

The interconversion between the enantiomers of estazolam is very fast at ambient temperature and the energy barrier was determined by DNMR.

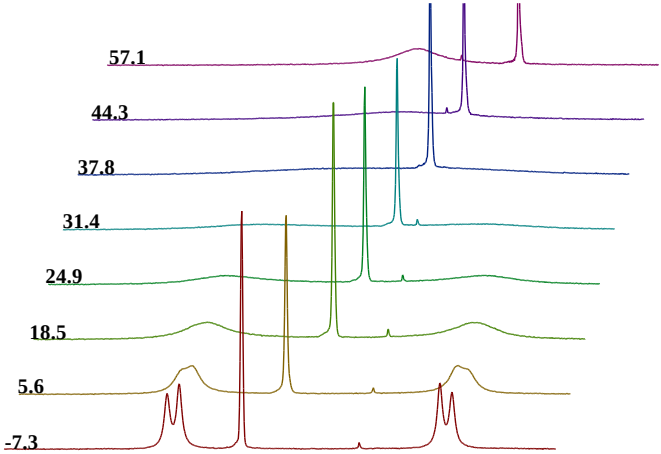


**Figure 22:** DMNR of estazolam in $CD_3OD$.

The energy barrier measured by D-NMR in $CD_3OD$ was 14.54 kcal/mol. Attempted resolution of the interconverting enantiomers of estazolam by cryo-HPLC (down to -70 °C) on the Chiralpak IA column were unsuccessful: a single, broad unsplit peak was observed as a result of fast

interconversion on the time scale of the HPLC separation. The low M/P interconversion barrier in estazolam is easily explained by the absence of the methyl group on the carbon atom of the triazole ring. In the other there benzodiazepines midazolam, alprazolam and triazolam, the methyl group faces the H on the fused benzene ring, and controls the rotational barrier of the molecule (see figure 23 , where a biaryl type substructure has been highlighted).

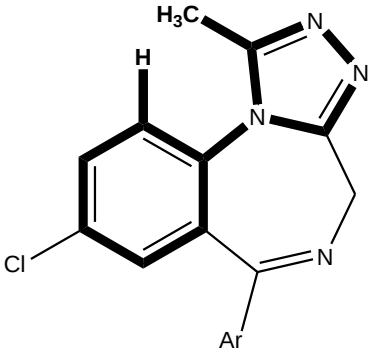


**Figure 23:** general structure of benzodiazepines with pentatomic fused ring on the N1-C2 bond. Bold lines indicate the biaryl-type substructure.

### 1.2.3 Clobazam

Clobazam, like the other benzodiazepines, lacks a chiral center and presents an additional carbonyl group on carbon C4 (Fig. 24). The additional carbonyl group is responsible of the conformational rigidity of the molecule and the stability of the two conformational enantiomers.

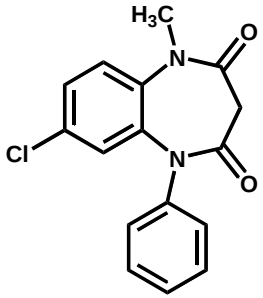


**Figure 24: s**tructure of clobazam.

The separation was performed on two different chiral columns Whelk-O1 and PhGlyDNB (N-3,5-dinitrobenzoyl-phenylglycine see part A2 for the chemical structure), using hexane/$CH_2Cl_2$/MeOH 60/60/1 as mobile phase. As shown in the left chromatogram of Figure 24 the separation at 22

°C is faster than the enantiomerization and two peaks, corresponding to the two enantiomers, are visible.

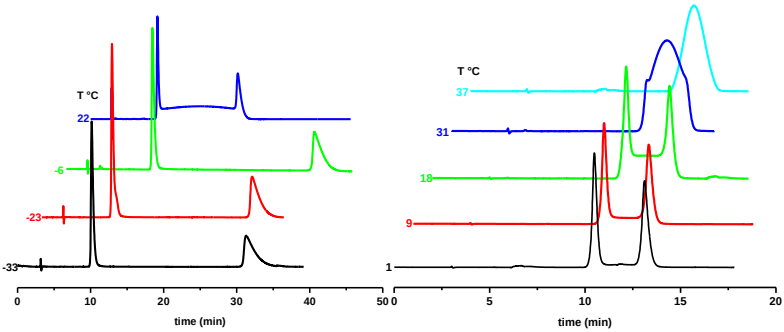


**Figure 25:** column (R,R)- Whelk-O1 (left), PhGly DNB (right), eluent hexane/$CH_2Cl_2$/MeOH 60/60/1, flow rate 1 ml/min, UV detection at 280 nm.

In the right figure the retention times are less than in the case of the Whelk-O1 and at 1 °C the enantiomerization process is completely locked and two peaks perfectly resolved at the baseline can be observed. At 37 °C the on-column interconversion is faster than the separation and it is impossible to separate the two enantiomers. With PhGly-

DNB it was possible to separate the two enantiomers in a range of temperature between 1 and 15 °C. Kinetic parameters for the on-column interconversion phenomena have been extracted from experimental peak profiles by computer simulation (Fig. 26). The corresponding averaged energy barrier is equal to $\Delta G^{\ddagger} = 21.07 \pm 0.2$ kcal/mol .

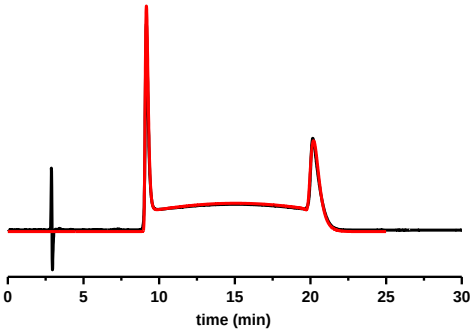


**Figure 26:** experimental (black traces) and simulated (red traces) HPLC of clobazam on (R,R)-Whelk-O1.

## 1.3 Conclusions

Dynamic HPLC on chiral stationary phases of the conformational enantiomers of several 1,4-benzodiazepines is a powerful technique that can be used to study in detail the stereochemistry of this class of interesting molecules. The technique allows for: 1) the physical separation of the individual enantiomers 2) the measurement of the interconversion barrier by computer simulation of exchange-deformed HPLC plots 3) the study of the interaction between the interconverting enantiomers and the immobilized chiral selector on the stationary phase.

The method is complementary to D-NMR in terms of time scale and temperature range available, as well as in terms of tolerance to different solvents (organic or aqueous).

## 1.4 Experimental section

### 1.4.1 Chemicals and materials

All solvents were purchased from Sigma Aldrich (St. Louis, MO, USA).

Benzodiazepines were gently provided by ISS (Istituto Superiore di Sanità) and FIS (Fabbrica Italiana Sintetici) Prior to use, all mobile phases were filtered on Nucleopore 0.4 µm.

### 1.4.2 Dynamic HPLC

*1.4.2 a Chromatographic apparatus*

Analytical chromatography was performed on a HPLC system composed by a Waters (Waters Associates, Milford, MA, USA) 1525 pump, a Rheodyne model 7725 20 µl injector, and a variable wavelength Waters 2487 ultraviolet spectrophotometric detector; and on a HPLC system composed by Jasco (Tokyo, Japan) with an universal Rheodyne 20 µl injector, Jasco PU 980 e Jasco PU 1580

$CO_2$ pumps, a Jasco UV 975 and a Jasco UV/CD 995 detectors.

HPLC runs were performed at flow rates of 1.0 ml/min and monitored by simultaneous UV and CD detections. Column temperature was maintained within -66 °C using a home made cooling device. Samples were dissolved in the eluent.

*1.4.2 b Simulation of dynamic chromatograms*

Simulation of variable temperature experimental chromatograms were performed by Auto DHPLC y2k (Auto Dynamic HPLC), that uses both stochastic and theoretical plates models. Both chromatographic and kinetic parameters can be automatically optimized by simplex algorithm until the best agreement between experimental and simulated dynamic chromatograms is obtained. All the simulations were performed with the stochastic model.

### 1.4.3 Dynamic NMR

Dynamic NMR was performed on a Bruker 400 MHz with $d_6$-DMSO and $d_4$-MeOH as solvents and TMS as internal standard.

### 1.4.5 Mass Spectrometry experiments

The experiments were performed using an ion trap LCQ DECA XP Plus or an Orbitrap Exactive (Thermo Fisher), equipped with an ESI source. Operating conditions for the ESI source were as follows: spray voltage, 5.00 kV; capillary voltage, 27 V; heated capillary temperature, 210 °C; tube lens offset voltage, 20 V; sheath gas ($N_2$) flow rate, 15 units (roughly 0.75 L/min). Methanolic/water solutions were infused via a syringe pump at a flow rate of 5 μL/min.

## 1.4.6 Circular dichroism (CD) measurements

CD spectra were recorded on a Jasco J-715 spectropolarimeter at room temperature, in a rectangular cell with 10 mm pathlength. The spectra were accumulated three times with a bandwidth of 1.0 nm. ICD spectra were

obtained as the difference of spectra of ligand(s)–protein mixture and of protein solution alone and ellipticities were expressed in millidegrees. Ligands were added in small aliquots of $10^{-5}$ M ethanolic solutions to 2 ml protein solutions.

## 1.5 References

[1] Ariens, EJ., Veringa, EJ. *Biochem. Pharmacol* 1988; 37:9-18.

[2] Waldech, B. *Chirality* 1993; 5:350-355.

[3] a) Clayden, J., Moran, WJ., Edwards, PJ., La Plante, SR. *Angew. Chem.* 2009, 121, 6516 – 6520; *Angew. Chem. Int.* Ed. 2009, 48, 6398 – 6401.

[4] M. Oki, *Topics in Stereochemistry* 1983, 14, 1 – 81.

[5] Rauwald, HW., Beli, A. *J. Chromatogr. A* 1993; 639:359-362.

[6] Kirby, DA., Miller, CL., Rivier, JE. *J. Chromatogr. A* 1993; 648:257-265.

[7] LaPlante SR., Edwards PJ., Fader, LD., Jakalian A., and Hucke, O. *Chem Med Chem* 2011, 6, 505 – 513.

[8] Polo C.-H. Lam and Paul R. Carlier *J. Org. Chem*. 2005, 70, 1530-1538.

[9] Vistolia, G., Testa, B., Pedrettia, A. *Helvetica Chimica Acta* 2013– Vol. 96.

[10] Paizs, B. and Simonyi, M. *Chirality* 1999, 11:651–658.

[11] (a) F. Gasparrini, L. Lunazzi, A. Mazzanti, M. Pierini, K. M. Pieyrusiewicz, C. Villani, *J. Am. Chem. Soc. 122 (2000) 4776*; (b) C. Dell'Erba, F. Gasparrini, S. Grilli, L. Lunazzi, A. Mazzanti, M. Novi, M. Pierini, C. Tavani, C. Villani, *J. Org. Chem. 67 (2002) 1663*; (c) A. Dalla Cort, F. Gasparrini, L. Lunazzi, L. Mandolini, A. Mazzanti, C. Pasquini, M. Pierini, R. Rompietti, L. Schiaffino, *J. Org. Chem. 70.*

[12] Cabrera, GC., Goldberg de Waisbaum, R. and Sbarbati Nudelman, N. *J. Phys. Org. Chem. 2005;18:156–161.*

[13] T. Peters Jr., *Biochemistry, Genetics and Medical Applications*, Academic Press, New York, 1996.

[14] He, XM and Carter, DC *Nature*, 1992; 358,209–215.

[15] Petitpas, I., Bhattacharya, AA., Twine, S., East, M. and Curry, S. *J. Biol. Chem.* 2001, 276, 22804–22809.

[16] Fehske, K. J., Schlafer, U., Wollert, U. and Muller, W. E. *Mol. Pharmacol.*1981, 21, 387–393.

[17] Ghuman, J., Zunszain, PA., Petitpas, I., Bhattacharya, AA., Otagiri, M. and Curry, S. *J. Mol. Biol.* 2005; 353, 38–52.

[18] Bertucci, C., Andrisano, V., Gotti, R., Cavrini, V. *J. Chromatogr. B* 2002, 768; 147–155.

[19] Lambert, HM., Janssen, S., Johannes, HM. Droge, Frans, CJ Durlinger, and Fruytier, FJ. *J. Biol. Chem.* 1985, 260,21;11442-11445.

[20] Salvadori, P., Bertucci, C., Ascoli, G., Uccello-Barretta, G. and Rossi, E. *Chirality* 1997, 9:495–505.

[21] Fitos, I., Visy, J., Zsila, F., Mady, J. and Simonyi. M. *Bioorganic & Medicinal Chemistry* 2007, 15, 4857–4862.

## PART A-2

# *The dynamic chromatographic behavior of tri-o-thymotide on HPLC chiral stationary phases*

# Tri-o-thymotide

## 2.1 Introduction

Tri-o-thymotide (TOT) is a 12-membered macrocyclic trilactone that adopts chiral conformations. The TOT molecule exists in solution as a rapidly equilibrating mixture of a time averaged $pC_3$ propeller conformation (major) and a $hC_1$ helical conformation (minor), as revealed by NMR spectroscopy (Fig. 1).

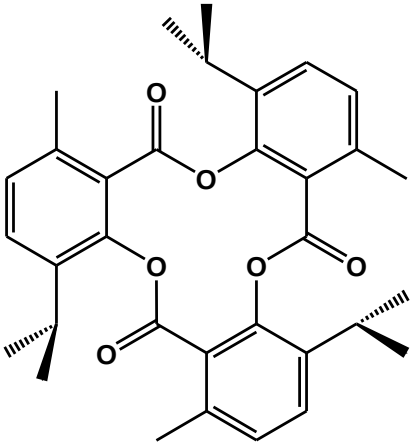


**Figure 1** Structure of Tri-*o*-thymotide

The TOT molecule has been shown by NMR to exist in solution as a mixture of a major, propeller, conformation (approximate molecular symmetry $C_3$-3) and a minor, helical conformation ($C_1$-1), each of which is present in two enantiomeric forms.

However, in its neat crystals and in its complexes it always has the shape of a somewhat flattened three-bladed propeller, with all three carbonyl oxygens on the same side of the mean ring plane.

The major propeller species has all three carbonyl oxygen atoms pointing to the same side of the macrocyclic ring whereas the minor helical has only two carbonyl oxygen atoms pointing in the same direction [1]. The pure crystalline phase of TOT is a racemic mixture of the two enantiomers of the propeller conformation.

The accepted interconversion scheme of TOT stereoisomers features a stepwise sequence from, for example, one enantiomer of the propeller conformation p$C_3$ to one enantiomer of the helical conformation with one blade reversed h$C_1$, then to the enantiomeric helix conformation

with two blades reversed ent-$hC_1$ and finally to the enantiomeric ent-$pC_3$ propeller conformation (eqn (1)).

$$pC3 \rightleftarrows hC1 \rightleftarrows ent\text{-}hC1 \rightleftarrows ent\text{-}pC3 \qquad (1)$$

The propeller to helix switch and its reverse process have energy barriers of 21.4 ± 0.9 kcal/mol and 20.7 ± 0.9 kcal/mol, respectively, as measured by D-NMR, while the barrier for the enantiomeric helix to helix exchange is unknown for TOT. However, the same helix to helix process in two trilactones closely related to TOT was investigated by D-NMR and gave energy barriers of 14.3 ± 0.5 kcal/mol for tris-3,6-dimethylsalicylide and 17.6 ± 0.2 kcal/mol for tri-o-carvacrotide, suggesting a much faster process compared to the propeller to helix exchange [2]. In the solid state, neat TOT as well as TOT complexed with guests are always found in a flattened three-bladed propeller conformation with approximate C3 symmetry [1c].

Upon cocrystallization with compounds with which it forms clathrate inclusion complexes, TOT often undergoes

spontaneous resolution. Any single crystal contains only *P* or only *M* TOT host molecule. The most common form of TOT clathrate crystallizes as discrete C2 symmetric cavities in the chiral space implying that the (-)-(M) and (+)-(P) forms separate spontaneously as crystallization occurs.

Interest in the TOT molecule and in its complexation behavior is due to the ability of TOT to give spontaneous resolution when forming clathrate inclusion crystals with a large variety of guests. Besides intrinsic scientific interest in TOT clathrate formation and properties, several studies have addressed specific applications of TOT in separation science, solid state asymmetric reactions, determination of absolute configuration of chiral guests, non-linear optical properties and sensor devices [3].

While solution and especially solid state chemistry of TOT is rich and varied, its HPLC chromatographic behavior on chiral stationary phases is completely unexplored. The fast room temperature exchange of TOT molecules between our populated species (the two enantiomers of the propeller and of the helix conformations) and the complex

chromatographic pattern expected under sub-ambient temperature condition shave certainly hampered progress in this field.

Here are presented the results on the dynamic chromatographic behavior of TOT at sub-ambient temperatures on different chiral stationary phases (CSP1-3, see further for their chemical structures) together with a computational investigation of TOT molecular conformation and chiroptical properties that were used to assign the absolute configuration to the isolated enantiomers of $pC_3$-TOT.

## 2.2 Results and discussion

Attempts to resolve the complex mixture of TOT stereoisomers by HPLC on CSPs at room temperature were unsuccessful. However, variable temperature HPLC runs on CSP1 showed temperature dependent chromatographic profiles that are indicative of on-column interconversion processes occurring on the same time scale of the separation process (Fig. 2, right panel) [4].

The UV trace shows a single, coalesced peak at 26 °C that broadens at 21 °C and eventually splits partially into two unequally intense peaks at 15 °C. As the column temperature is gradually lowered, the separation between the two peaks increases while the first eluted peak shows a decoalescence process that culminates at -12 °C with the appearance of a third peak. At this temperature, the integrated peak areas are 10 : 45 : 45 from low to high retention times.

Simultaneous CD monitoring (Fig. 2, left panel) of the dynamic behavior of TOT on CSP1 shows the absence of

signals at 26 °C and only two, equally intense, bisignated peaks at lower temperatures corresponding to the major peaks observed by UV detection.

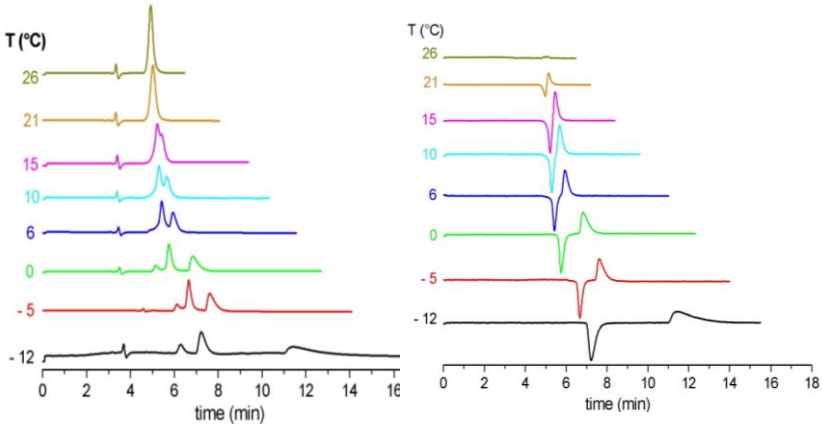


**Figure 2:** dynamic HPLC of TOT on (R,R)-CSP1, eluent hexane/$CH_2Cl_2$/2-propanol 40/40/10, flow rate 1 ml/min; UV (left panel) and CD (right panel) detections wavelength.

The UV dynamic pattern clearly shows that the three species are mutually interconverted during HPLC at higher temperatures, and this was easily confirmed by cycles of

low temperature HPLC peak collection, room temperature equilibration followed by low temperature HPLC analysis of the equilibrated fractions: each of the isolated peaks gave, after thermal equilibration, the same original three peaks mixture. These preliminary results are fully consistent with the known solution interconversion scheme of TOT stereoisomers. Thus, the two major peaks observed at lower temperatures can be assigned to the two enantiomers of the propeller conformation, $pC_3$ and ent-$pC_3$, while the third minor peak can be assigned to the unresolved, rapidly interconverting enantiomers of the helical conformation $hC_1$ and ent-$hC_1$. Attempted separations of these latter species by cryo-HPLC down to -78 °C (Fig. 3) on CSP1 were unsuccessful as a result of unfavorable changes of selectivity with temperature, leading to peak overlapping at low T.

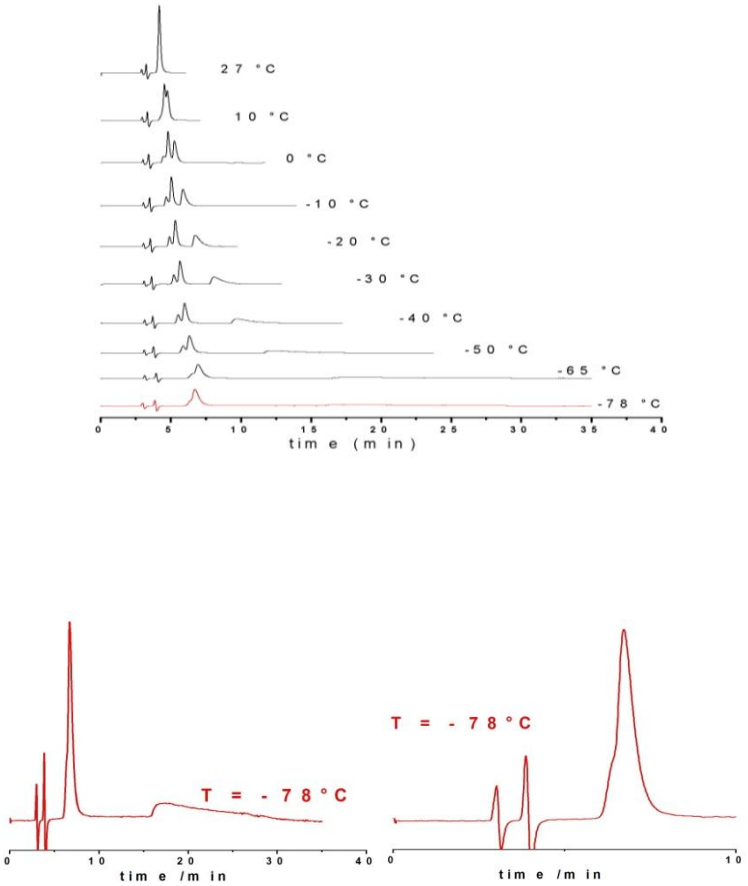


**Figure 3:** variable temperature, column CSP1, eluent hexane/$CH_2Cl_2$/2-propanol 40/50/10, flow rate 1 ml/min; UV detection at 245 nm. Insets show the peaks overlapping of C1 and 1$^{st}$ eluted C3 TOT.

CSP2 has no selectivity for the major, propeller $pC_3$-TOT species and a low selectivity for the minor, helical $hC_1$-TOT species that are marginally resolved. However, partial splitting of the minor peak was observed at -90 °C on CSP2, thus confirming the assignment and suggesting a much lower barrier to interconversion between the enantiomers of the TOT helical conformation (Fig. 4).

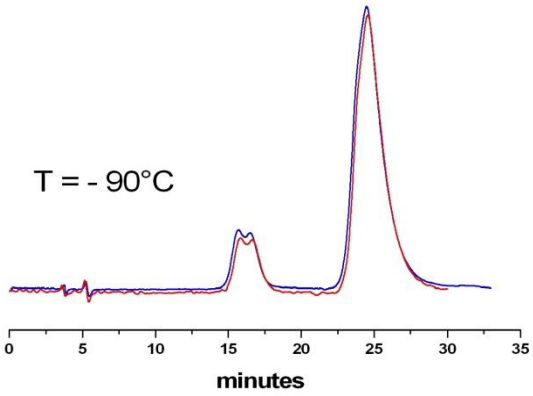


**Figure 4:** two replicate overlaid HPLC runs at -90 °C, column CSP2, eluent hexane/$CH_2Cl_2$/2-propanol 40/50/10; flow rate 1 ml/min; UV detection at 245 nm.

Low temperature micropreparative HPLC runs on CSP1 were also exploited to collect the individual enantiomers of the propeller conformation of TOT.

HPLC separation carried out with the column cooled at -10 °C allowed us to process milligrams of TOT by iterative chromatography. Collected fractions of the pure individual enantiomers, $pC_3$ and ent-$pC_3$, were stored at low temperatures and used to acquire CD spectra of the enantiomers as well as to monitor the CD signal decay as a function of time (Fig. 5).

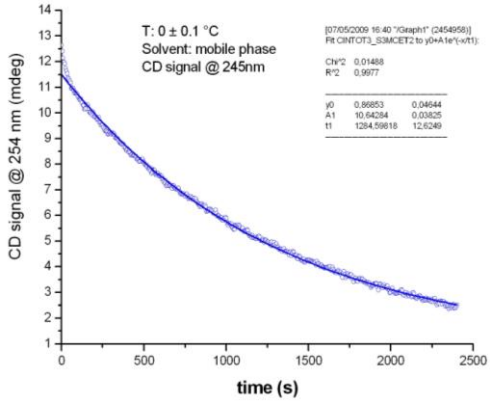


**Figure 5: d**ecay of CD signal for the 2nd eluted enantiomer as a function of time at T 0 °C.

The CD spectrum of the first eluted enantiomer from (R,R)-CSP1 shows a positive band centered at 245 nm, which is mirrored in the CD spectrum of the second eluted enantiomer. With the isolated enantiomers of the propeller form in hand, their thermal racemization [5] was monitored by CD at 245 nm in a thermostatted cuvette. Conversion of one propeller enantiomer $pC_3$ to the equilibrium mixture follows a first-order kinetic at T= 0 ± 0.1 °C in the HPLC eluent. From the linear logarithmic plot of CD signal vs. time, a first-order rate constant of 0.0385 $min^{-1}$ was calculated, corresponding to a free energy barrier $\Delta G^{\ddagger}$ = 19.93 ± 0.02 kcal/mol. This result is in good agreement with the values found by polarimetry at T = 23 °C in $CHCl_3$ ($\Delta G^{\ddagger}$= 20.3 ± 0.2 kcal/mol) and in benzene ($\Delta G^{\ddagger}$ = 20.2 ± 0.2 kcal/mol)[6]. We additionally used an independent HPLC approach to extract kinetic data for the propeller–helix interconversion process. When equilibrated solutions of TOT are analyzed by HPLC on the racemic version of CSP3 (Fig. 6), only two unequally intense peaks corresponding to the helical (10.1%, minor, $hC_1$ and ent-$hC_1$ coeluted) and to

the propeller (89.9%, major, $pC_3$ and ent-$pC_3$ coeluted) species are observed under conditions of slow on-column interconversion.

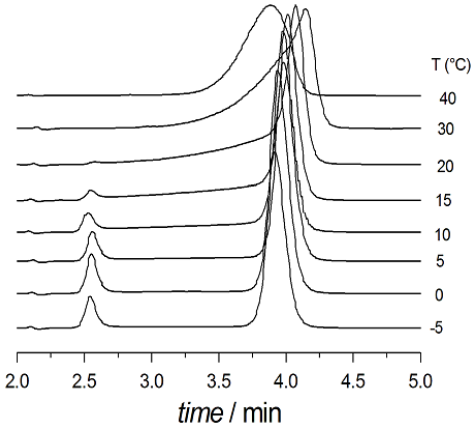


**Figure 6:** variable temperature HPLC of TOT on racemic CSP3.

As the column temperature is raised, accelerated on-column interconversion generates a plateau between the two resolved peaks that eventually coalesce at higher temperatures into a single broad peak. Computer simulation

[4f] of the dynamic HPLC profile recorded with the column temperature set at 15 °C (Fig. 7) yields the apparent rate constants $k_{1,2}$= 0.75 $min^{-1}$ for the on-column helix to propeller conversion and $k_{2,1}$= 0.08 $min^{-1}$ for the reverse process. The associated energy barriers $\Delta G^{\ddagger}_{1,2}$= 19.4 ± 0.1 kcal/mol and $\Delta G^{\ddagger}_{2,1}$= 20.6 ± 0.1 kcal/mol are consistent with the corresponding literature data and with the energy barrier measured here in the same solvent by off-column thermal equilibration of a single $pC_3$ enantiomer. It has to be noted that the computer simulation of the on-column exchange process yields only the apparent kinetic constants, and these are to some extent potentially perturbed by the presence of the stationary phase. Nonetheless, the simulation correctly reproduces the expected difference in the energy barriers for the $hC_1$ to $pC_3$ conversion.

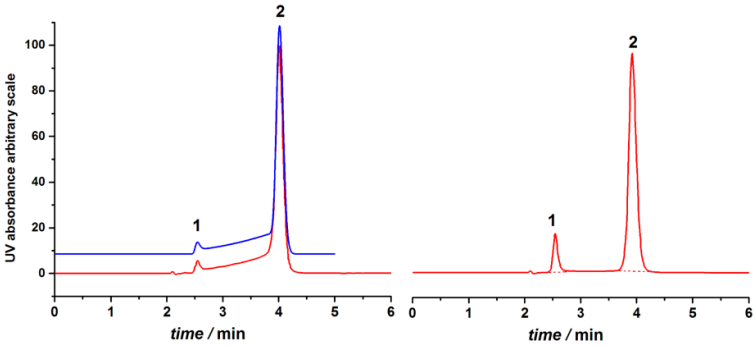


**Figure 7:** experimental (red) and computer (blue) simulated dynamic HPLC on racemic CSP3 thermostatted at T 15 °C (left panel) and at T -5 °C (right panel); eluent hexane/$CH_2Cl_2$/2-propanol 40/40/10, flow rate 1 ml/min, UV 250 nm. **1**: helical $C_1$-TOTconformer; **2**: propeller $C_3$-TOT conformer.

To assign the absolute configuration to the chromatographically isolated enantiomers of p$C_3$-TOT we used density functional theory (DFT) calculations of their Circular Dichroism (CD) spectra and compared them to those measured experimentally. The TOT molecule is conformationally flexible: the nonplanar 12-membered trilactone ring can adopt several conformations and the mutual orientation of the three phenyl rings varies easily as well. Since the measurements of the CD spectra have been carried out at 0 °C, a calculation of the structures and

percentage distribution of the populated conformations of $C_3$-TOT at that temperature is a prerequisite to the CD calculation. Structure of a TOT molecule was modelled in three steps: (1) exhaustive conformational search performed through stochastic Monte Carlo algorithm (for details see the Experimental Section), basing the structure optimization on MM2* molecular mechanics calculations in vacuum; (2) ranking of the obtained conformations according to their Boltzmann Populations (BP), and grouping into two ensembles on the basis of the orientation of the three carbonyl oxygen atoms with respect to the middle plane of the twelve membered macrocycle, limiting the choice to those structures found within an energy window of 5 kcal/ mol from the global minimum, (3) further optimization of the most stable conformation found in each of the two ensembles through DFT calculations (BLYP method with the QZ4P large core basis set), including dichloromethane solvent in the simulation. Step 2 gave a first ensemble consisting of propeller like conformations of $C_3$ symmetry with the three carbonyl oxygen atoms pointing in the same

direction (97.2% BP at 0 °C) and a second ensemble including helical like conformations of $C_1$ symmetry with only two carbonyl oxygen atoms paired (2.8% BP at 0 °C). Reoptimization with DFT in step 3 led to two unique structures (Fig. 8) with $C_3$ (499.9% BP at 0 °C) and $C_1$ symmetry (< 0.1% BP at 0 °C). At the same level of DFT theory, the C3 symmetry structure with M helicity has been submitted to simulation of the CD spectrum. Comparison of the DFT CD spectrum calculated for M-pC3-TOT to the CD traces registered for the enantiomers of p$C_3$-TOT isolated by HPLC on CSP1shows that the first eluted enantiomer with a negative CD band at 245 nm has the M propeller configuration (Fig. 9) [7].

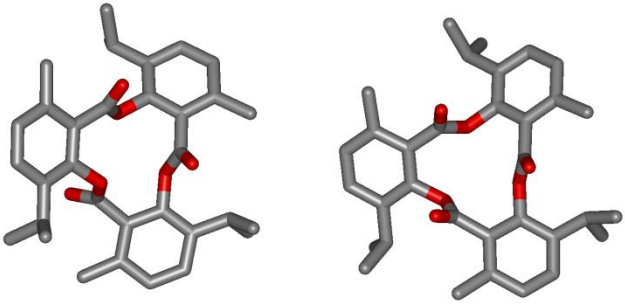

**Figure 8:** low energy structures of $hC_1$ (left) and $pC_3$ (right) TOT found by DFT optimization. Both are shown in the M configuration.

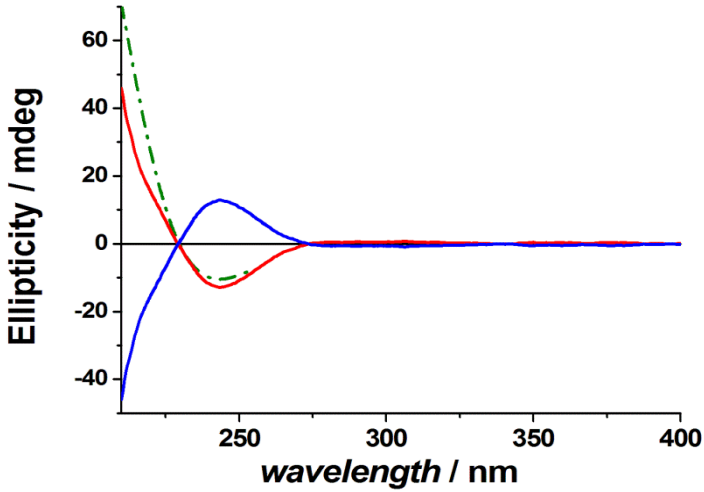


**Figure 9:** experimental (red line, first eluted and blue line, second eluted) and DFT calculated (green line, M configuration) CD spectra of the enantiomers of propeller $C_3$-TOT. Experimental spectra are recorded in the HPLC eluent at T 0 °C.

## 2.3 Conclusions

The dynamic HPLC behavior of TOT has been investigated in detail and the temperature regions where the TOT internal motions manifest themselves with exchange-deformed peaks have been identified. The absolute configuration of the $C_3$ propeller enantiomers was assigned by comparison of DFT calculated and experimental CD spectra.

## 2.4 Experimental sections

### 2.4.1 Low-Temperature Dynamic HPLC.

Columns packed with CSPs 1-3 (Fig. 10) are available from Regis Technologies, Morton Groove, IL.

Cryogenic HPLC was performed placing the column in a dry-ice/acetone or dry-ice/diethyl ether cooling bath, with a 1 m long inlet capillary wrapped around the column to ensure thermal equilibration of the mobile phase. Temperatures were maintained within ± 0.5 °C for at least two consecutive, replicate analysis.

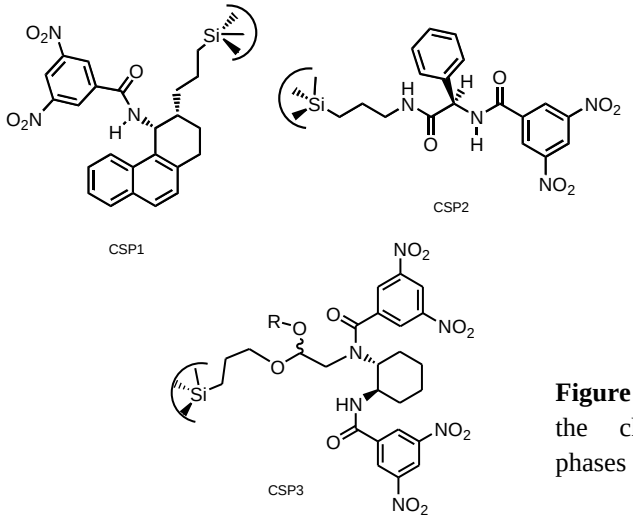


**Figure 10:** Structures of the chiral stationary phases CSP1-3.

### 2.4.2 Molecular Modeling Calculations.

Conformational search of TOT was carried out by the Batchmin computer program, version 4.5 (Columbia University, NY), using the following options: MM2* Force Field, Monte Carlo stochastic algorithm with 5000 generated structures, 100 most stable structures retained among all those obtained from the search, minimization by PR conjugate gradient. All the rotatable bonds resulting after temporary opening of the molecular cycle (eight torsional angles) were explored. The obtained geometries were analyzed by the home made computer program C.A.T. to exclude twin molecules and to make clusters based on energetic and geometric criteria. From this preliminary procedure fifteen geometries of TOT were obtained within an energetic window of 5 kcal/mol from the global minimum. Seven among these conformers display very similar geometries of C3 symmetry, with all the carbonyls of the three ester groups placed at the same side of the macrocycle. The other eight conformers, also very similar one to each other, are asymmetric and display only two of

the three carbonyl groups at the same side of the macrocycle. The most stable conformers of each of these two ensembles have then been further optimized by DFT calculations based on the BLYP method with the QZ4P large core basis set, as implemented in the Amsterdam Density Functional (ADF) package v. 2007.01. Solvation energies in dichloromethane were also computed with the same program by the Conductor like Screening Model (COSMO), with the cavity defined according to the Solvent Excluding Surface (SES) algorithm. Finally, the CD spectrum of the M enantiomer of the C3 symmetry structure was calculated with the same method. The options were set at: single point calculation; 40 singlet and triplet excitations; diagonalization method: Davidson.

## 2.5 References

[1](a) R.Gerdil, in Comprehensive Supramolecular Chemistry, *Solid-State Supramolecular Chemistry Crystal Engineering*, ed. D. D. MacNicol, F. Toda and R. Bishop, *Elsevier Science Ltd*, Oxford, 1996, vol. 6, pp. 239–280; (b)Crystalline Molecular Complexes and Compounds, ed. F. H. Herbstein, Oxford Science Publications, Oxford, 2005, vol. 1, pp. 423–436; (c) J. W. Steed and J. L. Atwood, *Supramolecular Chemistry*, Wiley, NY, 2009, pp. 410–413.

[2] W. D. Ollis, J. S. Stephanatou and J. F. Stoddard, *J. Chem. Soc.*, Perkin Trans. 1, 1982, 1629–1636.

[3](a) G. Faceyand J. A. Ripmeester, J. Chem. Soc., Chem. Commun., 1990, 1585-1587; (b) J. M. Gnaim, V. Schurig, H. Grosenickand B. S. Green, *Tetrahedron: Asymmetry*, 1995, 6, 1499–1502; (c) G. A. Facey, C. I. Ratcliffeand J. A. Ripmeester, *J. Phys. Chem.*, 1995,99, 12249–12256; (d) R. Gerdil, H. Liu and G. Bernardinelli, Helv. Chim. Acta, 1999,82, 418–434; (e) V. K. Gupta, A. K. Jain, P. Kumar, S.

Agarwal and G. Maheshwari, *Sens. Actuators*, B, 2006,113, 182–186.

[4](a) C. Wolf, Chem. Soc. Rev., 2005, 34, 595–608; (b) V. Schurig, *Chirality*, 2005, 17, S205–S226; (c) I. D'Acquarica, F. Gasparrini, M. Pierini, C. Villani and G. Zappia, *J. Sep. Sci*., 2006, 29, 1508–1516; (d) O. Trapp, *J. Chromatogr., B: Anal. Technol. Biomed. Life Sci.*, 2008, 875, 42–47; (e) C. Villani, F. Gasparrini, M. Pierini, S. Levi Mortera, I. D'Acquarica, A. Ciogli and G. Zappia, *Chirality*, 2009, 21, 97–103;

[6] W. A. Bonner, *Origins Life Evol. Biospheres*, 1999, 29, 317–328.

[7] R. Arad-Yellin, B. S. Green, M. Knossow and G. Tsoucaris, *Tetrahedron Lett.*, 1980, 21, 387–390.

# PART B

# *Enantioselective molecular recognition by mass spectrometry*

# Enantioselective molecular recognition by mass spectrometry

## 1.1 Introduction

Molecular recognition is an important step in any chemical and biological processes, enzyme catalysis, cellular signaling, protein-protein association, protein crowding, reactant transport, to name a few. The non-covalent binding between a receptor and a ligand molecule involve the recognition between two or more molecular binding partners, leading either to their association or to their rejection. In chemistry, non-covalent interactions influence virtually every chemical reaction and the design of building blocks held together by non-covalent bonds refers to a particular field known as supramolecular chemistry [1, 3]. The examination and understanding of the non-covalent bond, is useful to understand the action of biomolecules, to implement function into molecular devices such as sensors, to control mechanical movement, to passively and actively

transport molecules, and to use supramolecules as catalysts. The term molecular recognition refers to the specific interaction between a molecule (host) and another one (guest) through non-covalent bonding producing a new entity, defined complex or supramolecule, with properties different from those of each single component.

The idea of coordination chemistry was formulated by Alfred Werner in 1893 [4], the lock-and-key concept was introduced by Emil Fischer in 1894 [5], and Villiers and Hebd discovered cyclodextrins, the first host molecules in 1891 [6]. A few years later, Paul Ehrlich devised the concept of receptors in his studies on Immunity in 1906 [7] by stating that any molecule can have an effect on the human body only if it is bound (‘‘Corpora non agunt nisi fixata’’). Daniel Koshland formulated the induced fit concept (1958) for binding events to biomolecules which undergo conformational changes in the binding event.

Generally the host appears as the largest component, such as an enzyme or synthetic cyclic compounds with a central hole or cavity, while the guest correspond to a small organic

or inorganic ion, or ion pair, or a little molecule with biological activity such as hormone or neurotransmitter. The host is defined as the molecular entity possessing convergent binding sites (e.g. Lewis basic donor atoms, hydrogen bond donors etc.), while the guest is the entity possessing divergent binding sites (e.g. Lewis acidic metal cation or hydrogen bond acceptor halide anion). In turn a binding site is defined as a region of the host or guest capable of taking part in a non-covalent interaction [8]. The majority of work on this subject to date has focused on interactions in solution, where the results are strongly influenced by the presence of a solvent. However, more recently the study of supramolecular chemistry has taken to the electrospray ionization mass spectrometry, because is a "soft" technique for the transfer of solution species into the gas phase. This is because the interactions are studied in the absence (or using small controlled amounts) of solvent and because of the intrinsic sensitivity, molecular specificity, and tolerance to impurities of the technique. Mass spectrometry, especially tandem mass

spectrometry, provides a unique method by which intrinsic interactions between molecules can be studied; information on the relative stabilities of non-covalent complexes is obtained from their gas-phase dissociation behavior. To achieve chiral recognition, multiple-point interactions (the "three-point rule") are required; this means that the chiral analyte and chiral reference need to be bound together in a polydentate complex, even if only transiently.

Chiral recognition by MS is usually based on the measurement of following: (i) the relative abundance of non-covalent diastereomeric adducts between a chiral host and the two enantiomers of a guest; (ii) the relative stability of diastereomeric adducts by equilibrium measurements or by collision-induced dissociation (CID) experiments (Cooks' kinetic method) and (iii) the rates ion/molecule reactions between diastereomeric adducts and suitable chiral or achiral reactants [9, 10].

*Cooks' kinetic method*: the experiments were carried out by generating in the ESI source of an ion trap MS the proton-

bound three-body complexes $[M_2 \cdot H \cdot A]^+$, containing two molecules of the macrocycle M and one enantiomer of A, either $A^R$ or $A^S$. The homochiral $[M^R{}_2 \cdot H \cdot A^R]^+$ and the heterochiral $[M^R{}_2 \cdot H \cdot A^S]^+$ three-body complexes were individually subjected to collision-induced dissociation (CID) using He ($10^{-5}$ Torr) as the target gas. The different CID fragmentation patterns reflect the relative stability of the diastereomeric adducts. The chiral resolution factor $R_{chiral}$ corresponds to the $R_{homo}/R_{hetero}$ ratio ($R_{homo=}$ $[M^R \cdot H \cdot A^R]^+/[M^R{}_2 \cdot H]^+$ ; $R_{hetero=}$ $[M^R \cdot H \cdot A^S]+/[M^R{}_2 \cdot H]^+$) [11, 13].

*50% Treshold method:* the dimeric complexes $[M \cdot H \cdot A]^+$, either homochiral and heterochiral, generating in the ESI source were isolated inside the ion trap and dissociated at a by collision with neutrals at variable energy. The enantioselectivity is expressed as the difference in the collision energy required to dissociate 50% of the parent diastereomeric $[M \cdot H \cdot A]^+$ complex (two experiments with enantiomeric guests) [14].

Organic chemistry makes possible the construction of variable macrocyclic compounds. The most widely known macrocycles are crown ethers, cryptands, starands, cyclodextrins and calixarenes. In this work another group of synthetic receptors, macrocyclic amides, have been synthesized and their enantioselectivity have been investigated through mass spectrometry.

## 1.2 Results and Discussion

### 1.2.1 Synthesis of macrocycles

*1.2.1 a Synthesis of $A_2B_2$ hosts*

Chiral receptors were prepared by a common macrocyclization reaction of complementary A and B fragments to yield $A_2B_2$ macrocycles, where A are activated forms of isophthalic acid derivatives and B are chiral, C2 symmetric (S,S)-1,2-diamines, derived from (R,R)-1,2-bis-(2-hydroxyphenyl)-1,2-diaminoethane.

The subunits A have been synthesized by transformation of the 5-hydroxy-isophthalic acid into the chloride of 5-methoxy-isophthalic acid. We first carried out the protection of the carboxylic group by transformation in methyl ester through acetyl chloride in methanol heated at 50 °C. The reaction was monitored by TLC. The next step was the methylation of hydroxyl group. The suspension of compound **1** and potassium carbonate was stirred and heated at 80 °C for 1h under inert atmosphere and then dimethyl sulfate was added. The corresponding suspension was stirred and heated at 70 °C for 3h. After hydrolysis of the

ester groups, using KOH 5N in dioxane, we obtained as white solid 5-methoxy-isophthalic acid. The corresponding acid was quantitatively converted into the chloride derivative by reaction with thionyl chloride (Scheme 1).

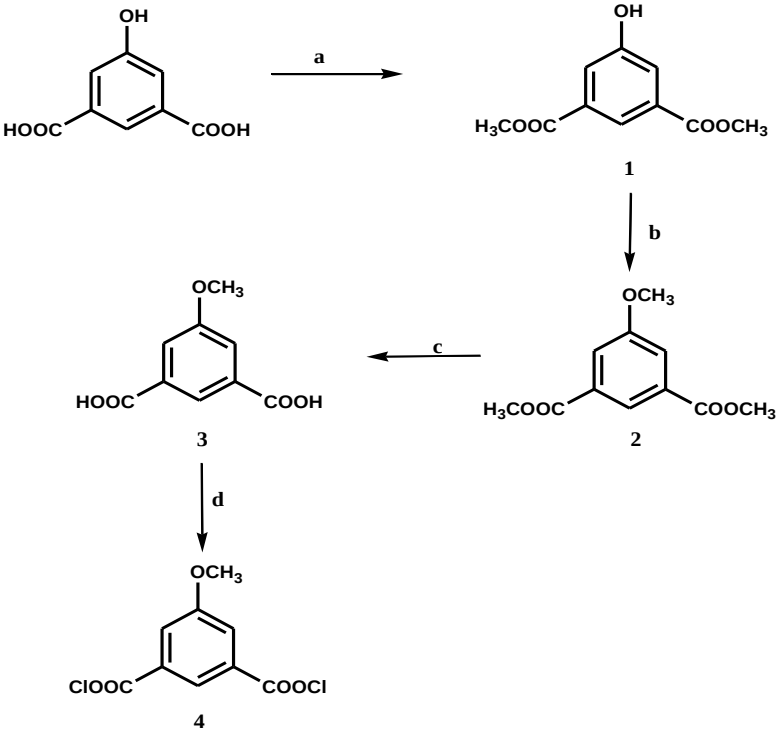


**Scheme 1**: (**a**) $CH_3OH$, $HCl_g$, T 50 °C, 4h; (**b**) $SO_4(CH_3)_2$, $K_2CO_3$, DMF; (**c**) KOH 5N, dioxane; (**d**) $SOCl_2$

All subunits B were prepared by a 3,3-aza-Cope-rearrangement described on JACS 2006, 130, 12184 [15]. Diaza-Cope rearrangement reaction can be used to synthesize meso-vicinal diamines by a unified approach for making enantiopure "daughter" diamines from a single "mother" diamine (Scheme 2).

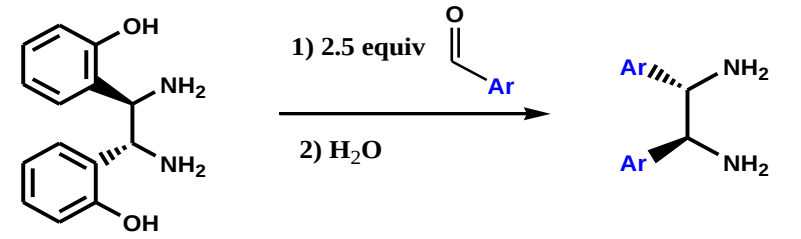


**(R,R)-hpen** **(S,S)-3a to (S,S)-3e**

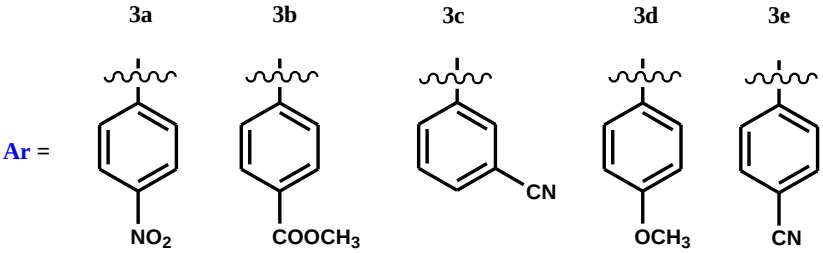


**Scheme 2:** synthesis of subunits B.

In a typical reaction, 2.5 equiv of an aldehyde is added to a solution of **1** dissolved in EtOH. The mother diamine 1 reacts with the aldehydes to form the initial diimines (Scheme 3). In general the initial diimines are not isolated since they rearrange very quickly to the product diimines at ambient temperature (Scheme 3a).

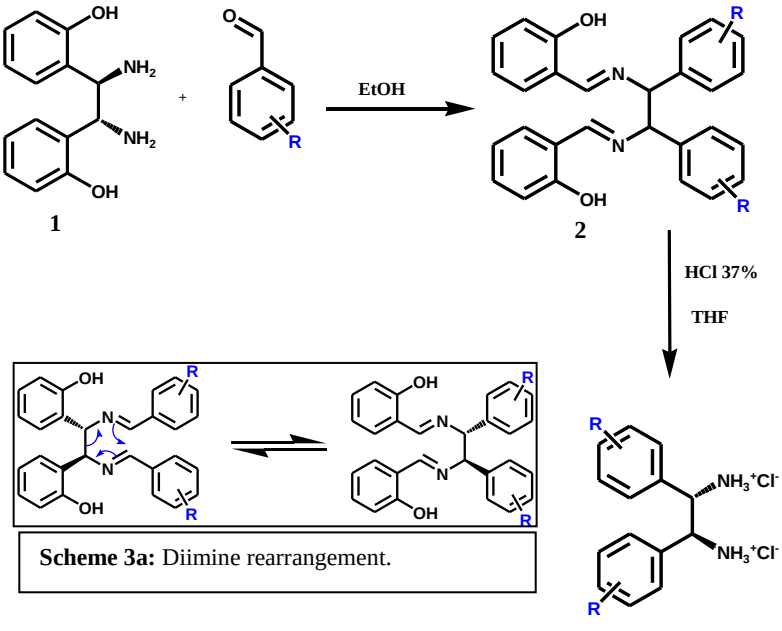


**Scheme 3a:** Diimine rearrangement.

**Scheme 3:** Diaza-Cope rearrangement.

Once the rearrangement is complete, extraction was used to isolate the product diimine. The extract was dried and hydrolyzed (3% conc HCl in THF) without further purification to the diamine dihydrochloride salt as a white powder in good yields (90-99%). The diamine dihydrochloride salt can be converted to the neutral form by extraction under basic conditions.

The macrocyclization reaction was carried out under very diluted condition of reaction (8 mM) between equimolar quantity of the two subunits (Scheme 4). The reaction was conducted in THF, in which both the subunits are soluble and in the presence of the Huning's base using as scavenger for HCl. After the mixture was stirred for 12 h at room temperature, the solvent was removed at reduced pressure, the residue was dissolved in $CH_2CI_2$, and the organic solution was washed with 0.1 N HCl and brine, dried over $Na_2SO_4$, and after solvent removal, purified by column chromatography on silica gel.

The diluted conditions are very important to obtain the cyclization and the ring closure and avoid the formation of

long linear chain, more polar, like $–[X\text{-}Y]_n–$. The more polar oligomeric linear byproducts were easily removed by chromatography on silica gel. The dihedral angle $N_1\text{-}C_1\text{-}C_2\text{-}N_2$ of the mother diamine and the orientation of the carboxy groups in the position 1-3 of subunits A are important structural parameter to obtain cyclic neutral products.

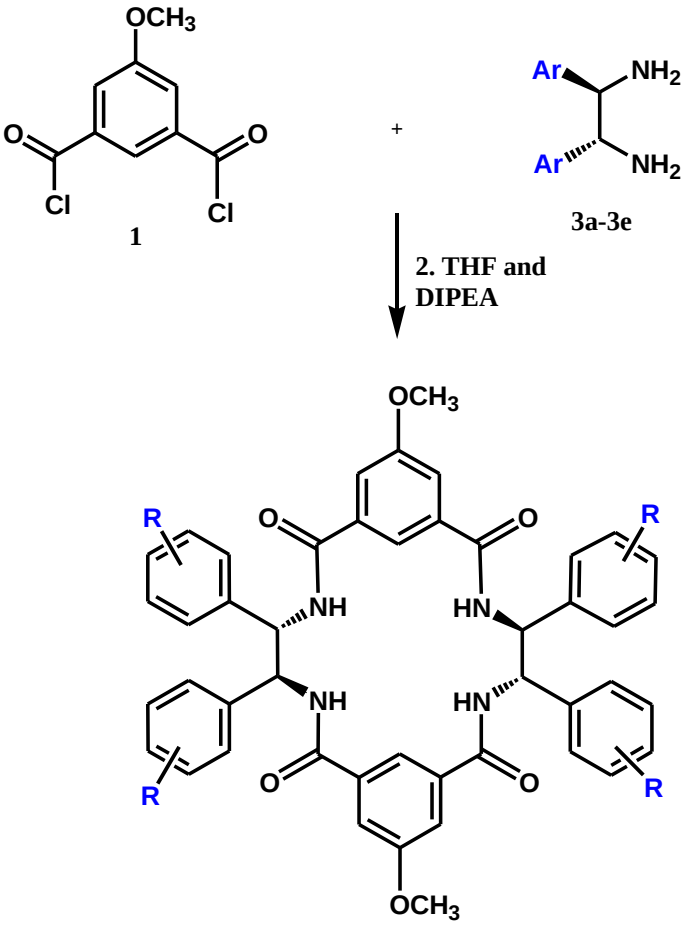


**Scheme 4:** macrocyclization reaction.

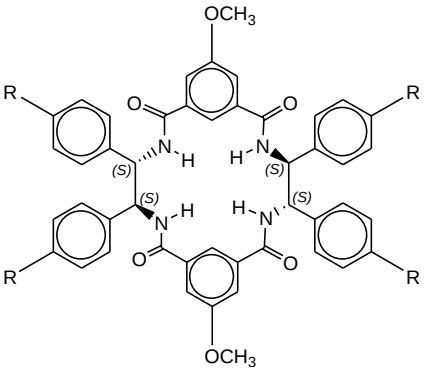


1] $A_2B_2$ 4a ; R = p-$NO_2$

2] $A_2B_2$ 4b ; R = p-$CO_2CH_3$

3] $A_2B_2$ 4c ; R = m-CN

4] $A_2B_2$ 4d ; R = p-$OCH_3$

5] $A_2B_2$ 4e ; R = p-CN

*1.2.1 b Synthesis of $A_2B_2T_2A'_2B_2$*

The $A_2B_2T_2A'_2B_2$ receptor was prepared via a click chemistry process, promoted by CuI, involving the dialkyne and diazide hosts derivatives to obtain the formation of cyclic compounds through molecular connections formed by an inter-intramolecular tandem process leading to discrete molecular receptors with only minor formation of the corresponding dimerization compounds. The azide-alkyne cycloaddition of bifunctional alkyne and azide monomers has proved to be a useful methodology for the formation of defined structures with 1,2,3-triazoles connecting units (Scheme 5). The reaction was carried out in toluene in presence of ([$(EtO)_3P$ CuI]) as catalyst and refluxed for 1h. After removing the solvent, the residue was purified by column chromatography to give a white solid.

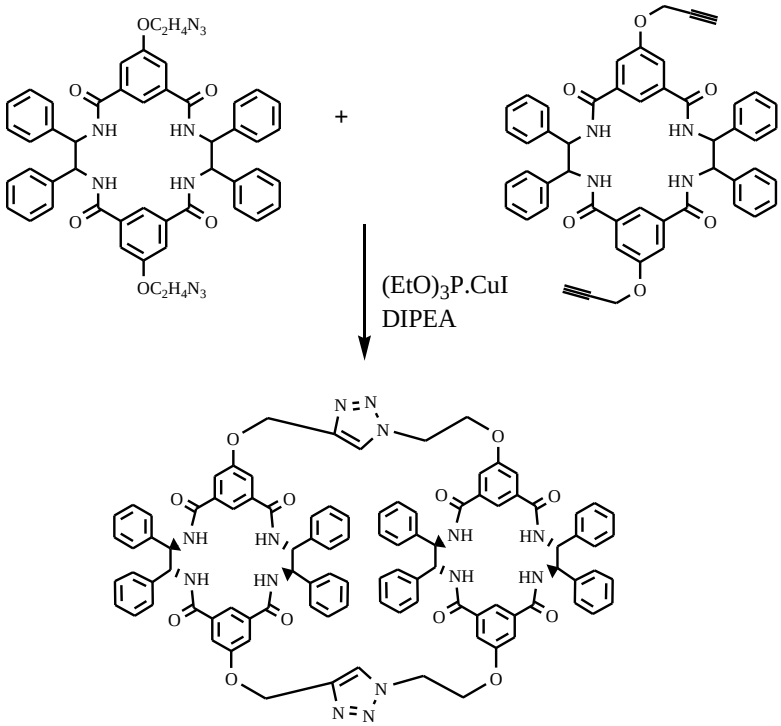


**Scheme 5:** click chemistry process.

### 1.2.2 Spectroscopic characterization

$^1$H-NMR spectra of receptors $A_2B_2$ type ($A_2B_2$ 4a to 4e) show a reduced number of signal due to their C2 symmetry. As shown in Figure 1 there is one signal at 5.57 ppm for all protons of the stereogenic carbons and one signal for the protons of amides at different chemical shift for the different receptors. The equivalence is due to a rapid process of flipping of the structure.

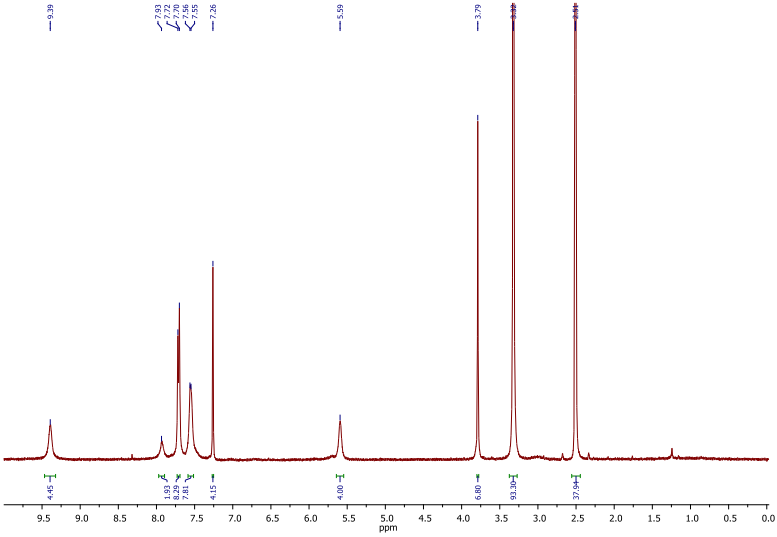


**Figure 1:** $^1$H-NMR spectrum of $A_2B_2$ 4a

The number of signals is also reduced in the $^{13}$C-NMR spectra due to the C2 symmetry. In Fig. 2 there is only one signal at 167 ppm for carbonyl groups and at 60 ppm one signal for stereogenic carbons.

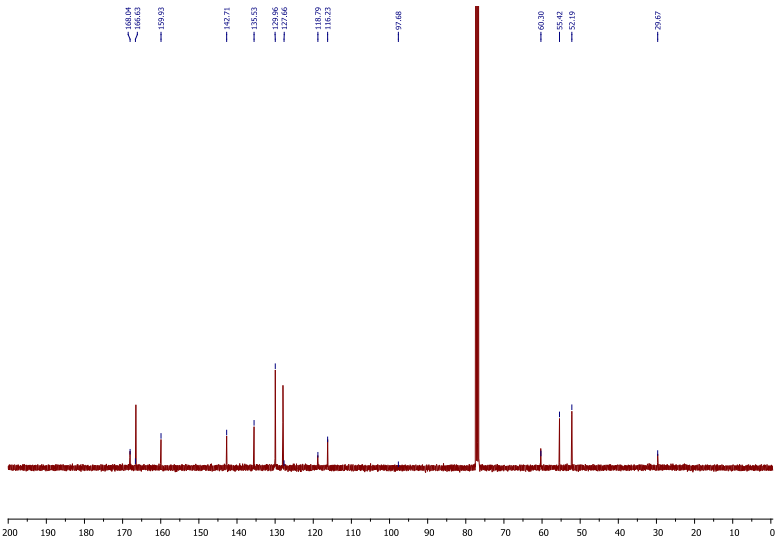


**Figure 2:** $^{13}$C-NMR spectrum of $A_2B_2$ 4a

In the case of $A_2B_2T_2A'_2B_2$, $^1$H-NMR spectrum shows four signals for the CO-NH- groups, two signals for each fragment $A_2B_2$, at 8.8, 8.75 and 8.68, 8.61 ppm (J=9.6 Hz;

7.2 Hz; 8 Hz; 8.8 Hz) because the structure is much more rigid for the presence of the triazole bridges, and the in-out flipping process is not observed. At 8.1 ppm the singlet signal corresponds to the protons in 2 of the isophthalic ring; the singlet signal at 7.78 ppm is the proton of the triazole ring. The presence of this only signal points out the possibility of only one regiochemistry of addition (Fig. 3).

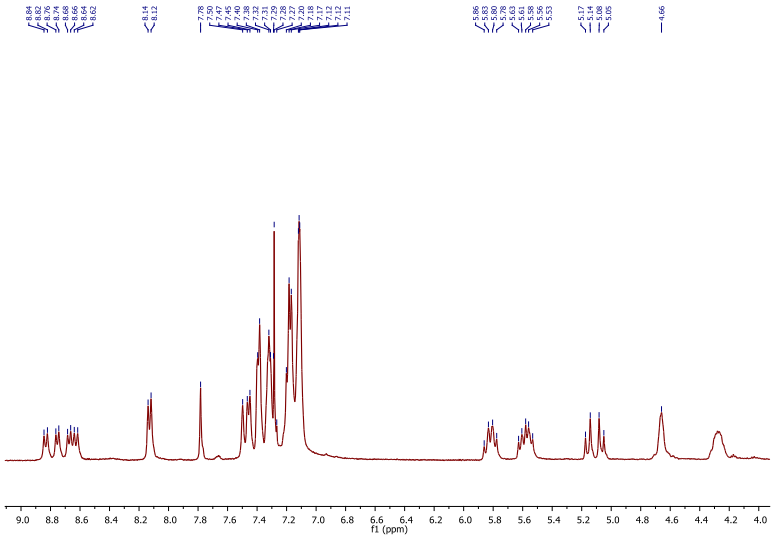


**Figure 3:** $^{1}$H-NMR spectrum of $A_2B_2T_2A'_2B_2$

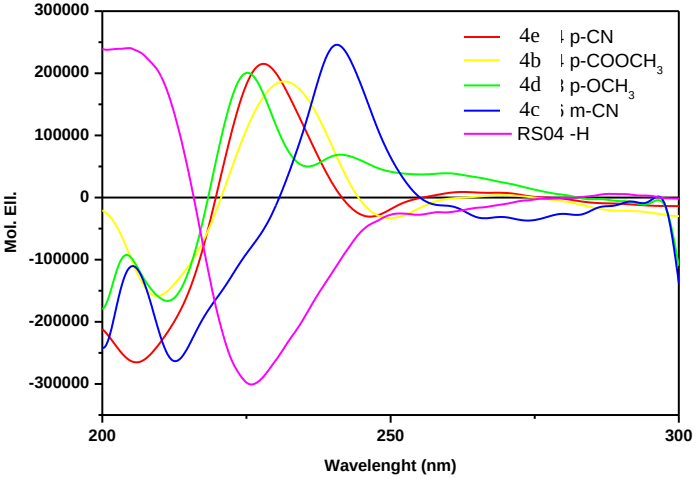


**Figure 4:** circular dichroism spectra of the $A_2B_2$ receptors with B units having (S,S) configuration ($A_2B_2$ 4a-e) or (R,R) configuration (RS04)

## 1.2.2 Gas Phase Enantioselectivity

### *1.2.2 a CID of host/guest non-covalent complexes*

Macrocyclic amides are a group of synthetic receptors important for their amphipilic properties of their amido groups in dipolar or H-bonding interactions, the carbonyl acting as a dipole donor and a H-bond and the N-H as a dipole acceptor and H-bond donor [16, 18].

Macrocyclic $A_2B_2$ tetramide receptors with polar groups on either A or B portions give weak signals for the proton bound species in positive ion mode. Intense signals are observed instead for the deprotonated species and for anion bound species in negative ion mode (Fig. 6).

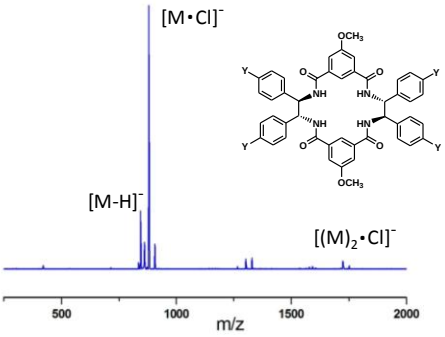


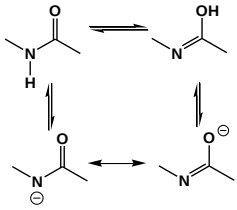

**Figure 6**

In a typical ESI-MS spectrum we can observe three different signals corresponding to the dimeric complex $[(M_2) \cdot Cl]^-$ generated by association, inside the ion trap, of two molecules of the complex in association with chloride ion, the signal $[M \cdot Cl]^-$ and the signal of the deprotonated host $[M-H]^-$. There are two possible deprotonation sites. Due to the electron-withdrawing nature of the carbonyl group, the lone pair of electrons on the nitrogen is delocalized by resonance, as shown in Fig 6, so during the electrospray we could observe charged species obtained by the loss of a proton, generating a resonance stabilized anion with the negative charge on either the nitrogen or carbonyl oxygen of the amide fragment.

Information about the relative stability of the homochiral and heterochiral $[M-H\cdot A]^-$ complexes has been derived from CID of the corresponding $[M-H\cdot A]^-$ adducts generated by electrospray ionization of M/A mixture; where M is a chiral host and A a chiral guest. The ability of our receptors to discriminate the enantiomers of a specific guest has been evaluated by isolating the dimers $[M-H\cdot A]^-$ inside the ion

trap followed by their dissociation by collision with neutrals (CID) at a different dissociation energy values. The lowest energy dissociation process involves the loss of the molecule of the guest, resulting in the free deprotonated hosts. In this way it was possible to monitor the decrease of the intensity of the dimeric complex and the increase of the $[M-H]^-$ signal due to the dissociation of the dimeric complex. The enantioselectivity of the system is extracted based on the decrease of the signal intensity of the complex $[M-H\cdot A]^-$ as a function of the collision energy. We obtained two sigmoidal curves one for each complex and enantioselectivity is expressed as the difference in the collision energy required to dissociate 50% of the parent diastereomeric $[M-H\cdot A]^-$ complexes (Fig. 7).

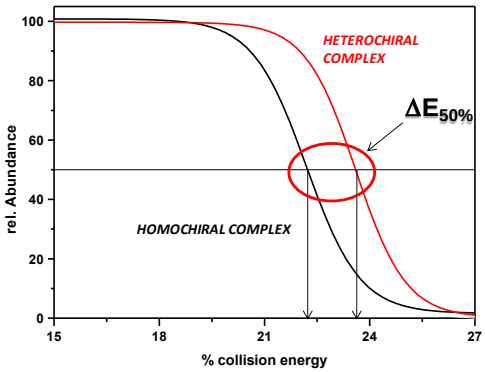


**Figure 7:** threshold method showing the energy resolved dissociation curves for the two diastereomeric host-guest complexes formed by a single enantiomer of the host and the two enantiomers of the guest.

The $E_{1/2}$ value for each complex was corrected for the degrees of freedom in the complex, relative to the deprotonated complex, chosen as a reference.

$$E_{1/2} = \frac{[\,E_{1/2}(\mathrm{complex})][\#\ \mathrm{DOF}(\mathrm{reference})]}{[\#\ \mathrm{DOF}(\mathrm{complex})]} \qquad (1)$$

*1.2.2 b Applications*

The gas phase enantioselectivity was evaluated using different enantiomers of aminoacids as guests. We selected six amino acids with different molecular complexity to evaluate the influence of the structure on enantioselectivity (Fig. 8).

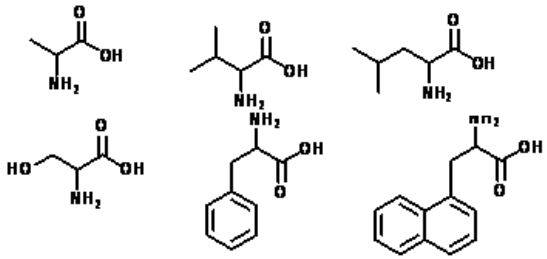

**Figure 8:** structures of the aminoacid guest used in this study.

The methodology employed was the 50% threshold, as explained before, the complex $[M\text{-}H \cdot A]^-$ generated by electrospray of an equimolar mixture of host and guest ($10^{-4}$ M in acetonitrile) was isolated inside the ion trap. The energy dissociation values, necessary to dissociate the

complex, range from about 15% to 28% of the maximum CID voltage of 5 V. At the lowest CID energy value the 100% of relative abundance corresponds to the intensity of the signal $[M\text{-}H\cdot A]^-$ that decrease with the increase of the dissociation energy. Figure 9 shows all the experiments carried out for all hosts with all guests.

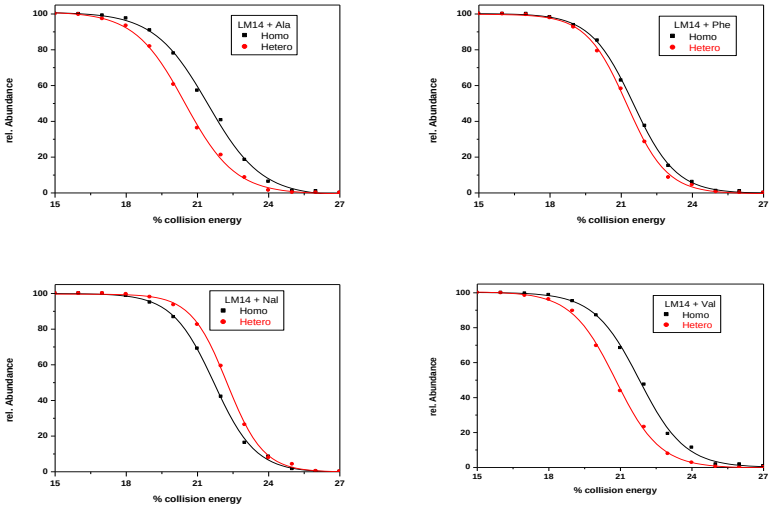

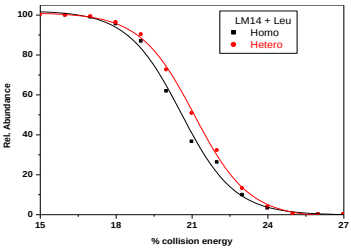
LM14 + Leu
Homo
Hetero
Rel. Abundance
% collision energy

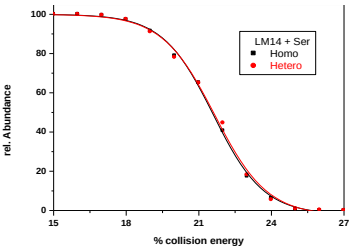
LM14 + Ser
Homo
Hetero
rel. Abundance
% collision energy

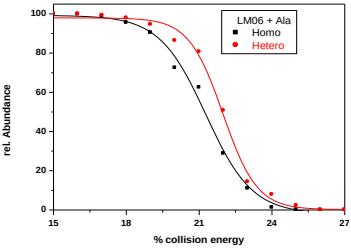
LM06 + Ala
Homo
Hetero
rel. Abundance
% collision energy

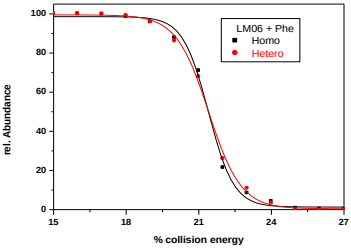
LM06 + Phe
Homo
Hetero
rel. Abundance
% collision energy

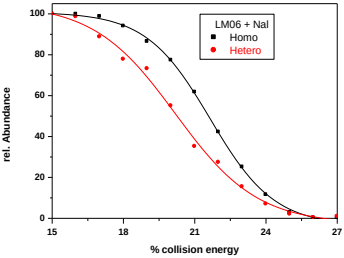
LM06 + Nal
Homo
Hetero
rel. Abundance
% collision energy

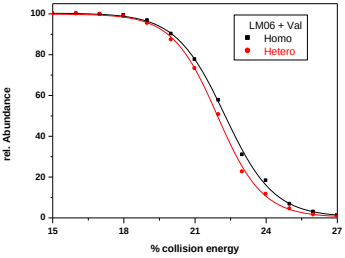
LM06 + Val
Homo
Hetero
rel. Abundance
% collision energy

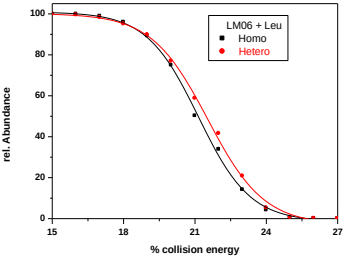
LM06 + Leu
Homo
Hetero
rel. Abundance
% collision energy

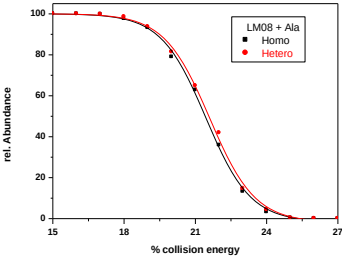
LM08 + Ala
Homo
Hetero
rel. Abundance
% collision energy

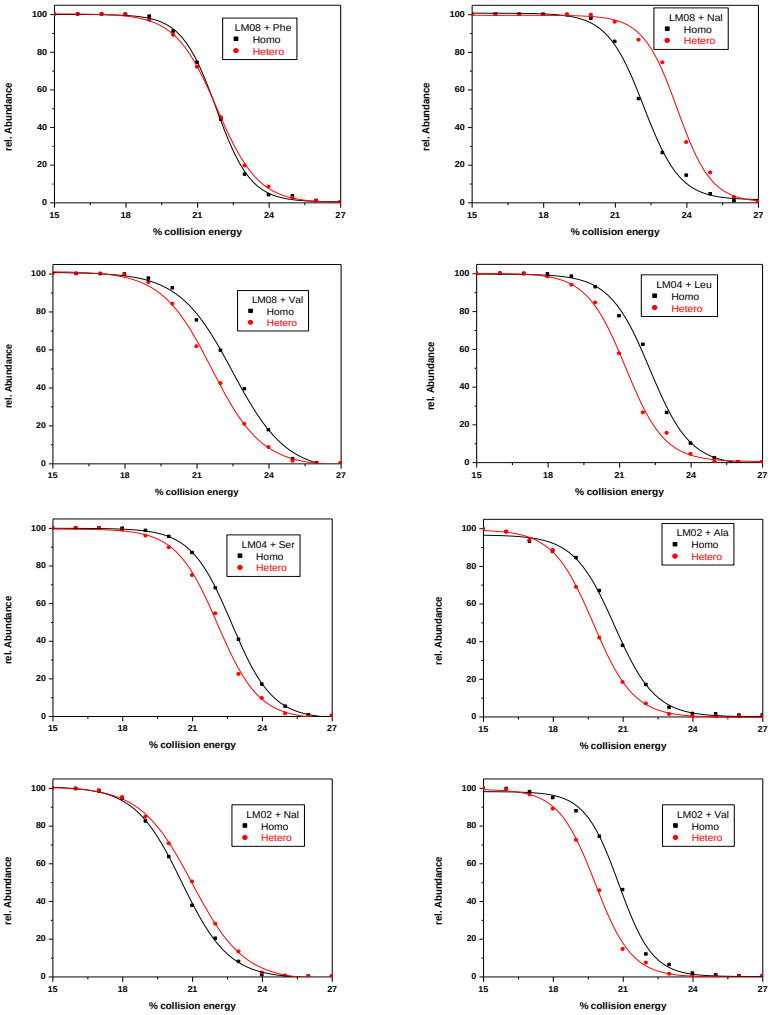


**Figure 9:** dissociation curves for the dimeric complexes $[M\text{-}H\cdot A]^-$ M: $A_2B_2$ hosts, A: amminoacids. Abbreviation within boxes: Ala: alanine, Val: valine, Leu: leucine, Ser: serine, Phe: phenylalanine, NaL: naphthylalanine.

Comparison of $E_{1/2}$ values for complexes involving the same host but different aminoacids shows that overall stability of the complexes is governed by the size of the guest: with large guests the dissociation of the complexes is more difficult because the energy acquired by the charged host-guest species by collision is distributed over a larger number of vibrational motions before culminating in the dissociation. The more stable complexes are usually those formed with naphthylalanine as guest, requiring greater energy value to be dissociated, around 23%. By contrast, complexes with the smaller alanine guest require only needs 21% of $E_{1/2}$ . However, size of the guests is not the only factor governing the overall stability of the complexes, as the presence of aromatic units in the guests and the electronic nature of substituents on the A or B units both affect the stability of the complexes.

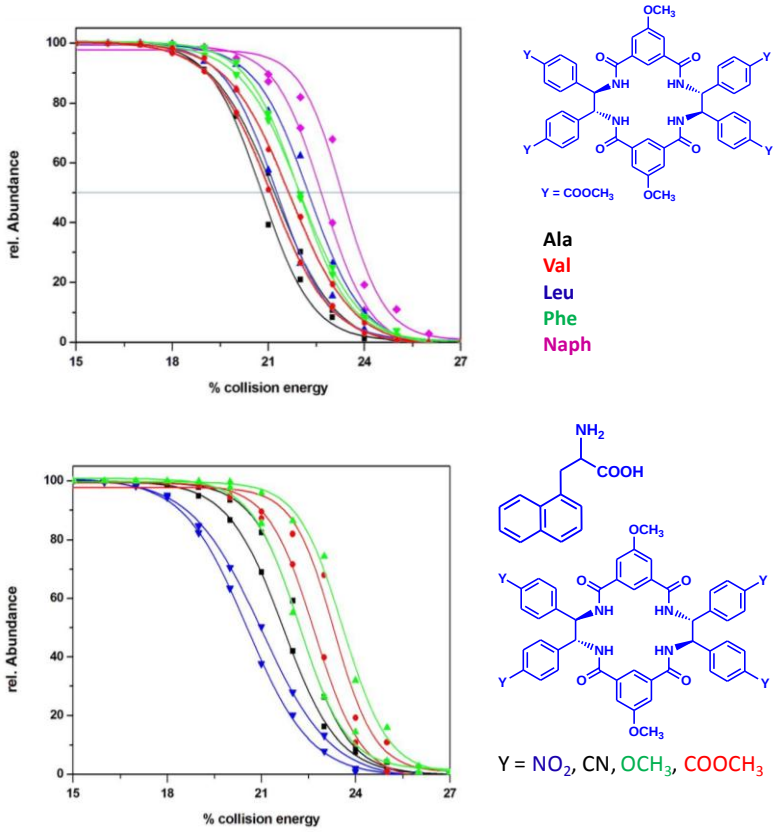


**Figure 10:** comparison of $E_{1/2}$ values for complexes involving the same host but different aminoacids (top) and the same aminoacid with different hosts (bottom).

This is evident when the dissociation threshold energies for complexes formed by the same guest (naphthylalanine in

figure 10, bottom) and different $A_2B_2$ hosts are compared. Here the hosts with electron withdrawing p-$NO_2$ and p-CN fragments on the phenyl rings of the B units have the lowest stability, and this is especially evident when compared with the p-OMe host: in spite of the similar size, the latter is much more stable than the other two, indicating either a beneficial effect of electron releasing groups on the stability or the presence of additional interaction sites stabilizing the complex. The host with the electron withdrawing p-COOMe fragments on the B units shows a mixed behavior: the host-guest complex in this case is more stable compared to those formed by the hosts with p-$NO_2$ and p-CN fragments and has a dissociation energy similar to that of the complex formed by the p-OMe host. In this case, the larger size and polarizability of the p-COOMe substituent together with its increased number of potential interaction sites, increase the stability of the host-guest system.

Enantioselectivity in the host-guest systems follow a similar trend, and can be visually observed by considering the shift along the collision energy axis of the dissociation curves for

the two enantiomeric guests with the same host. The largest differences are observed for naphthylalanine when the same host is scrutinized towards several aminoacid guests, and with hosts carrying electron releasing groups on either A or B units when the same aminoacid guests is screened for enantioselectivity towards different hosts. With only few exceptions, the homochiral host-guest combinations are more stable than the heterochiral ones.

*1.2.2 c $A_2B_2$-$T_2$-$A'_2B_2$*

The recognition abilities of $A_2B_2$-$T_2$-$A'_2B_2$ have been explored by ESI-MS using a linear ion trap and by screening for selective association a collection of potential guests ranging from small sized aminoacids and peptides (Fig. 11) to large octahedral $Ru(L_3)^{2+}$ complexes (L = bpy, phen) (Fig. 12). In the first case it didn't show enantioselectivity, the complex host-guest was so weak that at 6% of collision energy the complex was not stable and in MS/MS spectrum was already visible the signal of the complex and of the host.

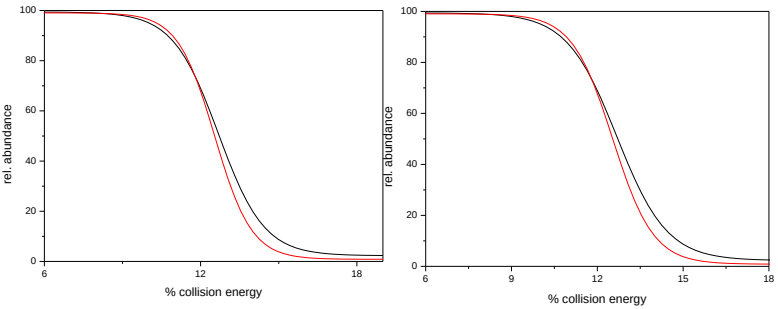


**Figure 11:** dissociation curves for the complexes $[M \cdot A]^{2+}$; M: $A_2B_2$ hosts, A: $[Ru(Phen)_3]^{2+}$.

ESI of equimolar solution ($10^{-5}$ M) of $A_2B_2$-$T_2$-$A'_2B_2$ and Δ- and Λ-$[Ru(Phen)_3]^{2+}$ in acetonitrile gave intense signals for the doubly charged $[host\text{-}guest]^{2+}$ complexes. $[host\text{-}\Delta\text{-}guest]^{2+}$ and $[host\text{-}\Lambda\text{-}guest]^{2+}$ were isolated inside the ion trap and dissociated at different values of collision energy. Energy resolved CID experiments for the two complexes yielded shifted dissociation curves, indicating enantioselective association in favor of Δ-$[Ru(Phen)_3]^{2+}$ (Fig. 12).

No enantioselectivity was observed for the same $[Ru(Phen)_3]^{2+}$ complexes with the smaller $A_2B_2$ receptors.

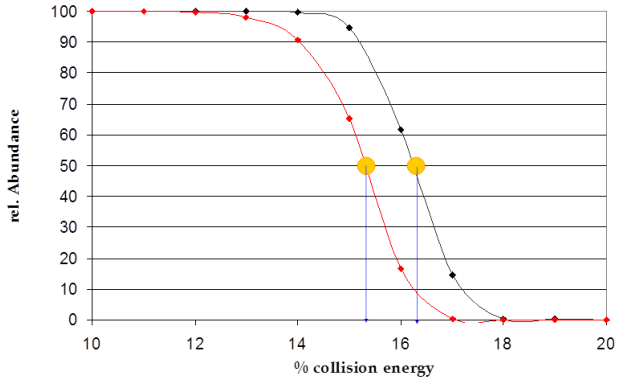


**Figure 12:** dissociation curves for the complexes $[M \cdot A]^{2+}$; M: $A_2B_2$-$T_2$-$A'_2B_2$ hosts, A: $[Ru(Phen)_3]^{2+}$.

## 1.3 Conclusions

All these data suggest the enantioselective recognition originates from a blend of different interactions, including H-bonding and π-π aromatic stacking interactions, and is modulated by the functionalities present at the subunits A and B and by the bulkiness of the guests.

The stability of the complexes increase as the size of guest and the number of degree of freedom increase as well.

There is also a correlation between the complex stabilities and gas-phase basicity of the hosts. Hosts with a greater basicity show a greater stability in gas phase and require higher values of collision energy.

## 1.4 Experimental Section

### 1.4.1 Chemicals and materials

All solvents, samples, and reagents were ordered from Sigma-Aldrich (St. Louis, Mo, USA). Prior to use, THF was freshly purified from alumina. All anhydrous reactions were carried out under argon atmosphere. Analytical thin layer chromatography was performed on Merck F254 precoated silica (0.2 mm) on glass and was revealed by UV-light. All chromatography separations were performed with Merck Kiesegel 60 (0.040-0.063 mesh).

### 1.4.2 Synthesis of chiral macrocyclic receptors

*a. Synthesis of subunit A*

A solution of 5-hydroxy-isophthalic acid (5 g, 0.027 mol) and acetyl chloride (5 ml) in 100 ml of MeOH was refluxed for 4 h, then the solvent was completely removed under reduced pressure recovering 4.2 g (0.021 mol yield = 96 %) of white powder consisting in pure **1**. Metil estere of 5-

hydroxy-isophthalic acid (2.5 g, 11.9 mmol) was added to a suspension of potassium carbonate (3.29 g, 23.8 mmol) in 112 ml of acetonitrile with stir. The resulting solution was stirred for 30 min at 80 °C in inert atmosphere. After 30 min $SO_4(CH3)_2$ was added and the solution was stirred for 3h at 70 °C. The mixture was neutralized with HCl 0.1 N and extracted with $CHCl_3$ and washed three times with water (3x15 ml). The solvent was completely removed to give 2.46 g of **2** (yield: 91.5%).

An aqueous solution of KOH 5N (75 ml) was added to a solution of **2** and stirred for 90 min at 70 °C. After 90 min, the solution was stirred over night at room temperature to give 1.96 g of **3** (yield 91%). A solution of **3** (0.35 g, 0.6 mmol) in $SOCl_2$ (8.15 g, 68 mmol) was refluxed and stirred for 4 h. After cooling to r.t., complete removal of $SOCl_2$ under reduced pressure afforded the compound **4** as a solid. The reaction is quantitative (Scheme 1).

*b. Preparation of C2 symmetric diamines by stereospecific Diaza-Cope Rearrangement (subunits B)*

B components were prepared by a 3,3-aza-Cope-rearrangement of imines derived from substituted benzaldehydes and the chiral parent diamine 1,2-bis-(2-hydroxyphenyl)-1,2-diaminoethane [JACS 2006, 130, 12184]. To a cloudy solution of 1,2-bis(2-hydroxylphenyl)-1,2-diaminoethane (**1**, 2.4 g 10 mmol) in 7.5 ml of methanol was added 25 mmol of aryl aldehyde. The resulting clear reaction mixture was stirred for 4h at room temperature to give **2** as a yellow precipitate. The solid was dried in vacuum (Scheme 3 in Results and discussion). To a solution of **2** in THF (2.5 ml) was added HCl (37%, 3 ml) and $H_2O$ (7,5 ml), the resulting solution was stirred for 5h at room temperature. The reaction was monitored by TLC, hexane/ethyl acetate 75/25 as eluent.

After removal of the solvent under reduced pressure, the was treated with water and extracted with $CH_2Cl_2$; the aqueous layer was rendered basic with NaOH 12N until pH12, and extracted with $CH_2Cl_2$. The solvent was removed

under reduce pressure to afford analytically pure **3** (130 mg, 0.43 mmol) as the free base.

*c. Synthesis of HOST $A_2B_2$ 4a*

$A_2B_2$ 4a was prepared by a general synthetic method in which the ethyl ester of 5-methoxy-ispophtalic acid in the minimum required amount of THF (100 ml) was added dropwise to a tetrahydrofuranic solution of the **3a** (130 mg, 0.4 mmol) in DIPEA (0.15 ml, 0.8 mmol) with stirring. The resulting solution was stirred over night at room temperature. After complete removal of the solvent under reduced pressure the residue was treated with water and extracted with $CH_2Cl_2$. The organic layer was dried over anhydrous $Na_2SO_4$ and the solvent removed under reduced pressure. The solid residue was purified by column chromatography ($SiO_2$, eluent: $CHCl_3$/MeCN 70/30) to give 84 mg (0.33 mmol, yield = 45 %) of pure 4a .

MS (ESI) m/z: 959.3 [ $(M \cdot Cl)^-$]

$^{1}$H-NMR ($CDCl_3$, 298 K) : δ 3.61 (s, 6H), 3.89 (s, 12H), 5.57 (s, 4H), 7.26-7.90 (m, 20H ), 8.05 (s, broad, 4H)
$^{13}$C-NMR ($CDCl_3$, 298 K): δ 29.67, 52.19, 55.42, 60.30, 97.68, 114.80, 116.79, 127.66, 129.96, 135.53, 142.71, 159.93, 167.54, 168.04
CD (nm) : (+) 232.05, (-) 210.43, (0) 220.87

*d. Synthesis of $A_2B_2$ 4b-4e*

These complex were prepared according to the procedure described for $A_2B_2$ 4a.

*$A_2B_2$ 4b*: 4b (270 mg, 0,82 mmol). Yield: 22%
MS (ESI) m/z: 1011.4 [ $(M \cdot Cl)^-$];
$^{1}$H.NMR ($CDCl_3$, 298 K) : δ 3.608 (s, 6H), 3.89 (s, 12H), 5.57 (s, 4H), 7.26-7.90 (m, 20H ), 8.05 (s, broad, 4H).
$^{13}$C-NMR ($CDCl_3$, 298 K): δ 29.67, 52.19, 55.42, 60.30, 97.68, 116.23, 118.79, 127.66, 129.96, 135.53, 142.71, 159.93, 166.63, 168.04
FT-IR (KBr): 3316, 2952, 1724, 1652, 1286, 1112, 709 $cm^{-1}$
CD (nm) : (+) 232.05, (-) 210.43, (0) 220.87

*$A_2B_2$ 4c*: 4c (220 mg, 0,84 mmol); Yield: 32%;

MS (ESI) *m/z*: 867.9 [ $(M \cdot Na)^+$], 1712.4 [ $(M_2 \cdot Na)^+$];

$^1$H-NMR (DMSO-$d_6$, 298 K): δ 3.80 (s, 6H), 5.59 (s, 4H), 7.30-7.99 (m, 22H), 9.32 (s, broad, 4H)

FT-IR (KBr): 3313, 3072, 2938, 2840, 2231, 1654, 1521, 1054, 700 $cm^{-1}$

CD (nm) : (+) 240.71, (-) 212.47, (0) 230.53

*$A_2B_2$ 4d*: 4d (190 mg, 0,7 mmol); Yield: 26%

MS (ESI) *m/z*: 887.42 [ $(M \cdot Na)^+$ ], 1752.17 [ $(M_2 \cdot Na)^+$];

$^1$H-NMR ($CDCl_3$, 298 K): δ 3.73 (s, 6H), 3.77 (s, 12H), 5.49 (s, 4H), 7.26-6.77 (m, 20H), 7.97 (s, broad, 6H)

$^{13}$C-NMR ($CDCl_3$, 298 K): δ 55.18, 55.64, 60.80, 113.96, 115.57, 118.13, 129.05, 130.67, 136.14, 159.05, 159.70, 168.68

FT-IR (KBr): 3309, 2998, 2937, 2836, 1648, 1513, 1249, 833 $cm^{-1}$

CD (nm) : (+) 225.18, (-) 211.18, (0) 21 8.31

*$A_2B_2$ 4e*: 4e (160 mg, 0,61 mmol); Yield: 30%

MS (ESI) *m/z*: 843.5 [ $(M - H)^-$ ], 879.3 [ $(M \cdot Cl)^-$ ];

$^1$H-NMR (DMSO-$d_6$, 298 K): δ 3.78 (s, 6H) 5.58 (s, 4H) 7.94-7.26 (m, 22H) 9,39 (s, broad, 4H);

$^{13}$C-NMR (DMSO-$d_6$, 298 K): δ 56.01, 58.75, 71.86, 110.72, 116.17, 118.55, 119.52, 129.56, 132.66, 136.70, 144.83, 159.49, 167.45;

FT-IR (KBr): 3307, 3068, 2938, 2840, 2229, 1662, 1525, 1340, 838 $cm^{-1}$;

CD (nm) : (+) 228.00, (-) 205.84, (0) 219.58

### 1.4.4 Synthesis of $A_2B_2T_2A'_2B_2$

A solution of 1 (0.130 g, 0.152 mmol), 2 (0.121 g, 0.152 mmol), DIPEA (0.11 g, 0.85 mmol), and the copper catalyst [$(EtO)_3P$•CuI] (0.013 g, 0.04 mmol) in toluene (65 ml) was refluxed for 1 h. Evaporation of the solvent yields a crude that was purified by column chromatography ($CHCl_3$/isopropanol 50/25) giving 3 (0.03 g) yield= 15 %

NMR, MS

### 1.4.5 $^{1}H$, $^{13}C$-NMR Spectroscopy

$^{1}H$ and $^{13}C$ spectra were recorded at 400 MHz on a Bruker 400. $CDCl_3$, $CD_3OD$, $CD_3CN$ and $(CD_3)_2SO$ were used as internal standard.

### 1.4.6 IR and CD Spectroscopy

Infrared (IR) spectra were recorded on

Circular Dichroism (CD) spectra were obtained on Japan Spectroscopic J-710/720 polarimeter in acetonitrile ($1 \times 10^{-5}$ M).

### 1.4.7 Mass Spectrometry experiments

The experiments were performed using an ion trap LCQ DECA XP Plus (Thermo Finnigan), equipped with an ESI source. Operating conditions for the ESI source were as follows: spray voltage, 5.00 kV; capillary voltage, 27 V; heated capillary temperature, 210 °C; tube lens offset voltage, 20 V; sheath gas ($N_2$) flow rate, 15 units (roughly 0.75 L/min). Acetonitrile solutions are infused via a syringe pump at a flow rate of 5 μL/min.

ESI of solutions of the macrocyclic tetraamides M = $A_2B_2$ 4a, $A_2B_2$ 4b, $A_2B_2$ 4c, $A_2B_2$ 4d and $A_2B_2$ 4e ($1 \times 10^{-4}$ M) containing a three times amount of the aminoacid ($1 \times 10^{-4}$ M), leads to the formation of appreciable amount of the corresponding $[M\text{-}H\bullet A]^-$ and $[(M)_2\text{-}H\bullet A]^-$ complexes. After individual isolation of the ions inside the ion trap, the isolated ions are subjected to a supplementary alternating current (AC) to excite them and cause fragmentation by collision with He gas (CID). Ion excitation time for CID is 30 ms with the amplitude of the excitation AC being optimized in each experiment and being kept the same for the measurement of the two enantiomeric guests with the same host. Optimized instrumental values of relative collision energy of 12-15% give exclusively the fragment ions of interest (relative collision energy values range 0-100% corresponding to 0-5 V resonant excitation potential). Spectra acquired in the centroid mode are the average of 100 scans, each consisting of three averaged microscans.

## 1.5 References

[1] M. I. Pagae, The chemisty of Enzyme Action, Elviser, Amsterdam, 1984

[2] E. C. Hulme , Receptor Biochemistry, Oxford University Press, New York, 1990

[3] S.M. Roberts, ed., Molecular Recognition-Chemical and Biochimical Problems, The Royal Society of Chemistry, Cambridge, 1989 [1] F. Vögtle and E. Weber, eds., *Host-Guest Complex Chemistry—Macrocycles*, Springer, Berlin-Heidelberg, 1985.

[4] E. Weber, ed., Supramolecular Chemistry II—Host Design and Molecular Recognition, Top. Curr. Chem., Vol. 175, Springer, Berlin-Heidelberg, 1995.

[5] J.-P. Behr, ed., The Lock and Key Principle, Perspectives in Supramolecular Chemistry, Vol. 1, Wiley, Chichester, 1994.

[6] J. W. Steed and J. L. Atwood, Supramolecular Chemistry, 2nd edition, John Wiley & Sons, Ltd, 2009.

[7] F. Vögtle and E. Weber, eds., *Host-Guest Complex Chemistry—Macrocycles,* Springer, Berlin-Heidelberg, 1985.

[8] D. Hamilton, in H. Dugas, ed., Bioorganic Chemistry Frontiers, Vol. 2, Springer, Berlin-Heidelberg, 1991, p. 115.

[9] Gasparrini F., Pierini M., Villani C., Filippi A., Speranza M. *J. Am. Chem. Soc*. 2008; 130, 522-534.

[10] Speranza, M.; Gasparrini F.; Botta B.; Villani C.; Subissati D.; Fraschetti C.; Subrizi F. *Chirality* 2009; 21, 68-86.

[11] Filippi A.; Gasparrini F.; Pierini M.; Speranza M., Villani C. *J. Am. Chem. Soc*. 2005; 127,11912-11913.

[12] Tao WA, Cooks RG. Chiral analysis by MS. *Anal Chem* 2003; 75:25A-31A.

[13] Tao WA, Cooks RG. *Anal Chem* 2003; 75:25A-31A.

[14] Wendi M. David and Jennifer S. Brodbelt, *J. Am. Soc. Mass Spectrom.* 2003, 14, 383–392.

[15] Kim, H., Nguyen, Y., Pai-Hui Yen, C., Chagal, L., Lough, A.J.,Monn Kim, B. and Chin, *J. Am. Chem. Soc.* 2008, 130, 12184–12191.

# PART C

# *Absolute quantitation of human milk proteins and their glycoforms using MRM*

# Absolute quantitation of human milk proteins and their glycoforms using MRM .

## 1.1 Introduction

Milk is the most important food for the newborn, due to its nutrient composition: immune components, anti-infective factors, and metabolic enzymes, which all contribute to the critical needs for growth and development during early life [1, 2]. Milk not only provide a digestible source of amino acids to infants, but it also confer immunological protection, perform developmental and regulatory functions and some proteins play a role in facilitating the digestion and uptake of other nutrients in breast milk . Human milk proteins are particularly important for infants who are born prematurely, it is well known that the protein composition of milk from preterm mothers is differ from that of term mothers. The protein content of human milk changes during the lactation, it decreases rapidly during the first month and declines much more slowly after that.

Milk proteins can be classified into 3 groups: mucins, caseins, and whey proteins. Mucins, also known as milk fat globule membrane proteins, contribute only a small percentage of the total protein content of human milk. The fat content of human milk does not vary during the course of lactation so the milk mucin concentration is most likely constant. The contents of casein and whey proteins change profoundly early in lactation; the concentration of whey proteins is very high, whereas casein is virtually undetectable during the first days of lactation (Fig. 1) [3, 4]. Casein synthesis in the mammary gland and milk casein concentrations increase, whereas the concentration of total whey proteins decreases, partially because of an increased volume of milk being produced.

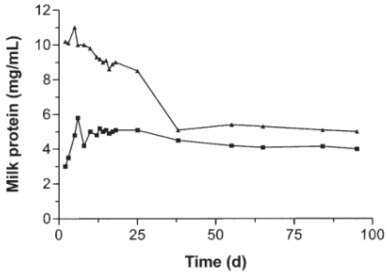


**Figure 1:** Changes in whey protein (▲) and casein (■) concentrations during lactation in one mother.

The frequently cited ratio of 60:40 is an approximation of the ratio during the normal course of lactation, but it does vary from 80:20 in early lactation to 50:50 in late lactation [5, 8]. A comprehensive understanding of the human milk protein profile is important to understand not only milk biogenesis and functions provided to the newborn but also to develop infant formulas more similar in protein composition to human milk and to study some eventually problems in the absorption and digestions of milk proteins.

Using gel electrophoretic method coupled with mass spectrometry less than 10 proteins were detected. More recently, proteomic studies employing strategies to deplete the high abundance proteins or to fractionate the sample prior to analysis have been more successful at identifying low abundance proteins than the gel-based methods [9, 12]. Two studies in particular have identified a large number of low abundance human milk proteins. Palmer et al. used immunodepletion columns to deplete the five most abundant proteins in colostrum prior to 2D LC−MS/MS analysis and were able to identify 151 proteins. More recently, Liao et al.

[13] employed combinatorial hexapeptide ligand libraries (ProteoMiner) to enrich the low abundance milk proteins before analysis by LC−MS/MS and identified 115 proteins. Liao et al. also showed that many of these proteins change in expression over the course of 12 months of lactation, highlighting the dynamic nature of milk composition. The changes in milk proteins during lactation, however, have not been comprehensively examined, but quantifying these changes is very important to understand changes in cell state at a molecular level.

Proteomic technologies based on mass spectrometry (MS) have emerged as preferred components for discovery of diagnostic, prognostic and therapeutic protein biomarkers [14, 17]. An important goal in proteomic is to quantify the profile changes of protein abundances in biological systems. The classical proteomic quantification methods utilizing dyes, fluorophores, or radioactivity have given very good sensitivity, linearity, and dynamic range, but they lack of two important shortcomings: first, they require high-resolution protein separation typically provided by 2D gels,

which limits their applicability to abundant and soluble proteins; and second, they do not reveal the identity of the underlying protein. Both of these problems are surmount by modern LC-MS/MS techniques. However, mass spectrometry is not inherently quantitative because proteolytic peptides exhibit a wide range of physicochemical properties such as size, charge, hydrophobicity, etc. which lead to large differences in mass spectrometric response. One major approach is based on stable isotope dilution theory which states that a stable isotope-labeled peptide is chemically identical to its native counterpart and therefore the two peptides also behave identically during chromatographic and/or mass spectrometric analysis. A mass spectrometer can recognize the mass difference between the labeled and unlabeled forms of a peptide, quantification is reached by comparing their respective signal intensities. Stable isotope labeling was introduced into proteomics in 1999 by three independent laboratories [18, 21] and has since been adopted widely in the field. Isotope labels can be introduced

as an internal standard into amino acids (i) metabolically, (ii) chemically, or (iii) enzymatically or, alternatively, as an external standard using spiked synthetic peptides. More recently, alternative strategies—often referred to as label free quantification-have emerged [22].

Label-free methods aim to compare two or more experiments by (i) comparing the direct mass spectrometric signal intensity for any given peptide or (ii) using the number of acquired spectra matching to a peptide/protein as an indicator for their respective amounts in a given sample. Proteomic studies are performed using a shotgun approach, in which the sample proteins are enzymatically degraded to peptides, which are analyzed by mass spectrometry using MRM (multiple reaction monitoring) [23].

Multiple reaction monitoring (MRM) is a technology that is valued for its potential towards the reliable quantitation of analytes of low abundance in complex mixture. MRM is a non-scanning technique, generally performed on a triple quadrupole (QQQ) instruments in which the fragmentation is used to increase the selectivity. In MRM mode two mass

analyzers are used as static mass filters, to monitor a particular fragment ion of a selected precursor ion. The first and the third quadrupoles act as a filter to specifically select predefines *m/z* values corresponding to the peptide ion and a specific fragment ion of the peptide (transition), whereas the second quadrupole serves as collision cell. The precursor ion selected by the first mass filter (Q1) enters in the collision cell (Q2) where it undergoes collision induced dissociation (CID). One fragment ions is then selected by the second mass filter (Q3) (Fig. 2) [24, 26]. A high selectivity is obtained due to the two selection steps that filter out co-eluting background ions. In this way mass spectrometer monitors both the intact peptide mass and one or more specific fragment ions of that peptide over the course of an LC-MS experiment. The combination of retention time, peptide mass, and fragment mass eliminates ambiguities in peptide assignments and extends the quantification range to 4-5 orders of magnitude. MRM measurements are quantitative analyses strictly targeting a

predetermined set of peptides and depend on specific MRM transitions for each targeted peptide.

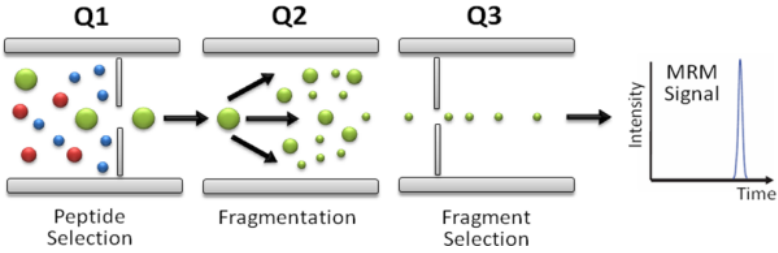


**Figure 2:** SRM/MRM analysis on QQQ MS.

Three types of information are necessary for a MRM project. First, the proteins that constitute the targeted protein set have to be selected. Second, for each targeted protein, it is necessary to identify peptides that present good MS responses and uniquely identify the targeted protein, or a specific isoform. Such peptides have been termed as proteotypic peptides (PTPs). Third, for each PTP, those fragment ions that provide optimal signal intensity and discriminate the targeted peptide from other species present

in the sample have to be identified. These optimized transitions are the essence of an MRM assay.

The aim of this project was the quantitation of seven human milk proteins and their glycoforms using a label free method through multiple reaction monitoring.

## 1.4 Results and Discussion

### 1.4.1 Method development

*1.4.1 b Proteins identification*

We selected seven proteins: lactoferrin, α-lactalbumin, IgG, s-IgA, IgM, $\alpha_1$-antitrypsin and lysozyme.

Some proteins, such as bile salt–stimulated lipase, amylase, β-casein, lactoferrin, haptocorrin, and $\alpha_1$-antitrypsin, assist in the digestion and utilization of micronutrients and macronutrients from the milk. Several proteins with antimicrobial activity, such as immunoglobulins, lysozyme, lactoferrin, α-lactalbumin, and lactoperoxidase, are relatively resistant against proteolysis in the gastrointestinal tract and may contribute to the defense of breastfed infants against pathogenic bacteria and viruses [27].

Lactoferrin presents antimicrobial activities, it has a strong bactericidal activity against several pathogens.

Lysozyme is one of the major components of the human milk whey fraction, it is capable of degrading the outer cell wall of gram positive bacteria.

α-lactalbumin binds $Ca^{2+}$ and $Zn^{2+}$ so it is possible that it has a positive effect on mineral absorption.

$\alpha_1$-antitrypsin may limit the activity of pancreatic enzymes in breastfed infants, it also escape digestion in part and are found in the stool of breastfed infants.

The major type of immunoglobulins in human milk is sIgA (> 90%)—a dimer of IgA linked together with a secretory component and a joining chain. This particular arrangement renders this molecule relatively resistant to intestinal proteolysis and modest amounts of sIgA have been found intact in the stool of breastfed infants. The immunoglobulins present antimicrobical activity.

We chose these proteins either for their important functions and for their quantity. α-lactalbumin, secretory immunoglobulin A, lysozyme and lactoferrin constitute over 90% of the total protein content in mature human milk [27, 28] obscuring the detection of less abundant proteins of potential biological. Usually the concentrations in milk are: lactalbumin 3-6 mg/ml, lactoferrin 2-5 mg/ml, IgA 0.5-3

mg/ml, IgM 0.01-0.1 mg/ml, IgG 0.01-0.1 mg/ml, antitrypsin 0.05-0.3 mg/ml and lysozyme 0.1-0.3 mg/ml.

*1.4.1 a Trypsin digestion*

Trypsin digestion is necessary cause, for most mass spectrometers, proteins are too big to be analyzed by tandem MS. The samples were dissolved in ammonium bicarbonate (AmBic, 50 mM), in which all the samples are soluble and it doesn't influence the electrospray, and added DTT (dithiothreitol) in water bath at 50 °C for 60 min, denaturation and reduction were carried out simultaneously by a combination of heat and a reagent. DTT is a strong reducing agent, that reduce the disulfide bonds and prevent inter and intra-molecular disulfide formation between cysteines in the protein. By combining denaturation and reduction, renaturation of the proteins can be avoided. Following protein denaturation and reduction, alkylation of cysteine is necessary to further reduce the potential renaturation. The most commonly used agent for alkylation

of protein is iodoacetamide (IAA). Samples were alkylated with 50 mM iodoacetamide, 1h, at room temperature in dark. After that trypsin was added, it hydrolyzes only the peptide bonds in which the carbonyl group is followed either by an arginine (Arg) or lysine (Lys) residue, with the exception when Lys and Arg are N-linked to Aspartic acid (Asp). The cleavage will not occur if proline is positioned on the carboxyl side of Lys and Arg. Tryptic digestion is performed at an optimal pH in the range 7.5-8.5 and at 37 °C for 18 h. Prior to LC-MS analysis, the resulting peptides were purified, to remove buffers and salts added during the sample preparation, by solid phase extraction (SPE) on a C18 column. The column were washed with 3 x 200 ml of water in 0.1% formic acid, 3 x 200 ml with acetonitrile in 0.1% formic acid and 3 x 200 ml of water in 0.1% formic acid. Total volume of digest were loaded, wash with 3 x 200 ml of water in 0.1% formic acid, and elute with 3 x 200 ml of 80% acetonitrile in 0.1% formic acid. Eluates were collected and dried in vacuum.

*1.4.1 b Fragmentation of peptides and glycopeptides*

After complete removal solvent the resulting peptides and glycopeptides were reconstituted with water and analyzed using LC-Q-TOF MS/MS in order to obtain information regarding the amino acid sequence of the peptide and further used for protein identification or characterization. In order to select specific peptides representative for each proteins we used our MS/MS information with publicly accessible databases. Global Proteome Machine Proteomics Database [28] was utilized to choose the appropriate peptides based on the most abundant b and y-ions representing our seven target proteins. The collision energy used for the LC-Q-TOF MS/MS experiment was calculated on the basis of the m/z values of each fragment (eq.1, low energy).

$$CE\ (eV) = 1.8\ m/z \times 100 - 2.4 \qquad \text{eq (1)}$$

The CID fragmentation method can use two different type of energy: low- or high-energy. The low-energy CID allows the rearrangement of the peptide after the loss of a fragment

[30] and it allows for multiple collisions (up to 100) in a time scale for dissociation of up to milliseconds whereas, the high-energy CID does not permit such process as it is too fast, breaking the peptide. The low energy CID fragmentation method generates two type of daughter ions due to the break of the CO-N bonds along the peptide backbone: the b-series ions extend from the N-terminal and the y-series ions extend from the C-terminal (Fig. 3) [30].

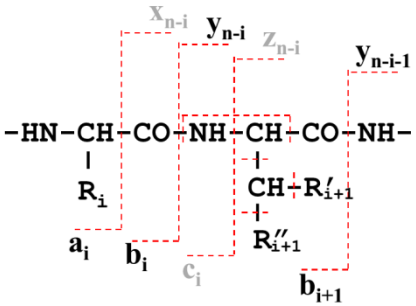


**Figure 3:** major fragment ions generated by CID of peptides.

The calculation of the mass difference between consecutive daughter ions belonging to the same ion series (for example b or y ion-series), allows the determination of peptide's primary sequence. CID fragmentation of peptides was

performed using helium, an inert gas, to hit the peptides resulting in the excitation of the molecular ion leading to the polypeptide chain breaking, and to a lower extent to that of the amino acid side chains, generating daughter ions.

Fig. 4 shows the tandem mass spectra of two different peptides of lactoferrin. These peptides generated mostly y and b-type ions. The CID (@23.7) of the peptide 1 of lactoferrin with a m/z values of 790.4 (doubly charge) gave different fragments, 228.1 $b_2$, 341.2 $b_3$, 488.3 $b_4$, 749.4 $y_6$, 863.4 $y_7$ 1239.6 $y_{10}$, to name a few. The same experiment were carried out for all the standards and the resulting MS/MS data were submitted to GMP where they compared our results with selected protein sequence databases.

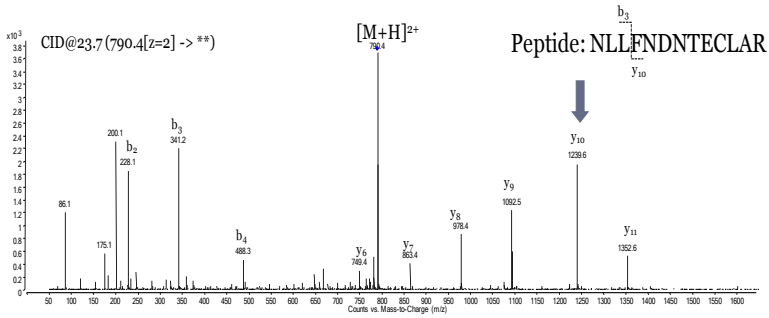

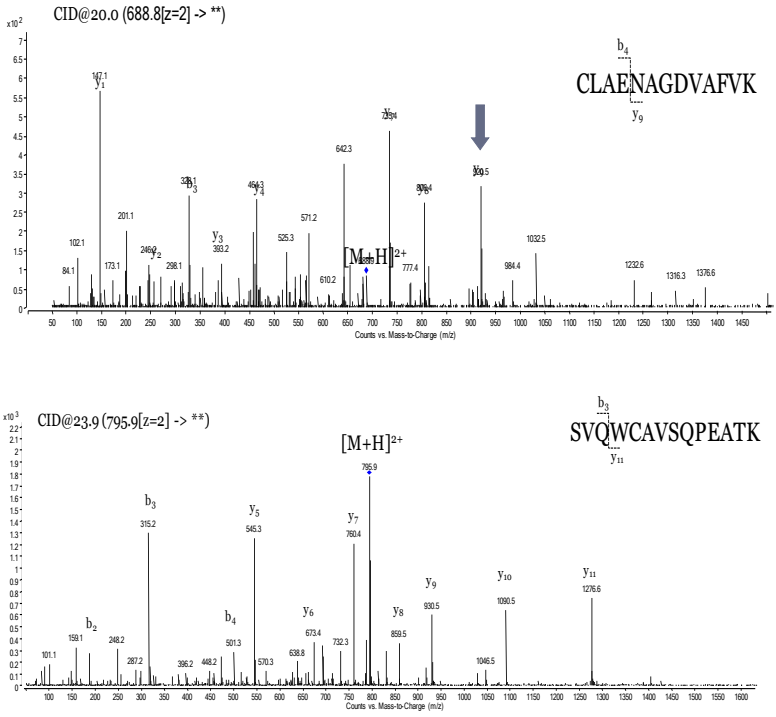


**Figure 4:** tandem spectra of lactoferrin peptides obtained by Q-TOF mass spectrometry.

The highest intensity fragment ions (y-ions in most cases) were selected for SRM transitions for each peptide (Table1).

*1.4.1 c Quantitation using MRM and calibration curves*

The peptides to quantify should have some characteristics, first they should be unique, second, peptides with post-translational modifications (PTMs) should be avoided to limit variation across the samples and they should not contain deamination or oxidation because these can vary across samples.

From the LC-Q-TOF-MS/MS experiments, MRM transitions were developed and they are summarized in Table 1 with their respective fragmentation voltages. For example: for lactoferrin nine transitions were determinate to be optimal: ($[M+2H]^{2+}$ 487.6→m/z 737.4 and 625.3) for peptide 93; ($[M+2H]^{2+}$ 795.9→m/z 1276.6) for peptide 795; ($[M+H]^{+}$ 621.6→m/z 272.2) for peptide 504; ($[M+2H]^{2+}$ 579.3→m/z 771.4) for peptide 544; ($[M+H]^{+}$ 510.8→m/z 506.3) for peptide 220; ($[M+2H]^{2+}$ 723.4→m/z 731.4) for peptide 364; ($[M+2H]^{2+}$ 790.4→m/z 1239.5) for peptide 2 790; ($[M+H]^{+}$ 668.4→m/z 300.2) for peptide 5 87.

| Compound Group | Compound Name | Precursor Ion (m/z) | Product Ion (m/z) | Ret Time (min) | Delta Ret Time | Collision Energy |
|---|---|---|---|---|---|---|
| ANTITRYPSIN | antitrypsin peptide 1 | 555.8 | 797.4 | 2.92 | 0.5 | 18 |
| ANTITRYPSIN | antitrypsin peptide 2 | 508.3 | 829.5 | 3.21 | 0.5 | 14 |
| IGA | IGA1/2-3 | 409.7 | 648.3 | 1.83 | 0.5 | 8 |
| IGA | IGA1-2 | 466.3 | 415.8 | 2.3 | 0.5 | 15 |
| IGA | IGA2-2 | 582.7 | 607.8 | 2.5 | 0.5 | 8 |
| IGA | IGA1/2-1 | 607.4 | 272.2 | 2.62 | 0.5 | 18 |
| IGA | IGA1/2-2 | 448.7 | 620.3 | 2.63 | 0.5 | 12 |
| IGA | IGA2-1 | 756.9 | 475.3 | 2.86 | 0.5 | 22 |
| IGA | IGA1-1 | 770.9 | 475.3 | 3.23 | 0.5 | 20 |
| IGG | peptide2_IgG1 | 419.8 | 327.7 | 2.22 | 0.5 | 6 |
| IGG | peptide1_IgG2 | 412.8 | 327.7 | 2.25 | 0.5 | 9 |
| IGG | peptide1234_2 | 418.2 | 506.3 | 2.32 | 0.5 | 9 |
| IGG | peptideIgG3 | 472.91 | 534.298 | 2.5 | 0.5 | 6 |
| IGG | peptideIgG1234 | 581.3 | 243.1 | 3 | 0.5 | 14 |
| IGG | peptideIgG1234Q | 581.82 | 244.1 | 3 | 0.5 | 14 |
| IGG | peptideIgG1_2 | 839.41 | 968.48 | 3.12 | 0.5 | 30 |
| IGG | peptideIgG1_3 | 593.83 | 699.4 | 3.18 | 0.5 | 20 |
| IGG | peptideIgG3_2 | 604.299 | 764.9 | 3.55 | 0.5 | 9 |
| IGG | IGG peptideIgG2_2 | 970.14 | 1100.62 | 4 | 0.5 | 28 |
| IGG | peptideIgG1 | 625.312 | 836.4 | 4.12 | 0.5 | 12 |
| IGG | peptideIgG4 | 634.98 | 425.214 | 4.2 | 0.5 | 9 |
| IGG | peptideIgG2 | 636.31 | 852.403 | 4.21 | 0.5 | 13 |
| IGM | IGM 3 | 534.3 | 426.3 | 2.4 | 0.5 | 9 |
| IGM | IGM 1 | 639.4 | 331.2 | 2.59 | 0.5 | 15 |
| IGM | IGM 2 | 572.95 | 654.9 | 2.77 | 0.5 | 9 |
| IGM | IGM 4 | 789.1 | 680.9 | 3.88 | 0.5 | 9 |
| J | J chain 2 | 469.8 | 613.3 | 2.63 | 0.5 | 12 |
| J | J chain 1 | 641.3 | 1035.5 | 2.73 | 0.5 | 24 |
| lactabumin | lactalbumin peptide 1 | 551.8 | 932.5 | 2.87 | 0.5 | 18 |
| lactalbumin | lactalbumin peptide 2 | 836.4 | 953.4 | 3.86 | 0.5 | 27 |
| Lactoferrin | LF peptide 93 | 487.6 | 737.4 | 2.18 | 0.5 | 10 |
| Lactoferrin | LF peptide 93 | 487.6 | 625.3 | 2.18 | 0.5 | 10 |
| Lactoferrin | LF peptide 1 795 | 795.9 | 1276.6 | 2.47 | 0.5 | 24 |
| Lactoferrin | LF peptide 504 | 621.6 | 272.2 | 2.59 | 0.5 | 24 |
| Lactoferrin | LF peptide 544 | 549.3 | 771.4 | 2.61 | 0.5 | 14 |
| Lactoferrin | LF peptide 220 | 510.8 | 506.3 | 2.8 | 0.5 | 13 |
| Lactoferrin | LF peptide 364 | 723.4 | 731.4 | 3.1 | 0.5 | 23 |
| Lactoferrin | LF peptide 2 790 | 790.4 | 1239.5 | 3.35 | 0.5 | 24 |
| Lactoferrin | LF peptide 587 | 668.4 | 300.2 | 4.27 | 0.5 | 20 |
| Lysozyme | lysozyme peptide 2 | 788.4 | 957.5 | 3.02 | 0.5 | 28 |
| Lysozyme | lysozyme peptide 1 | 700.8 | 764.4 | 3.33 | 0.5 | 20 |
| Lysozyme | lysozyme peptide 3 | 788.1 | 808.4 | 4.8 | 0.5 | 20 |
| SC | SC peptide 2 | 619.7 | 414.2 | 2.82 | 0.5 | 14 |
| SC | SC peptide 5 | 724.7 | 860 | 4.06 | 0.5 | 21 |

**Table 1:** MRM transitions peptides.

Fig. 5 shows the MRM overlaid of all transitions and the single extracted ion chromatograms (EIC) monitored transitions for all the seven proteins. The LC-MS runs were done in 16 minutes and peptides and glycopeptides were monitored in the same experiments.

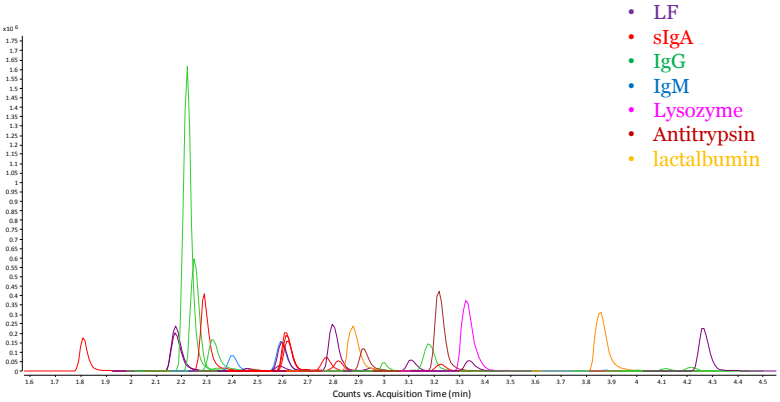


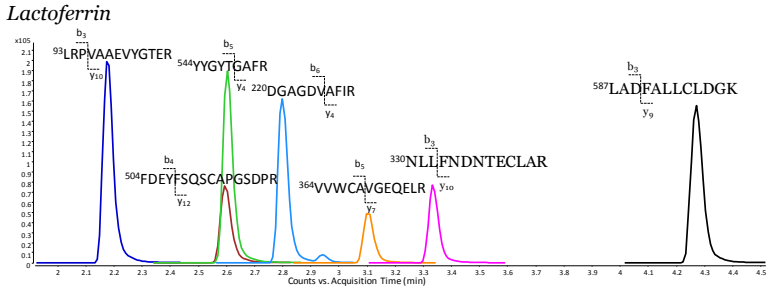

*Lactalbumin*

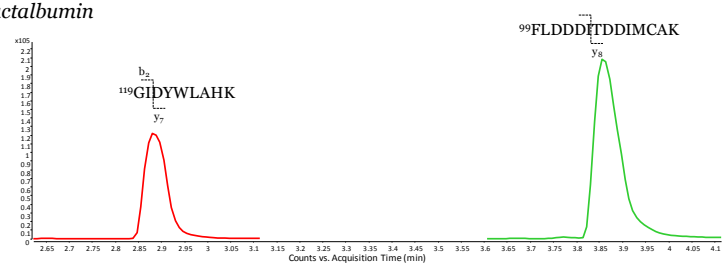


*Secretory-IgA*

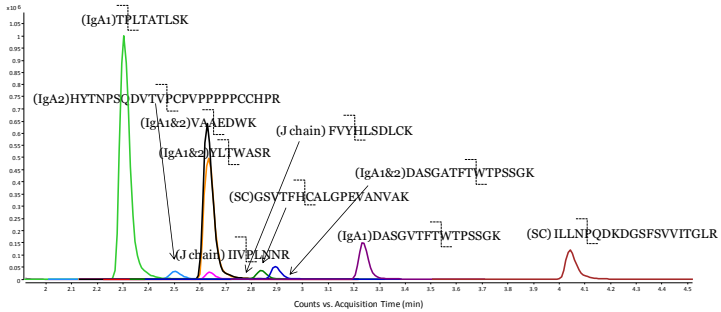


*IgG*

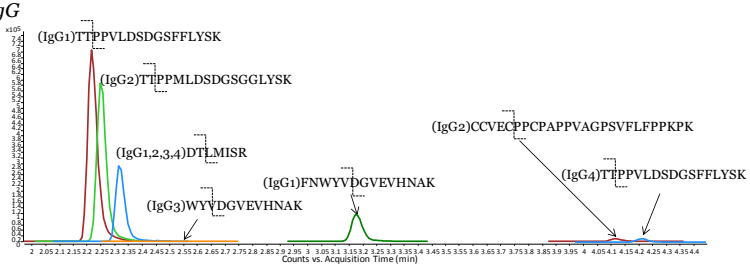

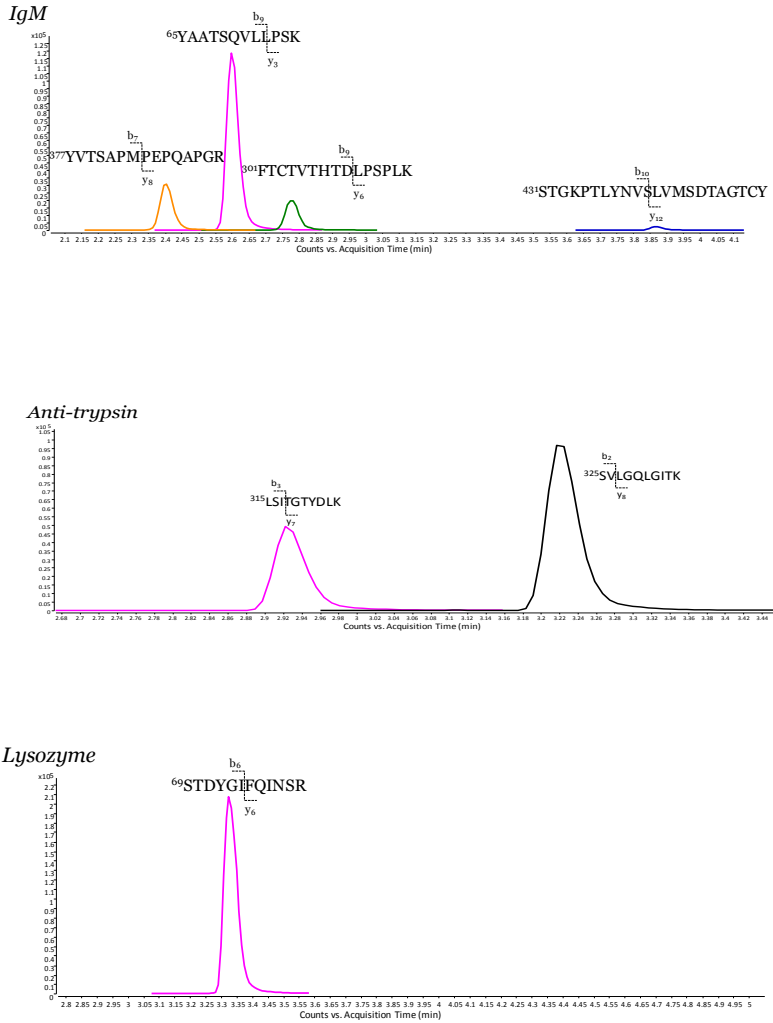


**Figure 5:** MRM overlaid and extracted ion chromatogram.

The IgG standard was observed to contain all four IgG subclasses: IgG1, IgG2, IgG3 and IgG4, the lactoferrin peptide 93, 795, 220, 790 and 587. Four for IgM: IgM1-2-3 and 4, three for lysozyme, two for antitrypsin and three for IgA and J chain.

For investigation of the assay linearity a dilution series of standard peptides containing constant amount of peptides were analyzed. Calibration curves were generated by linear regression analysis on the peak area ratios versus concentration ratios for all peptides. The calibration curves (Fig. 6) were fitted linearly with an $R^2$ of aost 1.

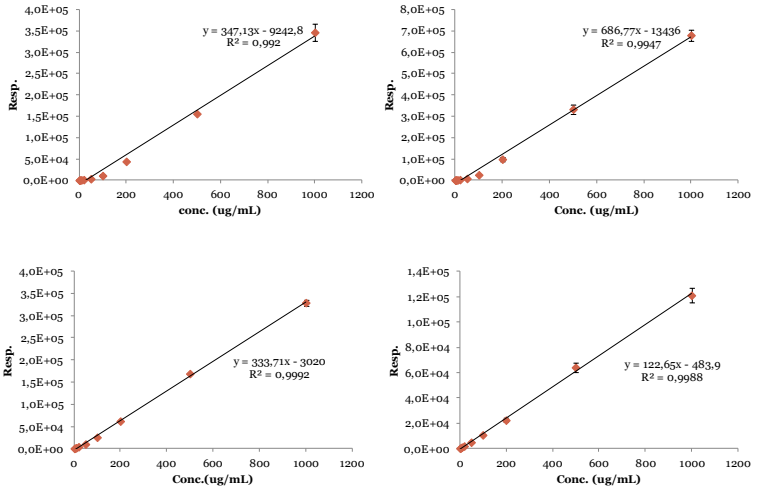

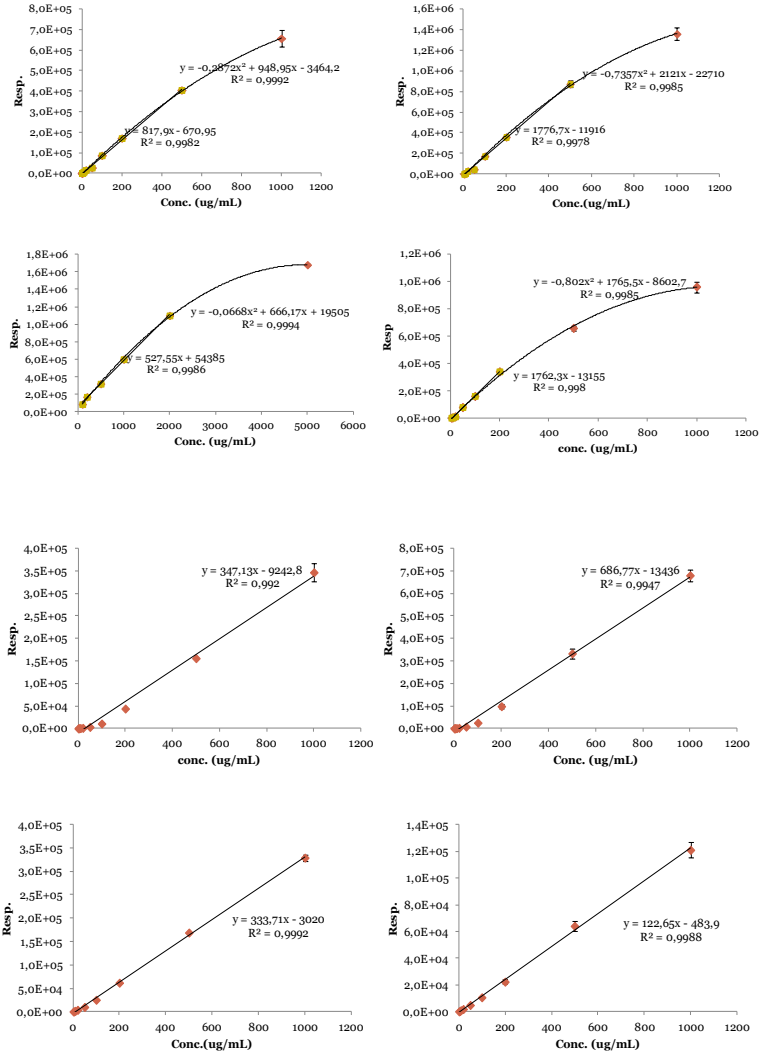


**Figure 5:** peptides calibration curves.

*1.4.1 d Glycopeptides quantitation*

Protein glycosylation is one of the most important post translational modifications that influence various functional aspects of proteins such as structural and modulatory functions. Changes in glycosylation have been correlated to a number of diseases, including Alzheimer's disease, diabetes mellitus, rheumatoid arthritis, and cancer. There are two major types of protein glycosylation N and O-glycosilation. Those where glycan are connected to asparagine residues are named N-linked, and those connected to serine or threonine residues, referred to as O-linked.

Glycopeptides were quantified using MRM in the same run with the peptides (Fig. 6). The absolute amount of the proteins was determined using a peptide calibration curve, while the degree of glycosylation was normalized to the total protein content. The MRM transitions for all the glycopeptides monitored are shown in Table 2.

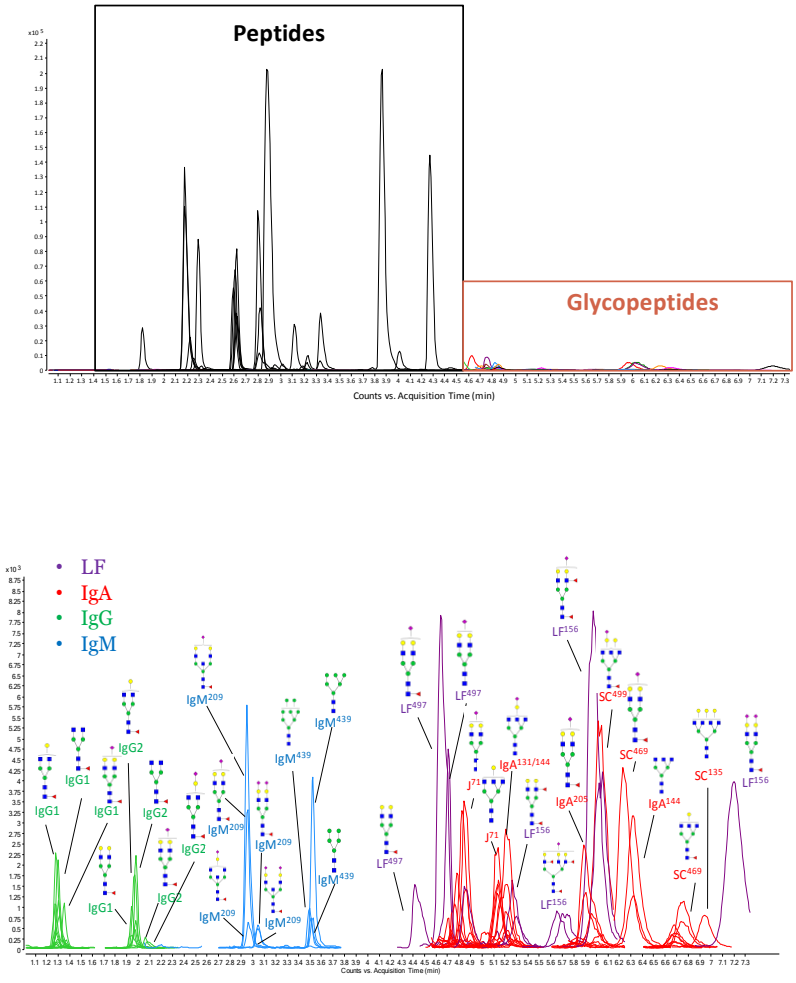


**Figure 6:** LC-QqQ profile of peptides and glycopeptides (top); MRM chromatogram of glycopeptides (bottom).

| Compound Group | Compound Name | Precursor Ion (m/z) | Product Ion (m/z) | Ret Time (min) | Collision Energy |
|---|---|---|---|---|---|
| IGA | IGA2 3510 205 | 869.4 | 204.1 | 4.85 | 23 |
| IGA | IGA 8200 131/144 | 934.1 | 204.1 | 4.8 | 29 |
| IGA | IGA 9200 131/144 | 966.5 | 204.1 | 4.8 | 30 |
| IGA | IGA 5401 131/144 | 976.3 | 204.1 | 5.2 | 24 |
| IGA | IGA2 5510-205 | 977.5 | 366.1 | 5.2 | 25 |
| IGA | IGA 4501 131/144 | 984.5 | 204.1 | 5.25 | 31 |
| IGA | IGA2 5411-205 | 1006.8 | 366.1 | 5.95 | 25 |
| IGA | IGA 3300 131/144 | 1015.5 | 204.1 | 4.91 | 32 |
| IGA | IGA 5501 131/144 | 1016.9 | 366.1 | 5.15 | 25 |
| IGA | IGA 5402 131/144 | 1034.5 | 204.1 | 5.85 | 32 |
| IGA | IGA 5200 131/144 | 1045.8 | 204.1 | 4.9 | 33 |
| IGA | IGA 3400 131/144 | 1066.3 | 204.1 | 4.83 | 34 |
| IGA | IGA2 5511-205 | 1074.5 | 366.1 | 6.73 | 25 |
| IGA | IGA 5502-131/144 | 1075.1 | 366.1 | 5.85 | 25 |
| IGA | IGA 3510 131/144 | 1102.8 | 204.1 | 5.05 | 32 |
| IGA | IGA1 3500-144 | 1117.1 | 366.1 | 6.4 | 25 |
| IGA | IGA 5400 131/144 | 1147.3 | 204.1 | 4.8 | 37 |
| IGA | IGA 4500 131/144 | 1157.6 | 204.1 | 4.8 | 31 |
| IGA | IGA2 6200-131 | 1168 | 204.1 | 4.8 | 36 |
| IGA | IGA 5301 131/144 | 1169.3 | 204.1 | 5.25 | 43 |
| IGA | IGA 4401-131/144 | 1179.6 | 204.1 | 5.25 | 41 |
| IGA | IGA1 5500-144 | 1198.1 | 366.1 | 4.76 | 25 |
| IGA | IGA1 5402-144 | 1292.9 | 366.1 | 5.9 | 30 |
| IGG | IGG H3N4F1_2 | 868.1 | 204.1 | 2 | 13 |
| IGG | IGG H4N4_2 | 873.4 | 204.1 | 1.98 | 13 |
| IGG | IGG H3N4F1_1 | 878.8 | 204.1 | 1.3 | 13 |
| IGG | IGG H4N4_1 | 884.1 | 204.1 | 1.3 | 14 |
| IGG | IGG H4N4F1_2 | 922.1 | 204.1 | 1.98 | 25 |
| IGG | IGG H4N4F1_3_4 | 927.4 | 204.1 | 1.3 | 14 |
| IGG | IGG H4N4F1_1 | 932.8 | 204.1 | 1.28 | 15 |
| IGG | IGG H3N5F1_2 | 935.8 | 204.1 | 1.98 | 14 |
| IGG | IGG H5N4_1 | 938.1 | 366.1 | 1.28 | 14 |
| IGG | IGG H3N5F1_3_4 | 941.1 | 204.1 | 1.28 | 15 |

| Compound Group | Compound Name | Precursor Ion (m/z) | Product Ion (m/z) | Ret Time (min) | Collision Energy |
|---|---|---|---|---|---|
| IGA | IGA2 3510 205 | 869.4 | 204.1 | 4.85 | 23 |
| IGA | IGA 8200 131/144 | 934.1 | 204.1 | 4.8 | 29 |
| IGA | IGA 9200 131/144 | 966.5 | 204.1 | 4.8 | 30 |
| IGA | IGA 5401 131/144 | 976.3 | 204.1 | 5.2 | 24 |
| IGA | IGA2 5510-205 | 977.5 | 366.1 | 5.2 | 25 |
| IGA | IGA 4501 131/144 | 984.5 | 204.1 | 5.25 | 31 |
| IGA | IGA2 5411-205 | 1006.8 | 366.1 | 5.95 | 25 |
| IGA | IGA 3300 131/144 | 1015.5 | 204.1 | 4.91 | 32 |
| IGA | IGA 5501 131/144 | 1016.9 | 366.1 | 5.15 | 25 |
| IGA | IGA 5402 131/144 | 1034.5 | 204.1 | 5.85 | 32 |
| IGA | IGA 5200 131/144 | 1045.8 | 204.1 | 4.9 | 33 |
| IGA | IGA 3400 131/144 | 1066.3 | 204.1 | 4.83 | 34 |
| IGA | IGA2 5511-205 | 1074.5 | 366.1 | 6.73 | 25 |
| IGA | IGA 5502-131/144 | 1075.1 | 366.1 | 5.85 | 25 |
| IGA | IGA 3510 131/144 | 1102.8 | 204.1 | 5.05 | 32 |
| IGA | IGA1 3500-144 | 1117.1 | 366.1 | 6.4 | 25 |
| IGA | IGA 5400 131/144 | 1147.3 | 204.1 | 4.8 | 37 |
| IGA | IGA 4500 131/144 | 1157.6 | 204.1 | 4.8 | 31 |
| IGA | IGA2 6200-131 | 1168 | 204.1 | 4.8 | 36 |
| IGA | IGA 5301 131/144 | 1169.3 | 204.1 | 5.25 | 43 |
| IGA | IGA 4401-131/144 | 1179.6 | 204.1 | 5.25 | 41 |
| IGA | IGA1 5500-144 | 1198.1 | 366.1 | 4.76 | 25 |
| IGA | IGA1 5402-144 | 1292.9 | 366.1 | 5.9 | 30 |
| IGG | IGG H3N4F1_2 | 868.1 | 204.1 | 2 | 13 |
| IGG | IGG H4N4_2 | 873.4 | 204.1 | 1.98 | 13 |
| IGG | IGG H3N4F1_1 | 878.8 | 204.1 | 1.3 | 13 |
| IGG | IGG H4N4_1 | 884.1 | 204.1 | 1.3 | 14 |
| IGG | IGG H4N4F1_2 | 922.1 | 204.1 | 1.98 | 25 |
| IGG | IGG H4N4F1_3_4 | 927.4 | 204.1 | 1.3 | 14 |
| IGG | IGG H4N4F1_1 | 932.8 | 204.1 | 1.28 | 15 |
| IGG | IGG H3N5F1_2 | 935.8 | 204.1 | 1.98 | 14 |
| IGG | IGG H5N4_1 | 938.1 | 366.1 | 1.28 | 14 |
| IGG | IGG H3N5F1_3_4 | 941.1 | 204.1 | 1.28 | 15 |

| Compound Group | Compound Name | Precursor Ion (m/z) | Product Ion (m/z) | Ret Time (min) | Collision Energy |
|---|---|---|---|---|---|
| IGA | IGA2 3510 205 | 869.4 | 204.1 | 4.85 | 23 |
| IGA | IGA 8200 131/144 | 934.1 | 204.1 | 4.8 | 29 |
| IGA | IGA 9200 131/144 | 966.5 | 204.1 | 4.8 | 30 |
| IGA | IGA 5401 131/144 | 976.3 | 204.1 | 5.2 | 24 |
| IGA | IGA2 5510-205 | 977.5 | 366.1 | 5.2 | 25 |
| IGA | IGA 4501 131/144 | 984.5 | 204.1 | 5.25 | 31 |
| IGA | IGA2 5411-205 | 1006.8 | 366.1 | 5.95 | 25 |
| IGA | IGA 3300 131/144 | 1015.5 | 204.1 | 4.91 | 32 |
| IGA | IGA 5501 131/144 | 1016.9 | 366.1 | 5.15 | 25 |
| IGA | IGA 5402 131/144 | 1034.5 | 204.1 | 5.85 | 32 |
| IGA | IGA 5200 131/144 | 1045.8 | 204.1 | 4.9 | 33 |
| IGA | IGA 3400 131/144 | 1066.3 | 204.1 | 4.83 | 34 |
| IGA | IGA2 5511-205 | 1074.5 | 366.1 | 6.73 | 25 |
| IGA | IGA 5502-131/144 | 1075.1 | 366.1 | 5.85 | 25 |
| IGA | IGA 3510 131/144 | 1102.8 | 204.1 | 5.05 | 32 |
| IGA | IGA1 3500-144 | 1117.1 | 366.1 | 6.4 | 25 |
| IGA | IGA 5400 131/144 | 1147.3 | 204.1 | 4.8 | 37 |
| IGA | IGA 4500 131/144 | 1157.6 | 204.1 | 4.8 | 31 |
| IGA | IGA2 6200-131 | 1168 | 204.1 | 4.8 | 36 |
| IGA | IGA 5301 131/144 | 1169.3 | 204.1 | 5.25 | 43 |
| IGA | IGA 4401-131/144 | 1179.6 | 204.1 | 5.25 | 41 |
| IGA | IGA1 5500-144 | 1198.1 | 366.1 | 4.76 | 25 |
| IGA | IGA1 5402-144 | 1292.9 | 366.1 | 5.9 | 30 |
| IGG | IGG H3N4F1_2 | 868.1 | 204.1 | 2 | 13 |
| IGG | IGG H4N4_2 | 873.4 | 204.1 | 1.98 | 13 |
| IGG | IGG H3N4F1_1 | 878.8 | 204.1 | 1.3 | 13 |
| IGG | IGG H4N4_1 | 884.1 | 204.1 | 1.3 | 14 |
| IGG | IGG H4N4F1_2 | 922.1 | 204.1 | 1.98 | 25 |
| IGG | IGG H4N4F1_3_4 | 927.4 | 204.1 | 1.3 | 14 |
| IGG | IGG H4N4F1_1 | 932.8 | 204.1 | 1.28 | 15 |
| IGG | IGG H3N5F1_2 | 935.8 | 204.1 | 1.98 | 14 |
| IGG | IGG H5N4_1 | 938.1 | 366.1 | 1.28 | 14 |
| IGG | IGG H3N5F1_3_4 | 941.1 | 204.1 | 1.28 | 15 |

**Table 2:** MRM glycopeptides transitions.

Quantitation of protein glycosylation is currently limited to relative quantitation due to the lack of glycan/glycopeptide standards so the glycopeptide signals were normalized to the protein abundances to separate out the contribution of protein concentration (Eq 2).

$$\text{Degree of glycosilation} = \frac{Glycopeptide \;\; ion \; abundance}{Protein \;\; ion \; abundance} \qquad (2)$$

## 1.4.2 Applications

*1.4.2 a Milk samples*

Milk samples, previously stored at -80 °C, were completely thawed and 50 µL were diluted with 150 µL of AmBic (50 mM) and subjected to trypsin digestion. Different times and enzyme amounts were used to evaluate changes in digestion. It was observed that 2 ug of trypsin are sufficient to digest 50 µL of milk. We tried also to eliminate fat layer from milk but there is no difference in digestion.

No dilution were performed before LC-QqQ analysis. LC-MRM experiments were carried out employing the method previously exposed. Figure 6 shows the LC-MRM profile of the peptides find in milk samples. Using Agilent MassHunter Quantitative Analysis B 6.0 software the response of each peptides was quantified and the concentration of proteins, from the corresponding calibration curves, was calculated. In tab. 3 have been reported the value in g/L found in milk samples. The concentration calculated of each proteins are in agreement

with literature, for example 0.65 ±0.05 g/L is the quantity found for lactoferrin employing our method, the literature value is 0.5-6 g/L.

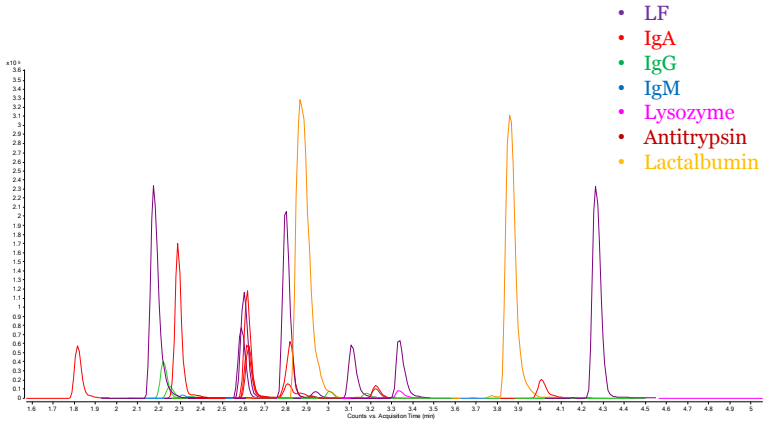


**Figure 6:** overlaid of LC-MRM profile for each peptides of all proteins.

| Milk Protein | Calc. Conc (g/L) | Theo. Conc (g/L) |
|---|---|---|
| Lactalbumin | 2.45 ± 0.13 | 0.4-3 |
| Lactoferrin | 0.65 ± 0.05 | 0.5-6 |
| IgA | 0.37 ± 0.05 | 0.2-2 |
| Antitrypsin | 0.075 ± 0.00034 | 0.05 – 0.3 |
| Lysozyme | 0.029 ± 0.0001 | 0.02-0.4 |
| IgM | 0.024 ± 0.0006 | 0.01-0.2 |
| IgG | 0.019 ± 0.0005 | 0.01-0.2 |

**Table 3:** Calculated and theoretical milk protein concentration.

*1.4.2 b Feces and urine samples*

50 mg of feces samples were diluted with AmBic 150 µL (50 mM), sonicated for 1 h and centrifuged for 30 min, to dissolve the most of the proteins. To the top layer was added chilled EtOH and placed 1h in -80 °C. The bottom layer was dried and reconstituted with AmBic and subject to trypsin digestion. In figure 7 is shown the LC-QqQ of the feces samples.

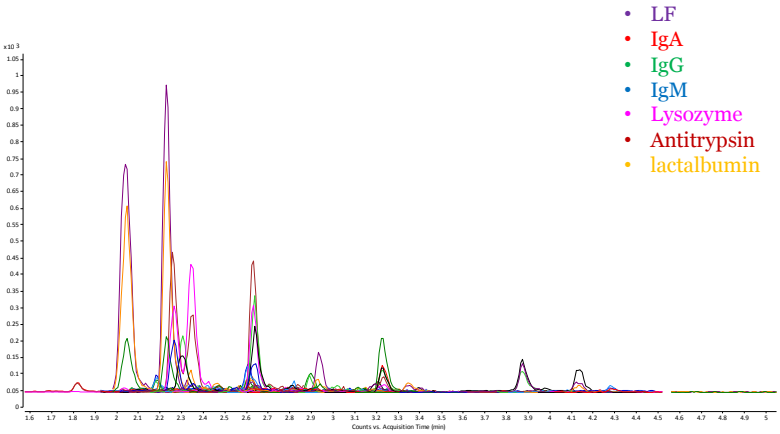


**Figure 7:** overlaid of LC-MRM peptides profile.

Most of the concentrations of the proteins found in the feces are very low compared to the milk proteins. The only exception is $\alpha_1$-antitrypsin, this is in agreement with its characteristic, it is a protein that survive digestion. The concentration found for the proteins are very close around 0.2 mg/g for each proteins, $\alpha_1$-antitrypsin is very abundant 4.6 mg/g and the other immunoglobulins (IgG and IgM) were not detected, but also in milk their concentration is really low (Table 4).

| Feces Protein | Calc. Conc (mg/g) |
|---|---|
| Lactalbumin | 0.23 |
| Lactoferrin | 0.13 |
| IgA | 0.18 |
| Antitrypsin | 4.6 |
| Lysozyme | 0.2 |
| IgM | --- |
| IgG | IgG1 and IgG2 peptides were enriched |

**Table 4:** feces proteins concentrations.

Urines were soaked in AmBic, extracted and dried. The samples were diluted with AmBic and, following the procedure, subjected to trypsin digestion and performed on a QqQ. Figure 8 shows the profile for the peptide transitions in urines.

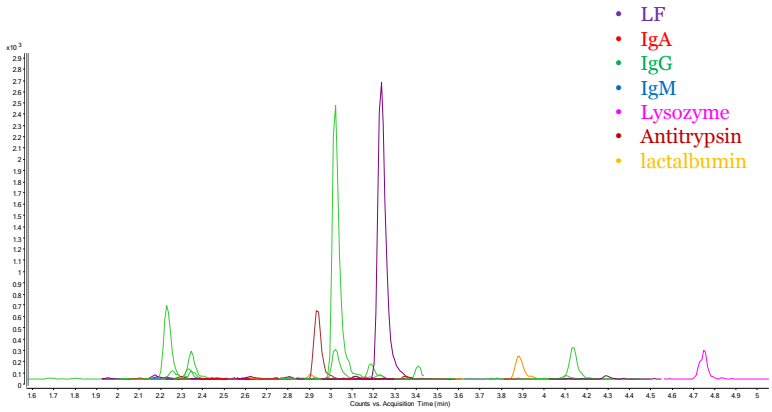


**Figure 8:** overlaid of LC-MRM peptides profile.

Also in this case we evaluated the concentration of the proteins from the linear regression of the calibration curves. $\alpha_1$-antitrypsin is the most abundant 278.2 mg/L, no detection

for s-IgA and IgM, IgG 67.1 mg/L, lysozyme 10.4 mg/L and α-lactoalbumin and lactoferrin around 2mg/L (Table 3).

| Urine Protein | Calc. Conc (mg/L) |
|---|---|
| Lactalbumin | 0.55 |
| Lactoferrin | 1.95 |
| IgA | --- |
| Antitrypsin | 278.2 |
| Lysozyme | 10.4 |
| IgM | --- |
| IgG | 67.1 |

**Table 3:** urine proteins concentrations.

### 1.4.3 Control and reproducibility of the method

In a large-scale MRM experiments, the control of the conditions and the reproducibility of the HPLC separations are critical. We evaluated the plate reproducibility, injecting 12 times the same sample placed in different position of the plate (Fig. 9) and also the injection reproducibility (Fig. 10).

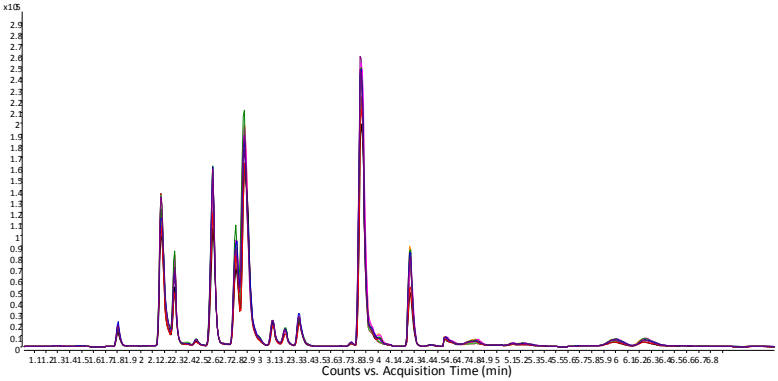


**Figure 9:** Plate reproducibility.

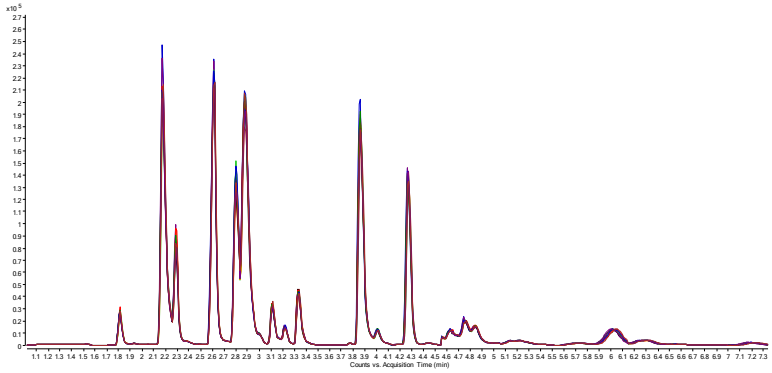


**Figure 10:** Injection reproducibility.

## 1.5 Conclusions

A method was developed to quantify proteins in biologic fluid by label free MRM. As expected the quantity of proteins in milk, feces and urines are very different and reflects their metabolic pathway. Some immunoglobulins could not be detected in feces and urine samples as the protein concentration is below the detection limit. Our results are in agreement with those of literature.

## 1.6 Experimental Section

### 1.6.1 Materials and Chemicals

Proteins standards were purchased from Sigma-Aldrich (St. Louis, MO). Milk and feces samples were collected from healthy patients by UC Davis Medical center; the samples were stored at -80 °C prior to use. Sequencing grade modified trypsin and dithiothreitol (DTT) were purchased from Promega (Madison, WI), iodoacetamide (IAA) was purchased from Sigma-Aldrich (St. Louis, MO).

### 1.6.2 Sample preparation

*1.6.2 a Standards*

Accurate amount of proteins standards were weighed using a micro balance (lactoferrin 200 ug, lactoalbumin 200 ug, IgA 100 ug, IgG 20 ug, IgM 20 ug, $\alpha_1$-antitrypsin 20 ug, lysozime 20 ug) mixted together and dissolved in 300 uL of 50 mM $NH_4HCO_3$ (AmBic). Sonication was applied for 1 h to dissolve the proteins. Proteins were reduced using 4 uL of 550 mM DTT (dithiothreitol) in a 60 °C water bath for 50

min, alkylated usig 8 uL of 450 mM IAA (iodoacetamide) at room temperature in the dark for 30 min. Then 2 ug of trypsin was added and proteins were incubated in a 37 °C incubator for 18 h. After that the samples were dryed and reconstituted with 50 uL of water and diluted serially and used to built a calibration curve (Fig. 11 for lactoferrin).

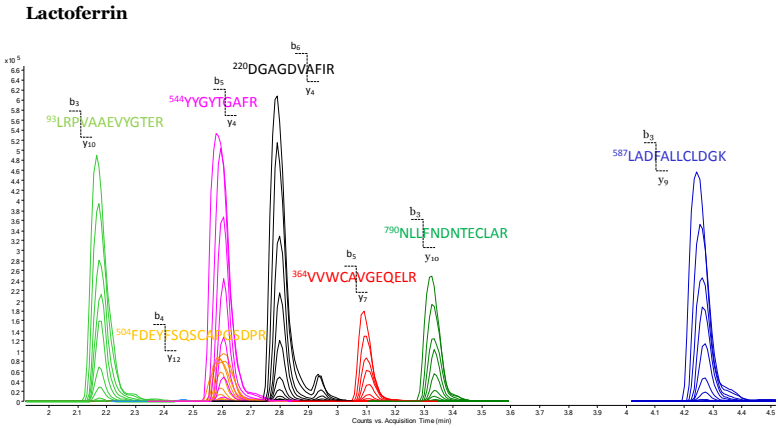


**Figure 11:** dilution serie for lacotoferrin

*1.6.2 b Milk samples*

50uL of milk samples, from different mothers at different stage of lactation, were diluted with 150 uL of 50 mM

$NH_4NCO_3$, reduced with 550 mM DTT (4 uL) in a 60 °C water bath for 50 min, and alkylated with 450 mM IAA (8 uL) at room temperature in the dark for 30 min. The samples were digested with trypsin (2 ug) for 18 h in a 37 °C water bath. The samples were cleaned up by C18 SPE (solid phase extraction), dried, reconstituted with 100 ul of water and analyzed on a QqQ, monitoring all the transition determined by the standards.

*1.6.2 Feces samples*

50 ug of feces was diluted with 150 uL of 50 mM $NH_4NCO_3$, sonicated for 1h and centrifuge for 30 min. 300 uL of chilled EtOH were added to the top layer and placed for 1 h at -80 °C. The top layer was collected to do HMOs analysis and the bottom (100 uL) dried. After reconstituting with 150 uL of AmBic, they were reduced with 550 mM DTT (2 ul) in a 60 °C water bath for 50 min, and alkylated with 450 mM IAA (4 ul) at room temperature in the dark for 30 min. The samples were digested with trypsin (2 ug) for 18h in a 37 °C water bath.

The samples were cleaned up by C18 SPE (solid phase extraction), dried, reconstituted with 100 uL of water and analyzed on a QqQ.

### 1.6.3 LC-MS Analysis

*1.6.3 a Nano-LC-Chip-QTOF analysis*

The peptide samples were reconstituted with 100 ul of water and 3 ul was injected for each sample run. The runs were carried out on an Agilent 1200 series HPLC-Chip system coupled to an Agilent 6520 QTOF (Agilent Technologies, Santa Clara, CA). The microfluid chip consisted of two C18 columns: one for enrichment (4 mm, 40 nL) and the other for separation (43 mm x 75 um). The LC separation was performed using a binary gradient solvent A of 3% acetonitrile, 0.1 % formic acid, solvent B of 90 % acetonitrile, 0.1 % formic acid in nano-pure water.

The MS was operated in positive mode with the parameters as follows: drying gas temperature 325 °C, drying gas flow rate 5L/min, fragmentor voltage 175 V, skimmer voltage 65V.

The collision energy used for the tandem experiment was calculated on the basis of the m/z value using the relationship (eq. 1)

$$CE\ (eV) = 1.8\ m/z \times 100 - 2.4 \qquad \text{eq (1)}$$

*1.6.3 b UPLC-ESI-QqQ analysis*

The standards were analyzed on an Agilent 1290 infinity LC system coupled with an Agilent 6490 triple quadrupole mass spectrometer (Agilent Technologies, Santa Clara, CA).

The LC separation was performed using a binary gradient at 0.5 ml/min flow rate solvent A of 3% acetonitrile, 0.1 % formic acid, solvent B of 90 % acetonitrile, 0.1 % formic acid in nano-pure water. The 16-minute gradient used was as follows: 0 min at 2.0% B; 15 min at 1.5% B; 3 min at 25% B; 4 min at 30% B; 10 min at 35% B; 11 min at 40% B; the column was washed at 100% B from 12 min to 14 min and re-equilibrated at 2% B from 14.1 min to 16 min. The MS was operated in the positive mode, Q1 and Q3 were

operated at unit resolution. The parameters used were: drying gas ($N_2$) temperature and sheath gas ($N_2$) temperature 290 °C, drying gas flow rate 11 l/min, sheath gas flow rate 12 L/min, nebulizer pressure 30 psi, capillary voltage 1800 V, fragmentor voltage 280 V, RF voltage amplitude of high pressure and low pressure ion funnel were 150 V and 60 V. The standards were diluted serially in nano-pure water to obtain a calibration curve for protein quantitation. The experiments were carried out using the MRM mode, in which transitions were monitored only when the target analyte was eluted. The cycle time was fixed at 500 ms. The MRM result was analyzed using Agilent MassHunter Quantitative Analysis B 6.0 software.

## 1.7 References

[1] Lonnerdal, B. *Am. J. Clin. Nutr.* 2003, 77, 1537S−1543.

[2] Srinivasan, M.; Patel, M. S. *Trends Endocrinol. Metab.* 2007, 19, 146−152.

[3] Kunz C, Lönnerdal B. *Am J Clin Nutr* 1990; 51:37–46.

[4] Kunz C, Lönnerdal B. *Acta Paediatr* 1992; 81:107–12.

[5] Lönnerdal, B. *Am J Clin Nutr* 2003; 77 (suppl):1537S–43S.

[6] Gao, X., Robert McMahon, J., Jessica Woo, G., Davidson, D. B., Ardythe Morrow, L., Zhang, Q. *J. Proteome Res.* 2012, 11, 3897−3907.

[7] Molinari, C. E., Casadio, Y. S., Hartmann, B. T., Livk, A., Bringans, S., Arthur, P. G. and Hartmann, *J. Proteome Res.* 2012, 11, 1696−1714.

[8] Liao,Y., Alvarado, R., Phinney, B. and Leonnerdal, B. *J. Proteome Res.* 2011, 10, 1746–1754

[9] Yamada, M.; Murakami, K.; Wallingford, J. C.; Yuki, Y. *Electrophoresis* 2002, 23, 1153−1160.

[10] Palmer, D. J.; Kelly, V. C.; Smit, A. M.; Kuy, S.; et al. *Proteomics* 2006, 6, 2208–2216.

[11] Mange, A.; Bellet, V.; Tuaillon, E.; Van de Perre, P.; et al. *J. Chromatogr., B* 2008, 876, 252−256.

[12] Picariello, G.; Ferranti, P.; Mamone, G.; Roepstorff, P.; et al. *Proteomics* 2008, 8, 3833−3847.

[13] H. Liao, J. Wu, E. Kuhn, W. Chin, B. Chang, M. D. Jones, S. O'Neil, K. R. Clauser, J. Karl, F. Hasler, R. Roubenoff, W. Zolg, B. C. Guild. *Arthritis Rheum.* 2004, 50, 3792.

[14] Bantscheff, M., Schirle, M., Sweetman, G. et al Quantitative mass spectrometry in proteomics: a critical review. *Anal. Bioanal. Chem.* 2007, 389(4):1017–1031.

[15] Ong, S. E., Foster, L. J., Mann, M. Mass spectrometric-based approaches in quantitative proteomics. *Methods* 2003 29(2):124–130.

[16] Ong, S. E., Mann, M. Mass spectrometry based proteomics turns quantitative. *Nat Chem Biol* 2005, 1(5):252–262

[17] Wilm, M. Quantitative proteomics in biological research. *Proteomics* 2009, 9(20): 4590–4605.

[18] Panchaud, A.; Kussmann, M.; Affolter, M. *Proteomics* 2005, 5, 3836−3846.

[19] Zhu, W., Smith, J. W. and Huang, CM *Journal of Biomedicine and Biotechnology* Volume 2010, Article ID 840518,6 pages.

[20] Bantscheff, M., Schirle, M., Sweetman, G., Rick, J., Kuster, B. *Anal Bioanal Chem* 2007, 389:1017–1031.

[21] Lange, V., Picotti, P., Domon, B. Aebersold, R. *Molecular System Biology* 2008, 4:222.

[22] Zhang, H., Liu, Q., Zimmerman, L. J., Ham, A. L., Robbert Slebos, L. C., Rahman, J., Kikuchi, T., Massion, P. P., Carbone, D. P., Billheimer, D. and Daniel Liebler, C. *Molecular & Cellular Proteomics* 10.6 10.1074/mcp.M110.006593–2.

[23] Gallien, S., Duriez, E. and Domon, B., *J. Mass. Spectrom.* 2011, 46, 298–312.

[24] Soares, R., Pires, E., Almeida, A. M., Santos, R., Gomes, R., Koči, K., Ferraz Franco, C. and Coelho, A. V.

(2012) *Tandem Mass Spectrometry of Peptides, Tandem Mass Spectrometry - Applications and Principles*, Dr Jeevan Prasain (Ed.), ISBN: 978-953-51-0141-3.

[25] Mange, A.; Bellet, V.; Tuaillon, E.; Van de Perre, P.; et al. *J. Chromatogr., B* 2008, 876, 252−256.

[26] Hong, Q., Lebrilla, C.B., Miyamoto, S. and Ruhaak, R. L. *Anal Chem.* 2013 17;85(18):8585-93.

[27] Smilowitz, J.T., S.M. Totten, J. Huang, D. Grapov, H.A. Durham, C.J. Lammi-Keefe, C. Lebrilla, and J.B. German *J Nutr*, 2013. 143(12): p. 1906-12.

[28] R. Craig, J. P. Cortens, R. C. Beavis. *J. Proteome Res*. 2004, 3, 1234.

[29] Wells, J.M. & McLuckey, S.A. (2005). Collision-Induced Dissociation (CID) of Peptides and Proteins, In: *Methods in Enzymology*, Burlingame A.L. (Ed.), pp.148-185, ISBN 978-0-12-182807-3.

[30] K. W. Lau, S. R. Hart, J. A. Lynch, S. C. Wong, S. J. Hubbard, S. J. Gaskell. *Rapid Commun. Mass Spectrom.* 2009, 23, 1508.

[16] Fraschetti C., Pierini M., Villani C., Gasparrini F., Filippi A., Speranza M  Collect. Czech. Chem. Commun 2009; 74 (2), 275-297.

[17] Fraschetti C., Pierini M., Villani C., Gasparrini F., Levi Mortera S., Speranza M. *Chem. Commun*. 2009; (36), 5430-5432.

[18] Fraschetti C., Pierini M., Villani C., Gasparrini F., Filippi A., Speranza M  *Collect. Czech. Chem. Commun* 2009; 74 (2), 275-297.

## List of Publications

1. Levi Mortera, S.; Sabia, R.; Pierini, M.; Gasparrini, F.; Villani, C. "*The dynamic chromatographic behavior of tri-o-thymotide on HPLC chiral stationary phases." Chem. Comm.* 2012; 48(26):3167-9.

2. Abbate, S.; Longhi, G.; Lebon, F.; Castiglioni, E.; Superchi, S.; Pisani, L.; Fontana, F.; Torricelli, F.; Caronna, T.; Villani, C.; Sabia, R.; Tommasini, M.; Lucotti, A.; Mendola, D.; Mele, A.; Lightner, D. "*Helical Sense-Responsive and Substituent-Sensitive Features in Vibrational and Electronic Circular Dichroism, in Circularly Polarized Luminescence and in Raman Spectra of Some Simple Optically Active Hexahelicenes" J. Phys. Chem. C,* Just Accepted Manuscript; DOI: 10.1021/jp4105695.

3. Sabia, R.; Ciogli, A.; Pierini, M.; Gasparrini, F.; Villani, C. *Dynamic HPLC on Chiral Stationary Phases. Low*

*Temperature Separation of the Interconverting enantiomers of diazepam, tetrazepam, prazepam and flunitrazepam* In preparation.

## Congress Communications

1. R. Sabia; F. Gasparrini, C. Villani, M. Pierini

*"A Chiral Macrotricyclic Receptor Prepared by Click Chemistry"*

Presented at the XXXIII National Meeting of Division of Organic Chemistry (SCI), San Benedetto del Tronto (Italy) 12-16/09/2010.

2. R. Sabia, M. Pierini, S. Levi Mortera, F. Gasparrini, C. Villani

*"Dynamic High-Performance Liquid Chromatography of Chiral Stereolabile Compounds: the conformational stereoisomers of Tri-O-thymotide"*

Presented at XXIV National Meeting of the Italian Chemical Society, Lecce (Italy), 11-16/09/2011.

3. R. Sabia, C. Villani, M. Pierini, F. Gasparrini

*"Gas phase enantioselectivity of chiral macrocyclic receptors by ESI-MS"*

Presented at 40° Anniversary of the Division of Mass Spectrometry (SCI), Palermo (Italy), 1-5/07/2012.

4. C. Villani, R. Sabia, A. Ciogli, M. Pierini, F. Gasparrini

*"Dynamic stereochemistry of chiral compounds by HPLC-ECD coupling"*

Presented at 14th International Conference on Chiroptical Spectroscopy- Nashville, Tennesee 9-13/06/2013.

*Oral Communication.*